Investigation of Mass Transfer Phenomena in Supercritical Antisolvent Precipitation Processes

by

Rajeshwar Balaji Chinnawar

A dissertation submitted to the Graduate Faculty of
Auburn University
in partial fulfillment of the
requirements for the Degree of
Doctor of Philosophy

Auburn, Alabama
August 1, 2015

Keywords: Precipitation, Micronization, Pharmaceuticals, Supercritical Fluids, High Magnification Imaging, Carbon Dioxide

Approved by

Steve R. Duke, Associate Professor, Chemical Engineering
Christopher B. Roberts, Professor, Chemical Engineering
Mario R. Eden, Professor, Chemical Engineering
Jayachandra B. Ramapuram, Associate Professor, Pharmacal Science

Abstract

This dissertation involves a detailed discussion of the production of organic and polymeric microparticles of controllable size and size distribution for several applications including certain pharmaceutical formulations. Particle size and particle size distribution are two key factors for the performance of active pharmaceutical ingredients. The supercritical antisolvent (SAS) precipitation process is one of the methods used to produce microparticles. SAS is performed by spraying a solution of an organic solvent and a solute through nozzle into a supercritical antisolvent. The solute is insoluble in the antisolvent and the organic solvent is soluble the antisolvent. The organic solvent and the antisolvent mix as the solution is sprayed which leads to supersaturation of the solute. This causes the solute to precipitate out as small particles.

The underlying phenomena of these processes are not fully understood which results in poor control of the particle formation. This research is focused on improving our understanding the mechanisms of particle formation in supercritical antisolvent precipitation processes. A high magnification visualization system was used to study the effects of process conditions on the spray characteristics and microparticles in the SAS precipitation process, quantifying drop size in SAS spray in an effort to examine solvent/antisolvent mass transfer. We carried out a number of SAS experiments to determine the relationship between the SAS spray characteristics and the

particle characteristics. To study the effects of pressure, temperature and density of the antisolvent on the produced particles, 1 wt% polymethyl methacrylate (PMMA) in acetone, 1 wt% budesonide in ethanol and varying compositions of 1wt% PMMA+budesonide in acetone were processed via the SAS precipitation process.

From these studies we found that spray characteristics were altered significantly by varying operating conditions, however, the resulting particle characteristics were relatively consistent for a range of operating conditions and spray characteristics. Thus, the ability to control the nature of the process spray is insufficient to control the particle characteristics, and as such, other phenomena are heavily influencing the particle characteristics in the SAS precipitation process. To better control this precipitation process, a clearer understanding of the mass transfer and concentration fields in this process is required.

Acknowledgements

I would like to thank my advisors Dr. Steve R. Duke and Dr. Christopher B. Roberts for providing me with the opportunity to join their research group at Auburn University and for their continued support and guidance. I would especially like to thank Dr. Steve Duke for giving me the independence to pursue my research goals in a way I saw fit, while at the same time ensuring I had the end result in sight.

I would like to thank my committee members Dr. Mario R. Eden and Dr. Jaychandra Babu Ramapuram for their guidance and help throughout my Ph.D. and in making this dissertation a worthy document. I would also like to thank Dr. Oladiran Fasina for undertaking the role as the outside reader for my dissertation. I would also like to thank Dr. Michael Miller for help with the scanning electron microscope. I would like to thank Brian Schwieker for his excellent assistance in the development and maintenance of the precipitation system. I would like to thank current and past members of the Duke Research Group. I would like to thank Dr. Daniel Obrzut for his assistance when I first started in the lab. I would like to especially thank Dr. Maninder Sandey and Dr. Payal Agarwal for being great friends, for helping me out countless times. I also like to appreciate the friendship of and express my gratitude to my fellow graduate students.

I would like to dedicate my dissertation to my parents, Anita Chinnawar and Balaji Chinnawar for being a beacon of support and for always being there for me. Their encouragement has been very helpful during my time at Auburn. The values they have imparted in me throughout my life have made me who I am today and I will be eternally grateful.

Table of Contents

List of Figures

List of Tables

Chapter 1

Introduction

Particle size and particle size distribution are two key factors for the performance of active pharmaceutical ingredients in drug delivery. By many estimates, up to 90% of new chemicals entities discovered by the pharmaceutical industry today and many existing drugs are poorly soluble in water or lipophilic compounds (Kommuru et al. 2001). The solubility issues obscuring the delivery of new drugs also affect the delivery of nearly 40% of existing drugs (Shakeel et al. 2008). The bioavailability of low solubility drugs is often intrinsically related to drug particle size. Decreasing the particle size of the drug may decrease the time necessary for it to dissolve in the body and, therefore, increase the bioavailability (Liversidge et al. 1995). Also, particle size and particle size distribution are important factors in inhaler application. Dry powder inhalers and nebulizers are widely prescribed for treating traditional diseases of the lung, particularly asthma and chronic obstructive pulmonary disease (Smith et al. 1996). In the case of oral delivery to the lower respiratory tract, it is widely recognized that particle size plays an important part in defining where the aerosol particles will deposit (Heyder et al. 2002, Sinko 2006). Hence a better control of the mechanisms of active pharmaceutical ingredient particle formation methods is required.

The formation of active pharmaceutical ingredient particles with suitable properties for dry powder inhalation presents an important challenge to drug delivery scientists. Conventional techniques involving direct crystallization from organic solvents are generally unable to provide aerosol products directly. In order to meet stringent particle size specifications, material is

processed further, usually by milling, to generate the required particle size properties. High energy milling techniques, such as air jet milling, are far from ideal as products formed are often cohesive, highly electrostatically charged, and difficult to process downstream. Also such processes can induce uncontrollable variations of crystal structure and crystallographic defects that result in reduced stability and increased sensitivity to moisture (Ward et al. 1995). Other methods for preparing micron-sized drug particles are spray-drying, spray freeze-drying, liquid-liquid emulsion and emulsion/coacervation techniques. Apart from spray drying, all other techniques are multi-stage. Hence there has been increase in interests in the techniques which result in particles with low residual solvent levels in pharmaceutical ingredients and excipients produced by conventional crystallization techniques. Supercritical fluids (SCFs), and compressed gas technologies in general, are single stage methods, which can give efficient particle formation. Hence supercritical fluids and compressed gas technologies for the formation of microparticles have been an active area of research (Yeo et al. 1993, Tom et al. 1994, Bertucco et al. 1996, Martin et al., 2002, Reverchon et al. 2007, Reverchon et al. 2008). Processes utilizing SCFs for particle formation include rapid expansion of supercritical solutions (RESS), supercritical antisolvent (SAS) precipitation, precipitation with compressed antisolvent (PCA), solution enhanced dispersion by supercritical fluids (SEDS), etc.

The supercritical antisolvent (SAS) precipitation process has been used to attempt the micronization of several kinds of compounds: pharmaceutical ingredients, superconductors, coloring matters, explosives, polymers, biopolymers, etc. (Reverchon 1999, Shariati et al. 2003, Hakuta et al. 2003). The SAS precipitation process works by spraying a solution of organic solvent and solute through a nozzle into supercritical fluid, an antisolvent (Dixon et al. 1993).

Many SCFs can be used for this purpose for example water, dimethylsulfoxide, methanol, ethanol, CO_2 etc. Supercritical CO_2 is particularly attractive because it has a moderate critical point (31.1 °C, 73.8 bar). The process is inexpensive, nonflammable, and nontoxic especially when used to replace freons and certain organic compounds. In addition, CO_2 is fairly miscible with many organic solvents.

The underlying phenomena of the processes are not fully understood which results in poor control of the particle formation. This research is aimed at developing an understanding of mechanisms of particle formation in supercritical antisolvent precipitation processes. A high magnification visualization system was used to study the effects of process conditions on the spray characteristics and micro particles in the SAS precipitation process, quantifying drop size in SAS spray to estimate solvent/antisolvent mass transfer.

1.1 Background of particle formation

The supercritical antisolvent precipitation process is a spray process used to produce small particles (Dixon et al. 1993). The supercritical antisolvent process involves three distinct components: solvent, solute and antisolvent. An organic solvent with a dissolved solute is sprayed into a supercritical fluid, which acts as the antisolvent. The antisolvent used is typically carbon dioxide because of the tunability of the solvents and mild working conditions. The critical point of carbon dioxide is 73.8 bar and 31.1 ºC. Carbon dioxide is FDA approved (Beckman et al. 2004) because residual CO_2 combination of high TLV (threshold limit value for airborne concentration at 298 K to which it is believed that nearly all workers may be repeatedly exposed

day after day without adverse effects) and high vapor pressure means that residual CO_2 left behind in substrates is not a concern with respect to human exposure. Different solutes can be used in the SAS precipitation process such as pharmaceuticals (Randolph et al. 1993), polymers (Mawson et al. 1997), proteins (Yeo et al. 1993), and dyes (Wu et al. 2005). The solvent is selected such that it dissolves the solute and mixes with antisolvent. For example, the solvent acetone dissolves the solute polymethyl methacrylate and mixes well with supercritical carbon dioxide. Toluene, methylene chloride, ethanol, dimethyl sulfoxide (DMSO), dimethyl formamide (DMF) etc. have all been used as the solvent in the SAS precipitation processes.

Dixon et al. (2003) studied spraying of a solution into a compressed fluid antisolvent to obtain micro particles. A solution of polystyrene and toluene was sprayed into carbon dioxide at subcritical and supercritical conditions. Low concentration of solute in the solvent resulted in the formation of particles, whereas high concentration of solute resulted in precipitation of the solute into polystyrene fibers instead of particles. An increase in particle size was observed as the temperature was increased from 10°C to 40°C at 0.86 g/cm^3. The increase in particle size was suggested to depend on the size of droplets breaking off the solution jet.

Randolph et al. (1993) studied the SAS precipitation process to form micro particles of PLA with the intention of developing particles for timed release delivery of pharmaceuticals. At working conditions above the critical point of carbon dioxide, spherical PLA micro particles were formed. At a temperature of 304 K and pressures of 75.8 bar, 82.7 bar, and 96.5 bar, the average size of the collected particles was observed to increase from 0.61 μm to 1.4 μm. The

authors concluded that the changes in the particle size with pressure can be related to the rate of mass transfer rather than the initial droplet size.

Lengsfeld et al. (2000) studied the jet break up of solutions and organic solvents sprayed into carbon dioxide. They estimated that, if the characteristic jet breakup length was shorter than 1 μm, the jet was predicted and shown to break up into a gas-like plume instead of atomizing into droplets due to the low surface tension. Particles formed in the core of the gas-like plume were predicted to be larger than particles formed in the carbon dioxide rich perimeter because it takes longer for carbon dioxide to diffuse into the core of the gas-like plume. In the case of a gas-like plume, particle size is controlled by inter diffusion of solvent and antisolvent rather than spray characteristics.

Dukhin et al. (2003) visualized the spray of ethanol into carbon dioxide and related the behavior to dynamic interfacial tension. They found that above the mixture critical point the jet breaks up through traditional jet breakup mechanism. Above the mixture critical point the jet break up regime was attributed to a dynamic interfacial surface tension. Thus, the jet break up time was shorter than the diffusion time. Well above the mixture critical point, a gas-like plume was seen.

Bell et al. (2005) developed an imaging system to obtain in situ images of the SAS precipitation process. The sprays of solutions were characterized by visualizing the sprays at various distances from the nozzle outlet to measure the jet breakup lengths and droplet sizes. Solutions included pure acetone, pure methylene chloride, 1 wt% poly(L-lactic) acid in methylene chloride, saturated poly(L-lactic) acid in methylene chloride, and 1 wt% budesonide

in methylene chloride. The visualization system developed by Stephens (2003) was used in the studies presented in this dissertation.

Gokhale et al. (2007) performed SAS on polyvinylpyrrolidone (PVP) to study the effect of dissolving a solute in a mixture of a good solvent, methylene chloride, and a poor solvent, acetone, on the resulting particle size. In a series of SAS experiments with several solutions of methylene chloride, acetone, and PVP at various concentrations, the average particle size of PVP decreased as the acetone concentration in the original solution was increased. As the jet break up transitioned from dripping to atomization, the dependence of the average particle size on the acetone concentration in the sprayed solution decreased. PVP with molecular weights of 1,300,000 and 360,000 were studied at 35 °C. The 1,300,000 molecular weight particles were slightly larger than the 360,000 molecular weight particles during dripping experiments. Obrzut (2008) studied the effect of polymer solute solubility on the SAS precipitation process and particle characteristics. Copolymers of methyl methacrylate and vinyl pyrrolidone were made at several theoretical monomer ratios; these were used as solute in ethanol as a solvent and processed via the SAS precipitation process. They found that, for sparingly soluble PMMA in ethanol, particles generated were approximately 0.4 μm. For copolymers at well above the critical point of the mixture, bimodal distribution of particles was observed. The diameters of copolymer particles were within the range of few microns to 100 micron balloons (hollow microspheres).

Werling et al. (2000) generated a model of the SAS process dealing with mass transfer between the droplets and bulk fluid in subcritical conditions. This model examined the mass flux

between a single droplet of organic solvent and a bulk fluid of carbon dioxide antisolvent. Mixing inside the droplet was assumed to be due to convective motion. The model was set up by assuming the flux of carbon dioxide following Fick's Law and the diffusion coefficient was related to the chemical potential gradient. They found that the carbon dioxide initially dominated the mass transfer by diffusing into the droplet. The interfacial flux approached zero when the rate of mass transfer into the droplet approached the rate of mass transfer out of the droplet. Then, the rate of mass transfer out of the droplet became the controlling mass transfer. When the SAS precipitation process was operated above the mixture critical point, droplets were predicted to shrink when the solvent density was below the bulk fluid density and swell when the density was greater in the droplet.

Reverchon et al. (2003) studied the effect of operating conditions on processing yttrium acetate (YAc) in solution with dimethyl sulfoxide (DMSO) using the SAS precipitation process. To study phase behavior, CO_2 and DMSO were sprayed continuously into a vessel at a CO_2 mole fraction of 0.98. At increasing temperatures, a higher pressure was necessary to reach the mixture critical point and, therefore, the transition from atomization to break up as a gas-like plume. When this experiment was performed with a 1.38 wt% YAc/DMSO solution, the mixture critical point was the same, but as the concentration of YAc increased (4.5 wt%) the pressure required to reach the mixture critical point also increased. Increasing the diameter of the nozzle was shown to result in a small increase in the particle size. The particle size was also shown to increase with increasing concentration of YAc in solution. The effect of phase behavior on particle size and morphology was studied by increasing the pressure at several temperatures to induce a transition from a two phase subcritical system to a one phase supercritical system. In the

subcritical system, nano-scale particles were shown to slightly decrease in size with increasing pressure. Near the transition from a two phase subcritical system to a one phase supercritical system, small particles coalesced to form large microballoon structures. When a one phase supercritical system was reached, smaller particles were obtained compared to those collected from a two phase subcritical system. This study showed that the relation between the operating conditions and the mixture critical point is very important when performing the SAS precipitation process.

1.2 Other processes to make particles

Supercritical antisolvent precipitation with enhanced mass transfer (SAS-EM) uses ultrasound to produce smaller droplets and, therefore, smaller particles (Chattopadhyay et al. 2001). A titanium horn delivers constant-amplitude vibrations near the nozzle tip. The ultrasonic vibration causes a rapid mixing of the solution and antisolvent. The jet also breaks up into smaller initial droplets. When compared to SAS, the particle size is greatly reduced.

SAS with coflow is the steady-state equivalent of the supercritical antisolvent precipitation process. This process allows for two flow rates to be changed: carbon dioxide flow rate and solution flow rate. Due to the change of jet break up related with a coflow jet, the droplet morphology is also altered.

A nozzle in which carbon dioxide is premixed with the solution prior to injection into the bulk carbon dioxide was developed by Hanna et al. (1994) as Solution-Enhanced Dispersion by

Supercritical fluids (SEDS). SEDS is performed by having a premixing section in the nozzle. This variation involves premixing of carbon dioxide and the solution before spraying into the bulk carbon dioxide. Adding CO_2 decreases the rate at which the droplets are supersaturated by decreasing the amount of CO_2 which needs to diffuse. By altering the time after spraying for the droplet to be saturated, the particle morphology can be controlled (Shekunov et al. 2001).

Atomized rapid injection for solvent extraction (ARISE) is a method similar to the SAS precipitation process (Sih et al. 2007). In this method the solution is mixed with the carbon dioxide as rapidly as possible. Initially there are two chambers which are filled with either CO_2 or the solution. A piece of tubing and a valve connects the two chambers. To operate the process the valve is opened and an inert gas forces the solution to rapidly transfer to the CO_2 filled chamber. The solute is then rapidly supersaturated and precipitates as micro particles.

1.3 Visualization and modeling studies of the SAS precipitation spray

Particle formation in the SAS precipitation process occurs due to the supersaturation of solute caused by counter diffusion of a supercritical antisolvent and the solvent (Werling et al. 2000). In the SAS precipitation process, varying spray characteristics with varying operating conditions have been observed (Obrzut et al. 2007) but the particles produced were similar in size and size distribution. In Obrzut (2008), for solutes with varying solubility the spray characteristics were similar but particles formed from these different solubility solutes had a wide range of particle sizes (0.4 μm to 100 μm). From the various visualization studies done in our laboratory it is clear that spray characteristics has no significant effect on the particle

characteristics. But solute solubility strength has some effect on the particle characteristics. Hence it is required to investigate concentration distribution and mass transfer in the SAS precipitation process to relate the precipitation mechanism and particle size.

Martin et al. (2004) developed a model of the solvent and solute concentration throughout a single phase spray. The size of particles was modeled as a function of nucleation, coagulation, and condensation. This method of calculation predicted that particle size depended on the location within the jet where nucleation occurs. The results from this model suggest that modifying temperature and pressure to induce supersaturation faster will produce smaller particles. Werling at el. (2000) worked on a model and examined the mass flux between a single droplet of organic solvent and a bulk fluid of carbon dioxide antisolvent. So it is clear that having understanding of the mass transfer and concentration fields in SAS process is required to better control particle characteristics. They suggested that the fact that supercritical conditions result in faster mass transfer suggests that supercritical operation should cause a higher degree of droplet supersaturation in the presence of a solute, resulting in higher nucleation rates and smaller particles.

1.4 Summary

Many studies have been conducted on the formation of particles using the SAS precipitation process. Initial studies were performed to understand how the particle characteristics change with operating conditions. These experiments led to the assumption that spray characteristics, specifically initial droplet size, may control the resulting particle

characteristics. While initial droplet size has some effect on the particle characteristics, the effect was not as dramatic as originally predicted. Then several simulation studies were performed to understand the effect of diffusion on SAS. Also several models were developed to understand the diffusion of solvent and the antisolvent. These models were developed to help understand how operating conditions control dynamic droplet behavior and relate mass transfer during the SAS precipitation process to the resulting particle characteristics.

This dissertation describes the experimental work performed to examine the underlying phenomena in the SAS precipitation process. To understand the particle formation mechanism in the SAS precipitation process, we processed many polymer and drug solutions in solvents via the SAS precipitation process, and the resulting particles where characterized using techniques such as scanning electron microscope and HPLC. The precipitation process spray was visualized at high magnification to allow us to correlate particle characteristics and spray characteristics for several systems. We also performed a feasibility study for a planar laser induced fluorescence method to estimate solute concentrations in SAS sprays.

Chapter 2

Effect of process conditions on the spray characteristics and particle size of PMMA in acetone via the SAS precipitation process

2.1 Introduction

The supercritical antisolvent precipitation process has been shown to be a method for producing microparticles. In the supercritical antisolvent process, an organic solvent with a dissolved solute is sprayed into a supercritical fluid, which acts as the antisolvent. The organic solvent is miscible in the supercritical fluid, but the dissolved solute is only weakly miscible in the supercritical fluid. The organic solvent and solute solution is typically sprayed into a precipitation chamber containing the supercritical fluid. The solution exits a nozzle with different spray characteristics depending on the process conditions. The antisolvent rapidly diffuses in the solution spray and solvent in the spray gradually diffuses in the antisolvent. This process causes supersaturation of solute leading to nucleation and precipitation of micron size particles (Dixon et al. 1993). This method takes advantage of the ability of antisolvent to show significant solvent strength when compressed to liquid-like densities. By operating in the supercritical region, the pressure and temperature of the system can be used to regulate the density of antisolvent fluid. This leads to different particle size and particle size distribution (Gokhale et al. 2007). The objective of this study is to investigate the relationship between process conditions, spray characteristics and particle characteristics.

I was assisted by NSF REU fellow Tyler McPherson with some of the data collection for these studies.

2.2 Materials

Experiments were conducted using a solution of the solute polymethyl methacrylate (PMMA) in acetone, the solvent. PMMA was obtained from Sigma Aldrich and has a molecular weight of ~15000 Daltons. Acetone was obtained from Fisher Scientific. Carbon dioxide of grade 5.5 was obtained from Airgas (Opelika, AL). All the materials were used as received.

2.3 Experimental setup and imaging system

The setup used to perform the SAS precipitation process (Figure 2.1) was modified from the system used by Obrzut et al. (2007). The precipitation chamber used was a Jerguson gage, model 19TM40, with volume of 57 cm^3, height of 48 cm. The precipitation chamber has transparent windows in front and back which facilitates the visualization of the spray. The solution was delivered at constant flow rate of 1.6 cm^3/min with a metering pump, the acuflow series II HPLC pump with pulse dampener, Scientific Systems, through a spray nozzle of 100 μm ID fused silica capillary tubing. An ISCO 500D syringe pump delivers the CO_2 to the precipitation chamber through the annular space between a capillary nozzle and a stainless steel sheath. The nozzle was made by cutting capillary tubing with a wire cutter and inspecting the ends with an optical microscope to achieve a flat tip. To safely operate the high pressure

precipitation chamber, a pressure gage, McDaniel Controls, and a blowout plug, HIP 16-63AF1, are attached. A RTD in the precipitation chamber was used as the input device for the temperature controller, Omega CSC32. The temperature controller regulates a heating tape, Omegaflux SRT051-080, to maintain the temperature of precipitation chamber. One more thermocouple was installed at the center of precipitation chamber to measure the temperature along the depth of the precipitation vessel. The membrane filter, Millipore FLGP02500, separates the precipitated particles from the vessel effluent. The membrane filter has a pore diameter of 0.22 μm and was mounted in a 25 mm filter holder, Millipore XX4502500, at the bottom of the precipitation chamber.

SAS involves jet spraying of the solution into a compressed antisolvent. Imaging and visualization techniques were used previously to study the jet flows, atomization and droplets (Lengsfeld et al. 2000, Obrzut et al. 2007). A high resolution monochrome CCD camera, COHU 2122, was used to image the SAS precipitation process. The camera has a chip size of 768 x 494 pixels with the pixel size of 8.4 x 9.8 μm. The shutter speed is 60 fps. Attached to the camera was a Questar QM100 MKIII long distance microscopic lens. The lens working distance ranges from 8 to 35 cm allowing visualization inside the precipitation chamber. The camera and lens were mounted on a tripod which facilitates X-Y-Z direction movement. A stroboscope, Monarch Nova Strobe DA Plus 115 with the pulse duration of 30 μs, provided backlight illumination (Bell et al. 2005).

The output of the COHU camera was digitized by an analog to digital video converter, Pinnacle Studio Moviebox Ultimate. The video was collected on a computer in .mpg format

using Pinnacle Studio 12 software. The frames of the video were separated into individual .bmp images using QuickTime media player. The images were then analyzed using image processing software, ImageJ. Jet break up length is the distance measured using the Straight Line tool, in ImageJ, from the edge of the capillary tubing to the point where the jet edge exhibits rippling. The same tool was used to measure the droplet diameters. Only droplets that were completely in focus were measured. To find pixel/μm, in-situ images of the 400 μm outer diameter nozzle with the same magnification as the droplet images were obtained and the known distances measured for pixel length.

The precipitated particles were analyzed using a scanning electron microscope (SEM), Zeiss EVO 500. Samples for the scanning electron microscope were prepared by transferring particles from the filter holder to a stub with double-sided carbon tape on the surface. The stub was sputter-coated for 2 minutes with gold. Images of the particles were obtained in .tif format. The particles were analyzed using ImageJ by measuring the diameter using the straight line tool.

2.4 Experimental procedure

To perform these experiments, the apparatus shown in Figure 2.1 was operated in batch mode. The precipitation chamber was initially filled with CO_2 using syringe pump, which was set to maintain the operating pressure in the precipitation chamber. The precipitation chamber was heated by using temperature controlled heating tape. The system was run until the temperature and pressure reached equilibrium. 1 wt% PMMA in acetone solution was pumped by the HPLC pump with all valves closed. The solution was sprayed at a fixed flow rate of 1.6

cm^3/min for 30 to 45 sec. The valve on the syringe pump was opened to resume the pressure control by the Isco syringe pump. Then, the two valves, downstream of precipitation chamber, were adjusted to control the chamber outflow. Usually outflow rate was adjusted to 5-7 cm^3/min, which can be monitored through the change in the volume of the Isco syringe pump. Four chamber volumes of CO_2 were purged through the precipitation chamber. Once the chamber reached the atmospheric pressure, the filter holder was removed to collect the dried PMMA particles on the membrane filter.

The visualization of the spray was done while spraying the solution in the precipitation chamber. The camera was positioned at the desired vertical distance from the tip of the nozzle. Images were typically obtained with the center of the spray in frame. In the case of visualization at 0 mm from the tip of nozzle (jet breakup visualization), the camera was rotated by 90º to take the greater advantage of the aspect ratio.

2.5 Experimental conditions

The SAS precipitation experiments were conducted with 1wt% PMMA in acetone solution sprayed into supercritical CO_2 at 1.6 cm^3/min for 30 to 45 seconds. Experimental conditions are listed in Table 2.1, grouped as three fixed density conditions and three fixed temperature conditions. The operating conditions were chosen to allow for characterization of the spray near the transition from two phases to one phase jet break up.

Experiments with a fixed initial carbon dioxide density of 0.32 g/cm^3 were performed at pressure and temperature combinations of 84 bar and 40 ºC, 89 bar and 45 ºC, and 94 bar and 50 ºC. Fixed temperature experiments at 50 ºC were performed at three pressure and density combinations: 84 bar and 0.24 g/cm^3, 89 bar and 0.28 g/cm^3, and 94 bar and 0.32 g/cm^3. The pressure values were selected to correspond to those of the fixed density experiments. The phase diagram for the binary mixture of CO_2-acetone indicates that after spraying the solution into carbon dioxide a supercritical mixture will be present at these conditions.

Videos were captured through a viewing window in the precipitation chamber. Visualization was done, for all the experimental conditions, at 0, 3, 7, 14, 24 and 34 mm from the tip of the nozzle. The flow rate of 1 wt% PMMA in acetone solution for these experiments was 1.6 cm^3/min, the pressure drop across the nozzle was estimated to be ~8 bar.

2.6 Results

Figure 2.2 represents the visualizations done by performing the SAS precipitation process at a fixed bulk CO_2 density of 0.32 g/cm^3 and select pressure and temperature combination with 1 wt% PMMA in acetone solution flow rate of 1.6 cm^3/min. Figure 2.3 represent the visualization done by performing the SAS precipitation process at a fixed bulk CO_2 temperature of 50 ºC and select pressure and density combination with 1 wt% PMMA in acetone solution flow rate of 1.6 cm^3/min. The data obtained from all the experiments is listed in Table 2.2. Figure 2.4 and Figure 2.5 show the jet break up lengths plots for experiments performed at fixed density and fixed temperature conditions, respectively. Figure 2.6 and Figure 2.7 are the plots of

average droplet diameter vs distance from the tip of the nozzle for experiments performed at fixed density and fixed temperature conditions, respectively. Error bars on all the plots represent the standard deviation due to the droplet size distribution.

2.6.1 Fixed density experiments

Figure 2.2 shows images of 1 wt% PMMA in acetone sprayed in CO_2 at fixed density of 0.32 g/cm^3. Column (a), column (b), and column (c) represent the images of 1 wt% PMMA sprayed in CO_2 at 84 bar and 40 ºC, 89 bar and 45 ºC, and 94 bar and 50 ºC, respectively. In all these conditions, the spray was clearly in the atomization regime as evidenced by the coherent jet and the presence of distinct droplets. Visualizations taken at 3 mm from the nozzle outlet show a section of the spray with the jet unbroken and droplets present. The average jet break up lengths for these three conditions are 586 ± 76 μm, 531 ± 75 μm, and 601 ± 60 μm, respectively. Jet break up length for these fixed density conditions remains similar. For column (a), the average droplet diameter increases from 67 μm at 3mm to 155 μm at 14 mm. For column (b), the average droplet diameter increases from 68 μm at 3mm to 170 μm at 14 mm. For column (c), the average droplet diameter increases from 58 μm at 3mm to 173 μm at 14 mm. After 14 mm the average droplet diameter decreased with increasing distance from the tip of the nozzle.

2.6.2 Fixed temperature experiments

Figure 2.3 shows images of 1 wt% PMMA in acetone sprayed in CO_2 at fixed temperature at 50 ºC. Column (a), column (b), and column (c) represent the images of 1 wt% PMMA sprayed in CO_2 at 84 bar and 0.24g/cm^3, 89 bar and 0.28g/cm^3, 94 bar and 0.32g/cm^3, respectively. In all these conditions, the spray was clearly in the atomization regime as evidenced

by the coherent jet and the presence of distinct droplets. But, the numbers of droplets seen in column (c) are fewer. This shows the transition regime for a gas-like plume. Visualizations taken at 3 mm from the nozzle outlet show a section of the spray with the jet unbroken and droplets present. For column (a), the average droplet diameter increases from 61 μm at 3 mm to 131 μm at 34 mm. For column (b), the average droplet diameter increases from 68 μm at 3 mm to 122 μm at 14 mm. At 89 bar and 0.28 g/cm^3, the average droplet diameter remains nearly similar. For column (c), the average droplet diameter increases from 58 μm at 3mm to 173 μm at 14 mm and then decreases with increasing distance from the tip of the nozzle.

2.7 Discussion

Figure 2.4 shows that the jet breakup length was similar for the fixed density experiments. Figure 2.5 shows that the jet breakup length decreases as pressure was increased for the fixed temperature experiments. Jet breakup length decreases with an increase in temperature or/and pressure which was consistent with the finding of Obrzut et al. 2007 and Lengsfeld et al. 2000. In fixed density experiments, an increase in pressure is accompanied by a decrease in temperature, hence no significant change in jet breakup length. But in the fixed temperature experiments, an increase in pressure increases affinity of the solvent towards the bulk CO_2, which contributes to a decrease in surface tension of the sprayed solution, and hence results in a decrease of the jet breakup length.

Figure 2.2 shows the jet breakup through atomization and droplet formation, and this was seen throughout the images for the fixed density experiments. The droplets occur due to the lack

of coherence in the jet. Figure 2.6 shows the average droplet diameter for the fixed density experiments. Figure 2.6 shows that the droplets initially swell then shrink as they travel away from the nozzle outlet. The analysis of the droplet diameters shows that for each operating pressure, the droplet diameters increased in size from 3 to 14 mm distances from the tip of the nozzle. The increase in size from the distances of 3 to 14 mm could be caused by the infusion of CO_2 into the droplet (Werling et al. 1999, Mukhopadhyay et al. 2004). After 14 mm from the tip of the nozzle, the average droplet diameter decreases. This was caused by the diffusion of acetone and CO_2 out of the droplet into bulk CO_2. Figure 2.3 shows the jet break up through atomization, and droplet formation was seen throughout the images for the fixed temperature experiments. But, the number density of the droplets decreases from the experiment at 84 bar and 0.24 g/cm^3 to 89 bar and 0.28 g/cm^3 to 94 bar and 0.32 g/cm^3. This trend was attributed to the fact that an increase in the pressure created a more miscible system. Figure 2.7 shows the average droplet diameter for the fixed temperature experiments. In the fixed temperature experiments, the average droplet diameter at 84 bar and 0.24 g/cm^3 increases for distances 3 mm to 34 mm, showing that droplets were still swelling. For 89 bar and 0.28 g/cm^3, the droplet diameter increases and then holds until the droplet dissipated in the bulk CO_2, showing that an increase in pressure causes the droplet to dissipate closer to the nozzle outlet. For 94 bar and 0.32 g/cm^3, the droplet diameter increases from 3mm to 14mm and then decreases. This highest pressure condition (more severe condition expected to be a gas like plume regime) was inconsistent with the findings of Lengsfeld et al. 2000.

For all three operating conditions, spherical PMMA micro particles were observed. The morphology of the particles was typically characterized as solid spheres as shown in Figure 2.8

and Figure 2.9. In the fixed density experiments, the average particle size for 84 bar and 40 ºC is 1.7 ± 0.7 µm, for 89 bar and 45 ºC is 0.8 ± 0.48 µm, for 94 bar and 50 ºC is 1.17 ± 0.53 µm. In the fixed temperature experiments, the average particle size for 84 bar and 0.24 g/cm^3 was 1.15 ± 0.77 µm, for 89 bar and 0.28 g/cm^3 was 1.10 ± 0.82 µm, for 94 bar and 0.32 g/cm^3 was 1.17 ± 0.53 µm. The particle sizes are also shown in Table 2.2. Despite the different spray characteristics at different experimental conditions, particles collected at these operating conditions were spherical in shape with similar average diameter and similar size distribution, as shown in Figure 2.10. Hence despite the different spray characteristics at different experimental conditions, the particle characteristics were similar.

2.8 Conclusion

This study shows that spherical, micron-sized PMMA particles can be created via the SAS precipitation process. The high magnification visualization system was used to study the spray characteristics of the SAS precipitation process. In fixed temperature experiments, an increase in pressure and density causes a decrease in jet break up length. In fixed density experiments, jet break up length was similar. Atomization of solutions of 1wt% PMMA in acetone was observed in all the experimental conditions. In the case of atomization, the average droplet diameter increased then decreased with the distance from the nozzle outlet. Despite different spray characteristics at different operating conditions, the particle size and particle size distribution of PMMA was very similar. This suggests that the spray characteristics are not the only phenomena influencing the particle characteristics in the SAS precipitation process.

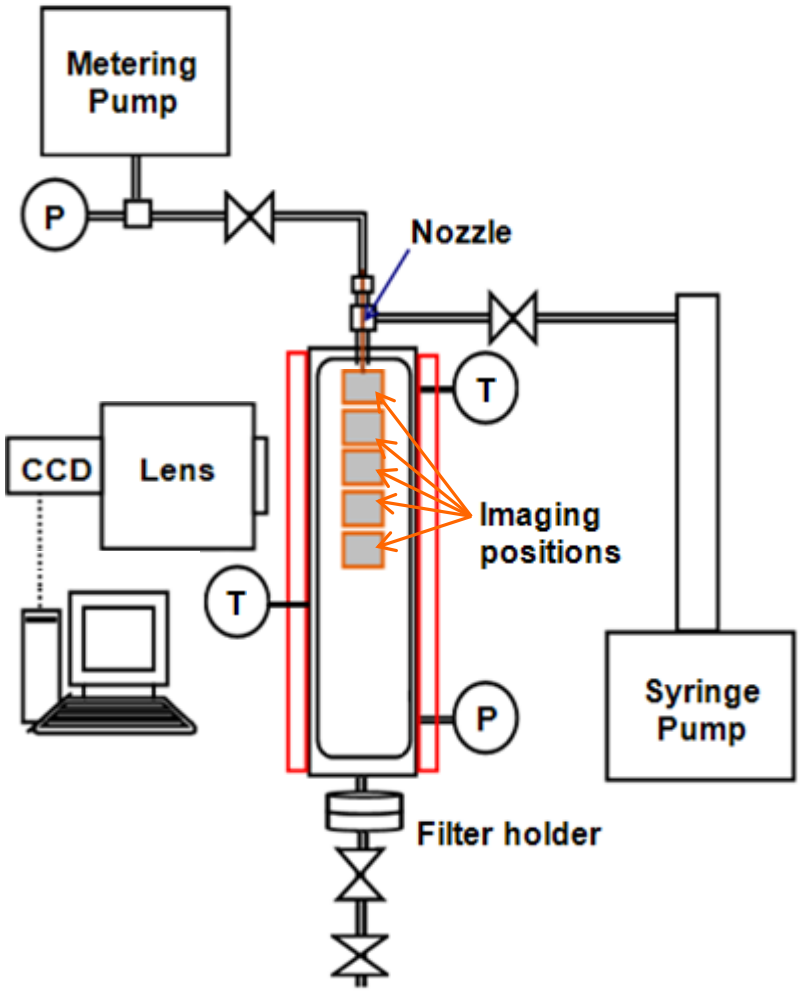

Figure 2.1 Diagram of the imaging system and the apparatus used to perform the supercritical antisolvent precipitation process. The imaging positions in the spray are represented by the shaded boxes inside the precipitation vessel

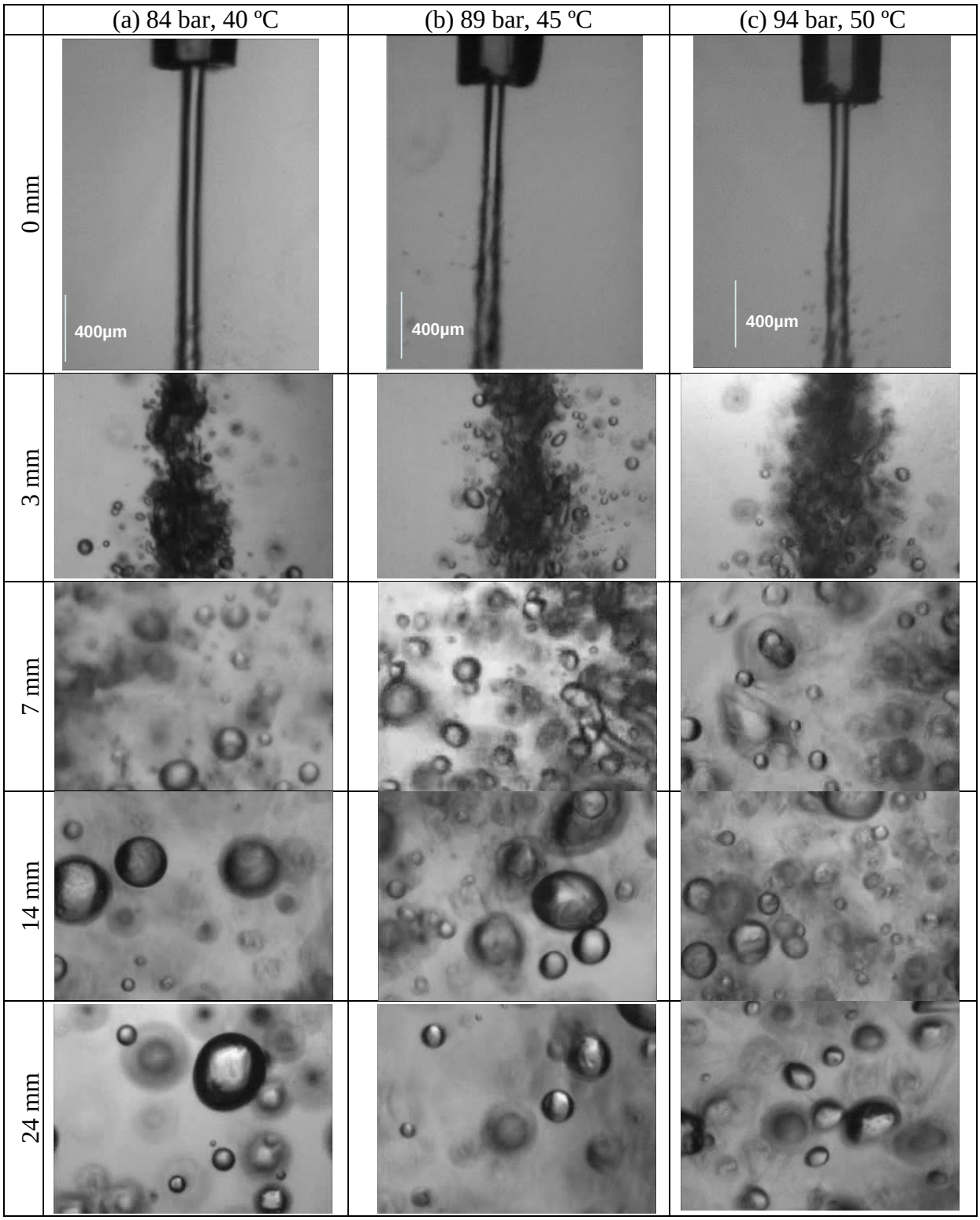

Figure 2.2 Selected frames taken from movies of the spray at given distances from the nozzle in the fixed density SAS experiments, bulk CO_2 density of 0.32 g/cm^3

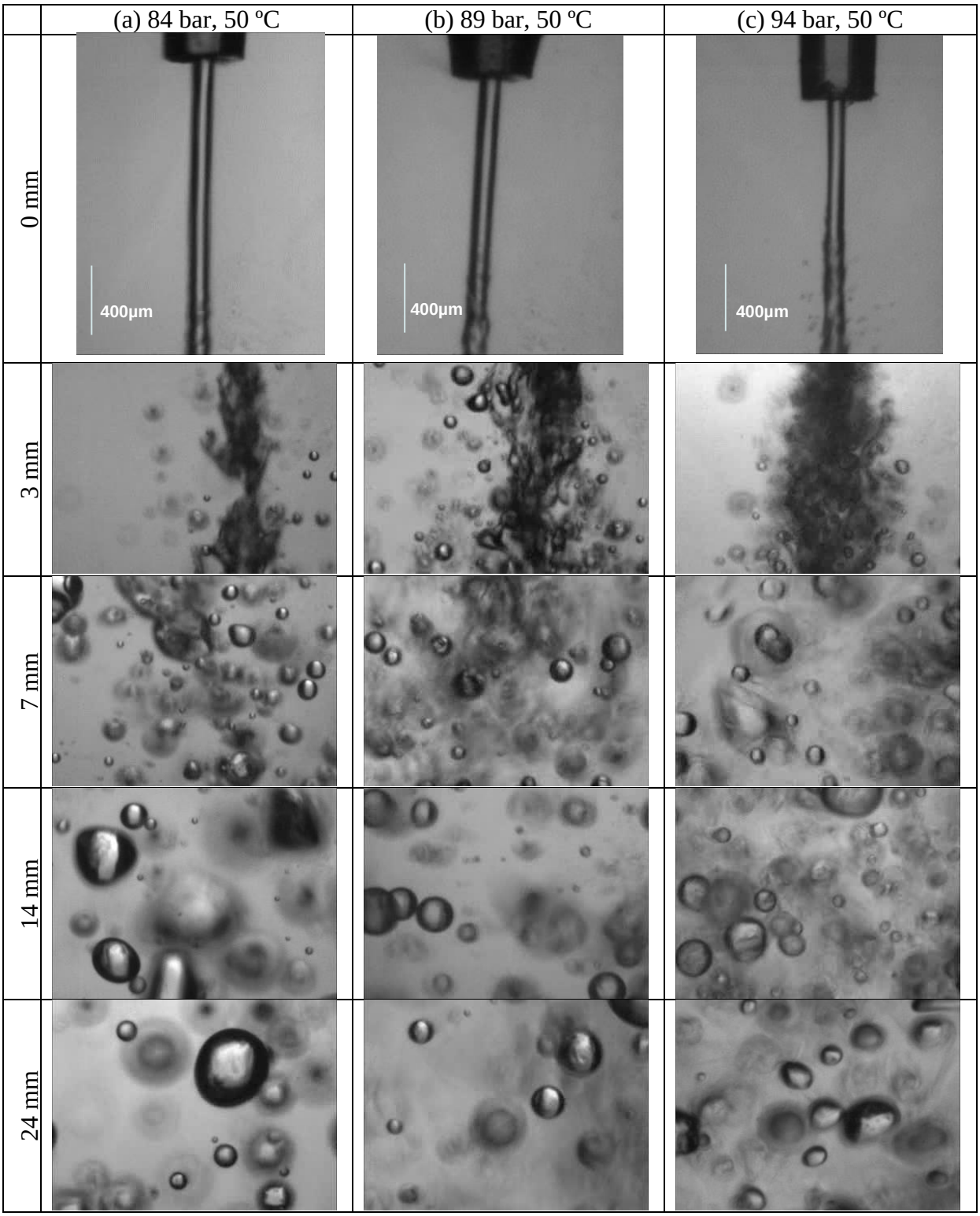

Figure 2.3 Selected frames taken from movies of the spray at given distances from the nozzle in the fixed temperature SAS experiments

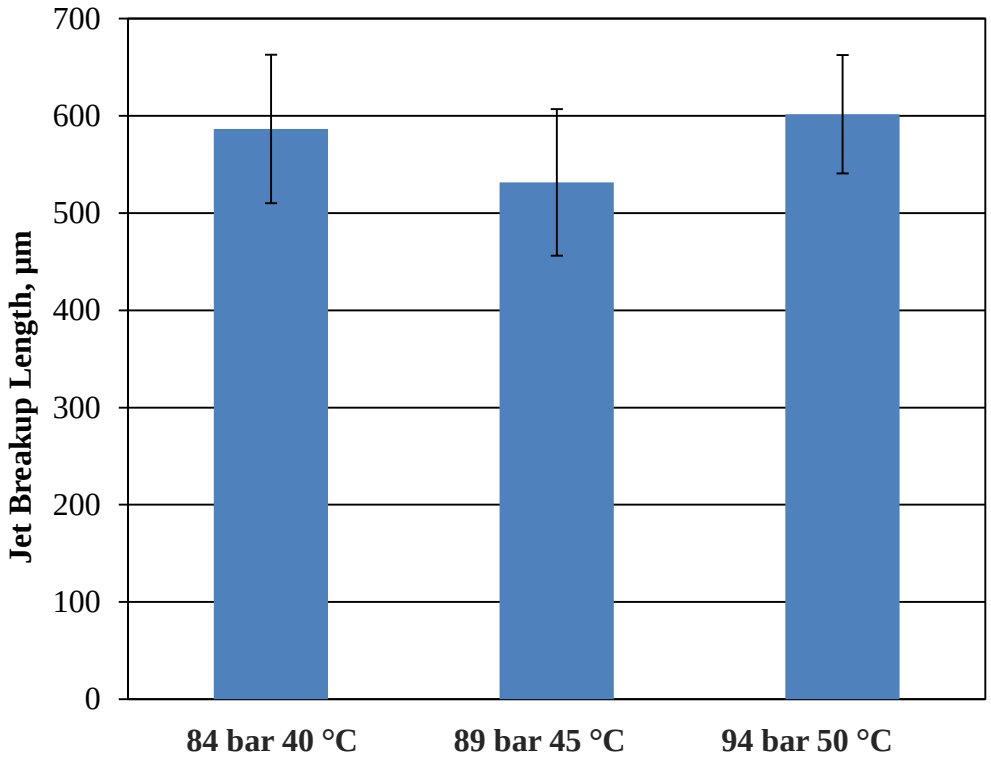

Figure 2.4 Jet breakup length for 1 wt% PMMA in acetone solution sprayed through a capillary nozzle of 100 μm in the fixed density SAS experiments, bulk CO_2 density of 0.32 g/cm^3

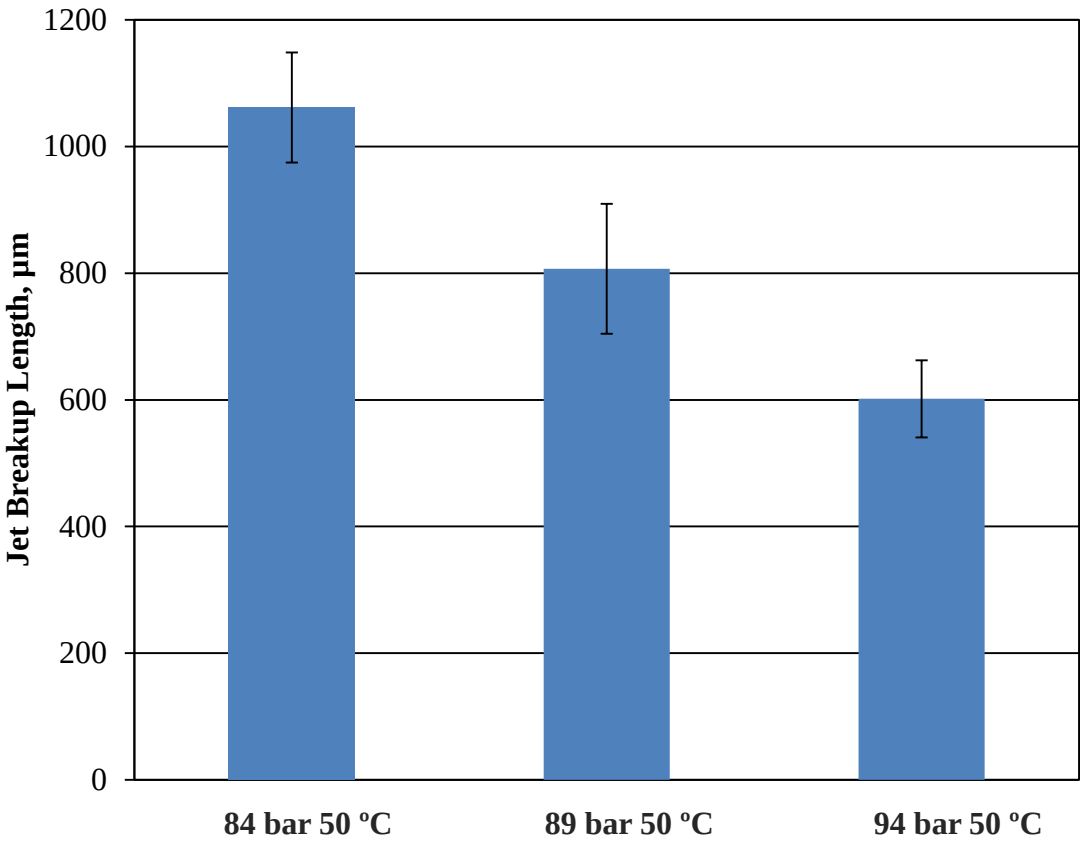

Figure 2.5 Jet breakup length for 1 wt% PMMA in acetone solution sprayed through a capillary nozzle of 100 µm in the fixed temperature SAS experiments

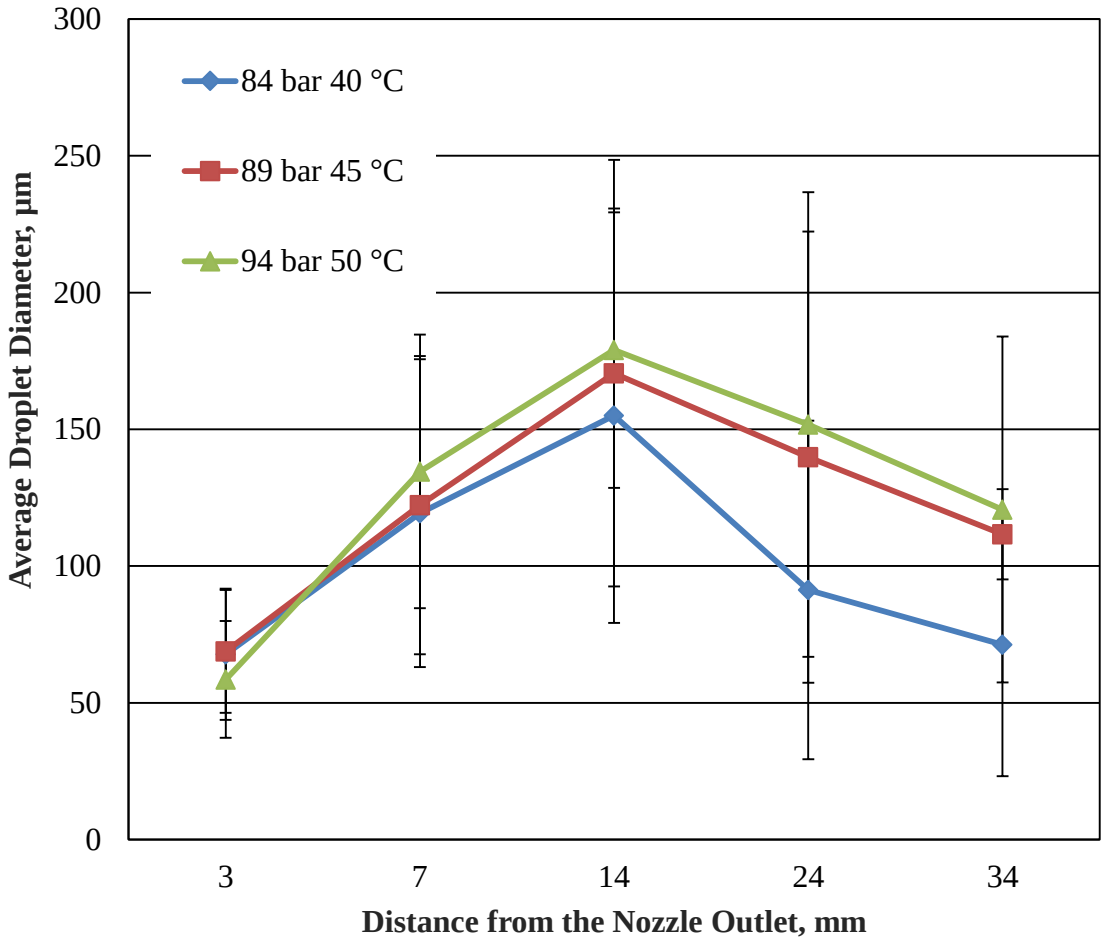

Figure 2.6 Average droplet diameter of 1 wt% PMMA in acetone solution sprayed into supercritical CO_2 at a constant density of 0.32 g/cm^3

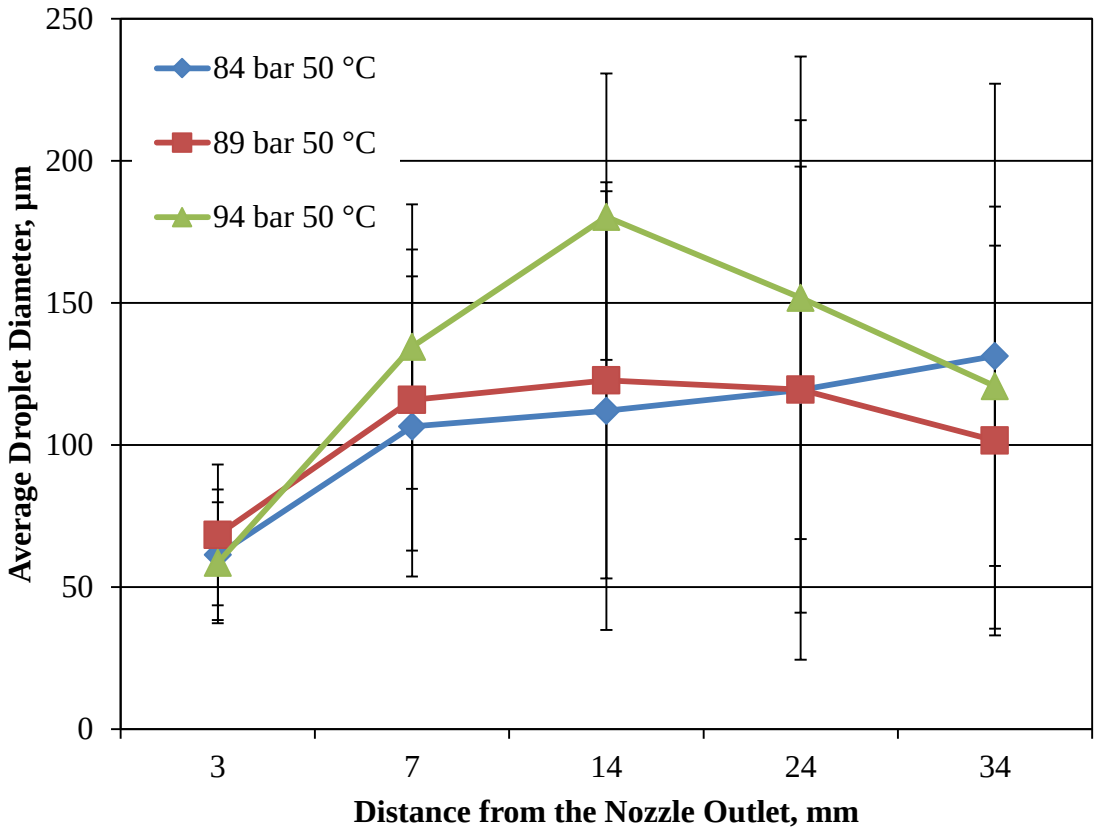

Figure 2.7 Average droplet diameter of 1 wt% PMMA in acetone solution sprayed into supercritical CO_2 at a constant temperature of 50 ºC

Bulk Supercritical CO_2				1 wt% PMMA in Acetone Solution		Visualizations
Density (g/cm^3)	Temperature (^oC)	Pressure (bar)	Viscosity (cP)	Flow Rate (cm^3/min)	Nozzle Velocity (m/s)	Distances from the Nozzle (mm)
Fixed Density						
0.32	40	84	0.025	1.6	0.8	0,3,7,14,24,34
0.32	45	89	0.025	1.6	0.8	0,3,7,14,24,34
0.32	50	94	0.025	1.6	0.8	0,3,7,14,24,34
Fixed Temperature						
0.24	50	84	0.021	1.6	0.8	0,3,7,14,24,34
0.28	50	89	0.023	1.6	0.8	0,3,7,14,24,34
0.32	50	94	0.025	1.6	0.8	0,3,7,14,24,34

Table 2.1 List of experimental conditions used to perform SAS as well as the distances from the nozzle imaged at each condition for 1 wt% PMMA in acetone

Density (g/cm^3)	Temp (ºC)	Pressure (bar)	Distance from Nozzle (mm)	Average Droplet Diameter (μm)	Standard Deviation (μm)	Droplets per Image	Number of Droplets Measured	Jet Break Up Length (μm)	Measured Jet Images	Standard Deviation of Jet Length (μm)
Fixed Density										
0.32	40	84	0					586.5	131	76.5
			3	67.8	24	2.9	756			
			7	119.4	56.3	-	153			
			14	155	75.8	-	123			
			24	91.3	61.9	-	341			
			34	71.3	48.1	-	155			
0.32	45	89	0					531.6	134	75.4
			3	68.8	22.5	-	203			
			7	122.3	54.5	-	218			
			14	170.5	78	-	207			
			24	139.9	82.5	-	265			
			34	111.6	36.5	N/A	N/A			
0.32	50	94	0					601.6	175	60.8
			3	58.6	21.3	-	146			
			7	134.6	50	-	157			
			14	173.8	59.3	-	246			
			24	151.8	84.9	-	166			
			34	120.7	63.2	-	263			
Fixed Temperature										
0.24	50	84	0					1061	249	86.9
			3	61.4	23	-	121			
			7	106.6	52.8	-	374			
			14	112.1	77.2	-	417			
			24	119.3	94.9	-	338			
			34	131.3	95.9	-	108			
0.28	50	89	0					807.2	228	102.6
			3	68.4	24.8	-	352			
			7	115.8	53	-	245			
			14	122.8	69.7	-	302			
			24	119.5	78.5	-	205			
			34	101.6	68.6	-	237			
0.32	50	94	0					601.6	60.8	175
			3	58.6	21.3	-	146			
			7	134.6	50	-	157			
			14	173.8	59.3	-	246			
			24	151.8	84.9	-	166			
			34	120.7	63.2	-	263			

Table 2.2 Analysis of 1 wt% PMMA in acetone processed via the SAS precipitation process

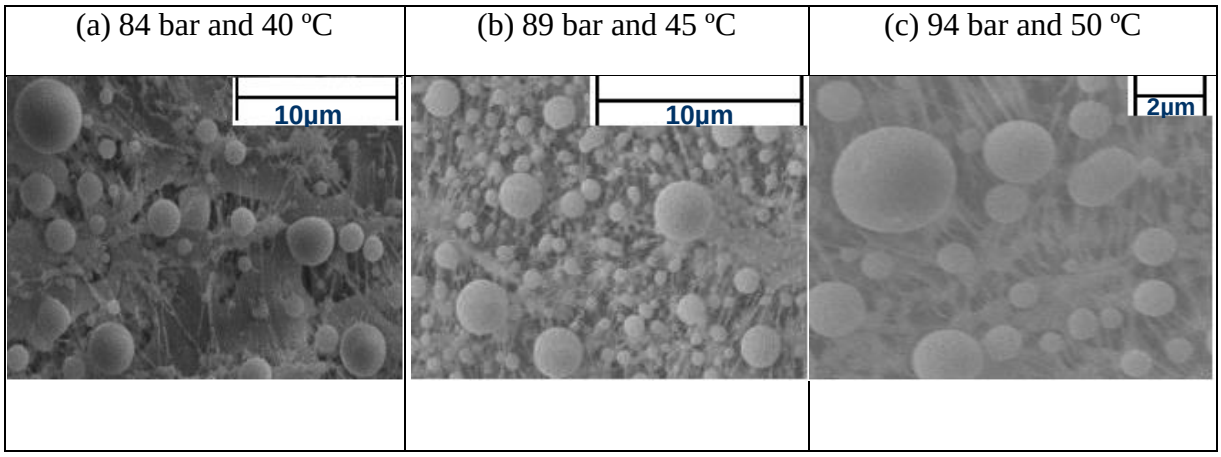

Figure 2.8 Scanning electron microscope images of PMMA particles produced by processing 1 wt% PMMA in acetone during the fixed density SAS experiments, bulk CO_2 density of 0.32 g/cm^3

(a) 84 bar and 0.24 g/cm^3	(b) 89 bar and 0.28 g/cm^3	(c) 94 bar and 0.32 g/cm^3
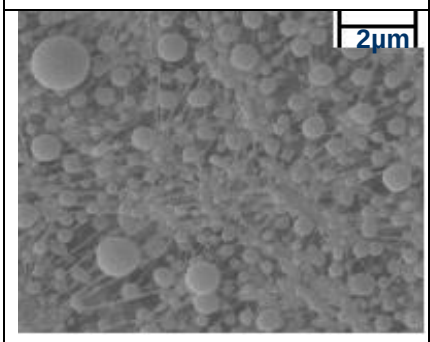	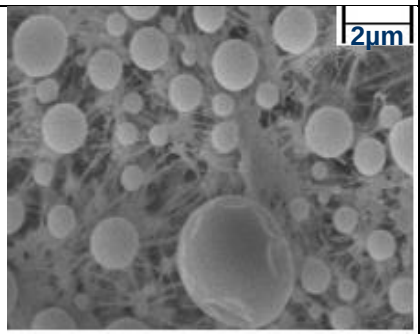	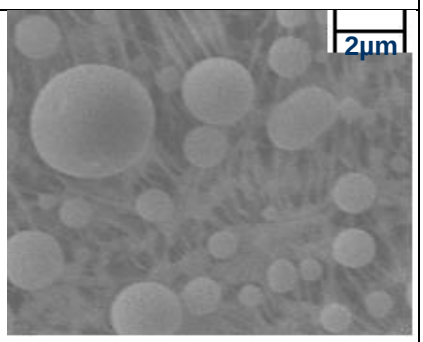

Figure 2.9 Scanning electron microscope images of PMMA particles produced by processing 1 wt% PMMA in acetone via the fixed temperature SAS experiments performed at 50 ºC

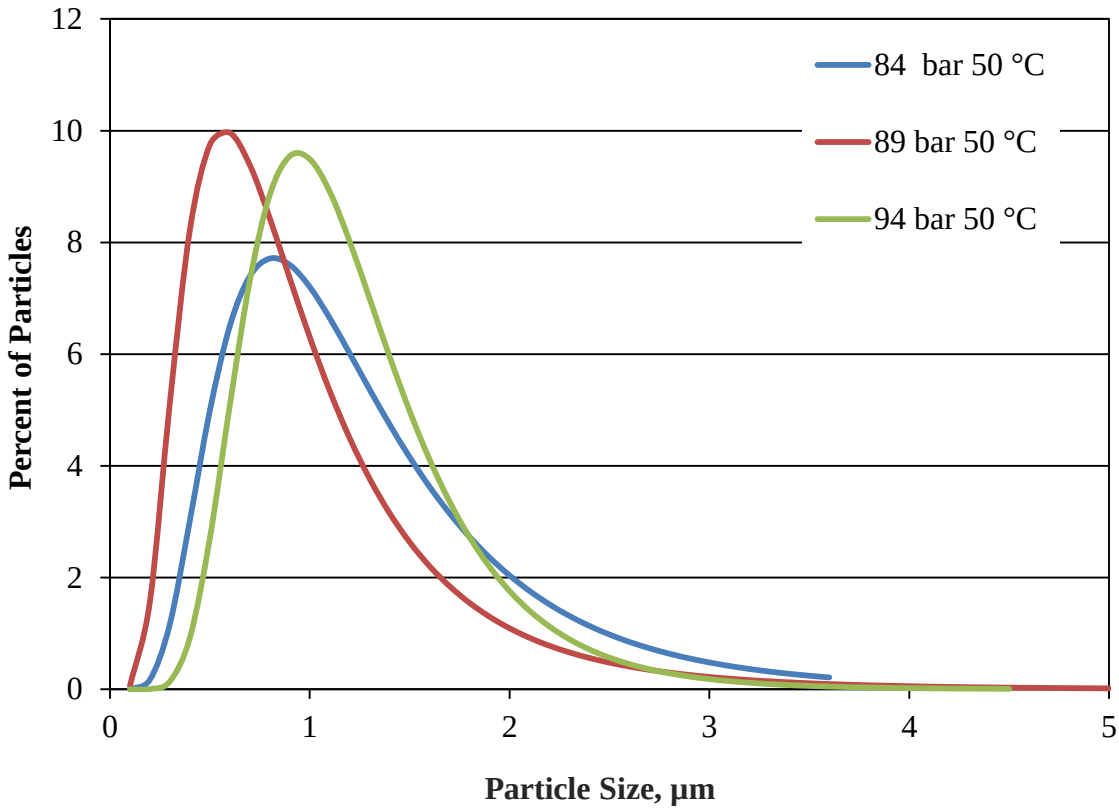

Figure 2.10 Size distribution of PMMA particles produced via the SAS precipitation process during the fixed temperature SAS experiments performed at 50 ºC

Chapter 3

Effects of pressure and temperature on precipitation of budesonide in ethanol during the supercritical antisolvent precipitation process

3.1 Introduction

Budesonide is an anti-inflammatory corticosteroid that exhibits potent glucocorticoid activity and weak mineralocorticoid activity. Budesonide is a white to off-white, tasteless, odorless powder that is practically insoluble in water. The field of drug delivery has attracted tremendous attention during the last three decades. The principle reason for this attention is the awareness that substantial improvement over current therapies will likely occur primarily through improved delivery of current and yet to be discovered drugs. Delivery system can address and correct problems related to the physical characteristics of drugs, including solubility and stability. A common method for the controlled release of drugs is the use of micro particles of carrier-drug composite (Langer 1998). Particular subset of drug delivery systems those that are based on synthetic polymers, appears particularly promising (Hubbell 1998). Many studies have been done to form the various sizes of polymer particles through the SAS precipitation process. This study attempts to understand the effect of process conditions on the spray characteristics and the micro particles of drug through the SAS precipitation process. The particles formation of method composite of polymer-drug will behave in between that of drug and polymer formation methods.

To perform the SAS precipitation process, a solution was sprayed into a supercritical antisolvent, typically CO_2. The solution exits a nozzle with different spray characteristics depending on the process conditions. The organic solvent and the antisolvent counter diffuse as the solution was sprayed into the precipitation chamber. The spray characteristics of a solute budesonide in a solvent ethanol sprayed into a vessel containing supercritical CO_2 were visualized and studied to understand the effect of process conditions on the spray characteristics and particle size. A high magnification imaging system was used to capture images through a viewing window on the sides of the supercritical CO_2 vessel. 1 wt % budesonide in ethanol solution was sprayed into supercritical CO_2 to form micro particle.

I was assisted by undergraduate research student fellow Andrew Klinger while carrying out experiments and the data collection of these studies.

3.2 Experimental

3.2.1 Materials

Experiments were conducted using a solution of the solute budesonide in ethanol, the solvent. Budesonide (99.9%) was obtained from Fisher Scientific. Budesonide has a molecular weight of 430.5 Daltons. Ethanol was obtained from Pharmco-Aaper (Brookfield, CT). Carbon dioxide of grade 5.5 was obtained from Airgas (Cinnaminson, NJ). All the materials were used as received.

3.2.2 Experimental setup and imaging system

The setup used to perform the SAS precipitation process is shown in Figure 3.1 was modified from the system used by Obrzut et al. 2007. The precipitation chamber used was a Jerguson gage, model 19TM40, with volume of 57 cm^3, height of 48 cm. The precipitation chamber has transparent windows in front and back, which facilitates the visualization of the spray. The solution was delivered at constant flow rate of 1.6 cm^3/min with a metering pump, the acuflow series II HPLC pump with pulse dampener, Scientific Systems, through a spray nozzle of 100 μm ID fused silica capillary tubing. An ISCO 500D syringe pump delivers the CO_2 to the precipitation chamber through the annular space between a capillary nozzle and a stainless steel sheath. The nozzle was made by cutting capillary tubing with a wire cutter and inspecting the ends with an optical microscope to achieve a flat tip. To safely operate the high pressure precipitation chamber, a pressure gage, McDaniel Controls, and a blowout plug, HIP 16-63AF1, were attached. A RTD in the precipitation chamber was used as the input device for the temperature controller, Omega CSC32. The temperature controller regulates a heating tape, Omegaflux SRT051-080, to maintain the temperature of precipitation chamber. One more thermocouple was installed at the center of precipitation chamber to measure the temperature along the depth of the precipitation vessel. The membrane filter, Millipore FLGP02500, separates the precipitated particles from the vessel effluent. The membrane filter has a pore diameter of 0.22 μm and is mounted in a 25 mm filter holder, Millipore XX4502500, at the bottom of the precipitation chamber.

SAS involves jet spraying of the solution into a compressed antisolvent. Imaging and visualization techniques were used previously to study the jet flows, atomization and droplets (Lengsfeld et al. 2000, Obrzut et al. 2007). A high resolution monochrome CCD camera, COHU 2122, was used to image the SAS precipitation process. The camera has a chip size of 768 x 494 pixels with the pixel size of 8.4 x 9.8 μm. The shutter speed is 60 fps. Attached to the camera is a Questar QM100 MKIII long distance microscopic lens. The lens working distance ranges from 8 to 35 cm allowing visualization inside the precipitation chamber. The camera and lens were mounted on a tripod which facilitates X-Y-Z direction movement. A stroboscope, Monarch Nova Strobe DA Plus 115 with the pulse duration of 30 μs, provides backlight illumination (Bell et al. 2005).

The output of the COHU camera was digitized by an analog to digital video converter, Pinnacle Studio Moviebox Ultimate. The video was collected on a computer in .mpg format using Pinnacle Studio 12 software. The frames of the video were separated into individual .bmp images using QuickTime media player. The images were then analyzed using image processing software, ImageJ. Jet break up length was the distance measured using the Straight Line tool, in ImageJ, from the edge of the capillary tubing to the point where the jet edge exhibits rippling. The same tool was used to measure the droplet diameters. Only droplets that were completely in focus were measured. To find pixel/μm, in-situ images of the 400 μm outer diameter nozzle with the same magnification as the droplet images were obtained and the known distances measured for pixel length.

The precipitated particles were analyzed using a scanning electron microscope (SEM), Zeiss EVO 500. Samples for the scanning electron microscope were prepared by transferring particles from the filter holder to a stub with double-sided carbon tape on the surface. The stub was sputter-coated for 2 minutes with gold. Images of the particles were obtained in .tif format. The particles were analyzed using ImageJ by measuring the diameter using the straight line tool.

3.2.3 Experimental procedure

To perform these experiments, the apparatus shown in Figure 3.1 was operated in batch mode. The precipitation chamber was initially filled with CO_2 using syringe pump, which was set to maintain the operating pressure in the precipitation chamber. The precipitation chamber was heated by using temperature controlled heating tape. The system was run until the temperature and pressure reached equilibrium. 1 wt% budesonide in ethanol solution was pumped by the HPLC pump into the Jerguson guage with downstream valve closed. The solution was sprayed at a fixed flow rate of 1.6 cm^3/min for 30 to 45 sec. The valve on the syringe pump was opened to resume the pressure control by the Isco syringe pump. Then, the two valves, downstream of precipitation chamber, were adjusted to control the chamber outflow. Usually outflow rate is adjusted to 5-7 cm^3/min, which can be monitored through the change in the volume of the Isco syringe pump. Four chamber volumes of CO_2 were purged through the precipitation chamber. Once the chamber reached atmospheric pressure, the filter holder was removed to collect the dried budesonide particles on the membrane filter.

The visualization of the spray was done while spraying the solution in the precipitation chamber. The camera was positioned at the desired vertical distance from the tip of the nozzle.

Images were typically obtained with the center of the spray in frame. In the case of visualization at 0 mm from the tip of nozzle (jet breakup visualization), the camera was rotated by 90º to take the greater advantage of the aspect ratio.

3.2.4 Experimental conditions

The SAS precipitation experiments were conducted with 1 wt% budesonide in ethanol solution sprayed into supercritical CO_2, at 1.6 cm^3/min for 30 to 45 seconds. Experimental conditions are listed in Table 3.1, grouped as three fixed density conditions and three fixed temperature conditions. The operating conditions were chosen to allow for characterization of the spray near the transition from two phases to one phase jet break up.

Experiments with a fixed initial CO_2 density of 0.32 g/cm^3 were performed at pressure and temperature combinations of 84 bar and 40 ºC, 89 bar and 45 ºC, and 94 bar and 50 ºC. Fixed temperature experiments at 50 ºC were performed at three pressure and density combinations: 84 bar and 0.24 g/cm^3, 89 bar and 0.28 g/cm^3, and 94 bar and 0.32 g/cm^3. The pressure values were selected to correspond to those of the fixed density experiments. The phase diagram for the binary mixture of CO_2-ethanol indicates that after spraying the solution into carbon dioxide a supercritical mixture will be present at these conditions.

3.3 Results

Videos were captured through a viewing window in the precipitation chamber. Visualization was done, for all the experimental conditions, at 0, 3 and 14 mm from the tip of the nozzle. The 0 mm distance was used to measure the jet breakup. The 3 and 14 mm distance

visualizations were used to measure the size of the droplet diameters and creation of droplets of the sprayed solution. The droplet diameters and jet break up length were measured from the still frame images. Table 3.2 shows a summary of the data collected in the analysis from each experimental condition at constant temperature. Figure 3.5 and Figure 3.6 show the jet break up lengths plots for experiments performed at fixed density and fixed temperature conditions, respectively. The droplet distributions for each process condition at 14 mm can be seen in Figure 3.7, Figure 3.8 and Figure 3.9. The droplet distributions were plotted in order to find any correlation between the droplet diameter and particle diameter.

3.3.1 Fixed temperature experiments

Figure 3.3 shows images of 1 wt% Budesonide in ethanol sprayed in CO_2 at fixed temperature at 50 ºC. The columns (a), (b) and (c) represent the images of 1 wt% budesonide sprayed in CO_2 at 84 bar and 0.24g/cm^3, 89 bar and 0.28g/cm^3, 94 bar and 0.32g/cm^3, respectively. In all these conditions, the spray is clearly in the atomization regime as evidenced by the coherent jet and the presence of distinct droplets. But, the numbers of droplets seen in column (c) are fewer. This shows the transition regime for a gas like plume. Visualizations taken at 3 mm from the nozzle outlet show a section of the spray with the jet unbroken and droplets present.

For 1 wt% budesonide in ethanol at 84 bar and 50 ºC, the average jet break up length was determined to be 871 μm with a standard deviation of 67 μm. The average droplet diameter at 3 mm from the nozzle for 84 bar and 50 ºC was determined to be 88 μm with a standard deviation of 39 μm. The average droplet diameter at 14 mm was determined to be 140 μm with a standard

deviation of 89 μm. This shows that from 3 to 14 mm from the nozzle the droplets grew in size. The high standard deviations appear to come from the large variations in the sizes of the droplets, as shown in Figures 3.7, 3.8 and 3.9, the droplet distribution at 14 mm covered a very broad range. This variation in droplet diameter was seen for all the three process conditions and at the different distances from the nozzle.

For 1 wt% budesonide in ethanol at 89 bar and 50 ºC, the average jet break up length was determined to be 549 μm with a standard deviation of 42 μm. The average droplet diameter at 3 mm was determined to be 72 μm with a standard deviation of 36 μm, and the average droplet diameter at 14 mm was determined to be 127 μm with a standard deviation of 80 μm. A distribution of the droplet diameters at 14 mm for 89 bar and 50 ºC was narrower than the distribution at 84 bar.

For 1 wt% budesonide in ethanol at 94 bar and 50 ºC, the average jet break up length for the solution sprayed at 1.6 cm^3/min at 94 bar was 508 μm with a standard deviation of 53 μm. The average droplet diameter at 3 mm was determined to be 28 μm with a standard deviation of 12 μm, and the average droplet diameter for 14 mm was determined to be 87 μm with a standard deviation of 57 μm. The droplet diameter distribution for 14 mm at 94 bar, 50 ºC was much narrower than the distributions at 84, 50 ºC and 89 bar, 50 ºC.

3.3.2 Fixed density experiments

Figure 3.4 shows images of 1 wt % budesonide in ethanol sprayed in CO_2 at fixed density of 0.32 g/cm^3. The columns (a), (b) and (c) represent the images of 1 wt% budesonide in ethanol sprayed in CO_2 at 84 bar and 40 ºC, 89 bar and 45 ºC, and 94 bar and 50 ºC, respectively. In all

these conditions, the spray was clearly in the atomization regime as evidenced by the coherent jet and the presence of distinct droplets. Visualizations taken at 3 mm from the nozzle outlet show a section of the spray with the jet unbroken and droplets present. The average jet break up lengths for these three conditions is 456 ± 62 μm, 589 ± 31 μm and 508 ± 53 μm, respectively. For column (a), the average droplet diameter increases from 71 μm at 3 mm to 163 μm at 14 mm. For column (b), the average droplet diameter increases from 92 μm at 3 mm to 149 μm at 14 mm. For column (c), the average droplet diameter increases from 28 μm at 3 mm to 87 μm at 14 mm.

3.4 Discussion

Figure 3.5 shows that the jet breakup length decreases as pressure was increased at the fixed temperature. This trend has also been noted in other studies such as Obrzut (2008) which used different solvents and solutes in the sprayed solution. The main reason for the decrease in the jet break up length may be attributed to a decrease in surface tension of sprayed solution due to the increased pressure of the supercritical CO_2 (Sullivan et al. 2009). For all the experimental conditions droplet formation was seen, the droplets occur due to the lack of coherence in the jet.

The analysis of droplet for the fixed temperature experiments, in Figure 3.10, shows that the droplet diameters increased in size from 3 to 14 mm distances from the nozzle. The increase in droplet size from the distances of 3 to 14 mm could be caused by the infusion of CO_2 into the droplet (Werling et al. 1999, Mukhopadhyay et al. 2004). Solvent is transferred out of the droplet, but the rate of solvent transfer leaving the droplet is much lesser than the rate of

supercritical CO_2 transfers into the droplet. This causes the droplet to swell. The droplets also decreased in size as the supercritical fluid pressure increased keeping the temperature constant. This trend is most likely attributed to the solutions surface tension interactions with the supercritical CO_2 similar to that of the jet break up length.

For all three operating conditions, spherical, micron-sized, budesonide particles were found. The particles morphology was typically characterized as solid spheres as shown in Figure 3.12 and Figure 3.13. Unrefined budesonide was in crystallize, rod structure as seen in Figure 3.14. In fixed temperature experiments, the average particle size for 84 bar and 0.24 g/cm^3 was 1.36 ± 0.83 µm, for 89 bar and 0.28 g/cm^3 was 1.29 ± 0.73 µm, for 94 bar and 0.32 g/cm^3 was 1.13 ± 0.77 µm. In the fixed density experiments, the average particle size for 84 bar and 40 ºC was 0.87 ± 0.68 µm, for 89 bar and 45 ºC was 0.79 ± 0.62 µm, for 94 bar and 50 ºC was 1.13 ± 0.77 µm.

Comparison of the droplet sizes and distributions to that of the particle sizes and distributions shows that, there was no apparent relation between the droplet size and particle size. The only similarity between the droplets and particles reside in the spherical morphology that both exhibit and the narrowed distributions at higher pressures. Despite different spray characteristics at different operating conditions, the particle size and particle size distribution of budesonide was similar. The particle size distribution for the fixed temperature experiments is shown in Figure 3.15.

3.5 Conclusion

This study demonstrates that spherical micro particles of budesonide can be created via the SAS precipitation process. The high magnification visualization system was used to study the spray characteristics of the SAS precipitation process. In fixed temperature experiments, an increase in pressure and density causes a decrease in jet break up length. In fixed density experiments, jet break up length was similar. Atomization of 1 wt% budesonide in ethanol was observed in all the experimental conditions. Despite different spray characteristics at different operating conditions, the particle size and particle size distribution of budesonide was similar. This suggests that the spray characteristics are not the primary phenomena influencing the particle characteristics in the SAS precipitation process.

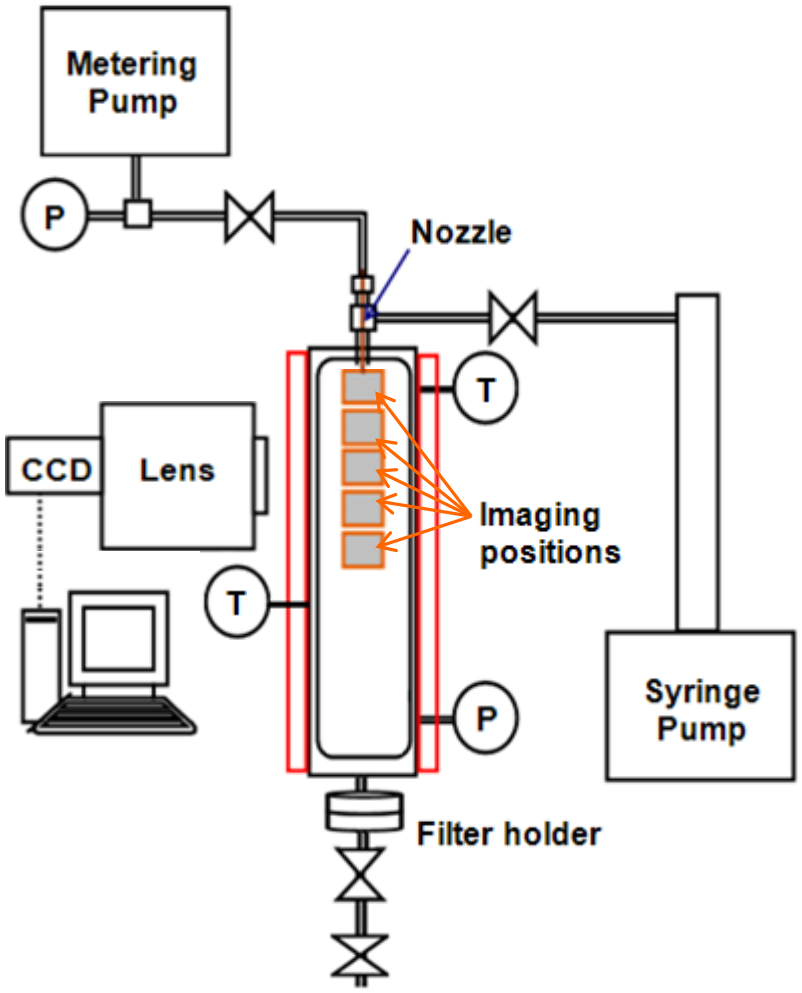

Figure 3.1 Diagram of the imaging system and the apparatus used to perform the supercritical antisolvent precipitation process. The imaging positions in the spray are represented by the shaded boxes inside the precipitation vessel

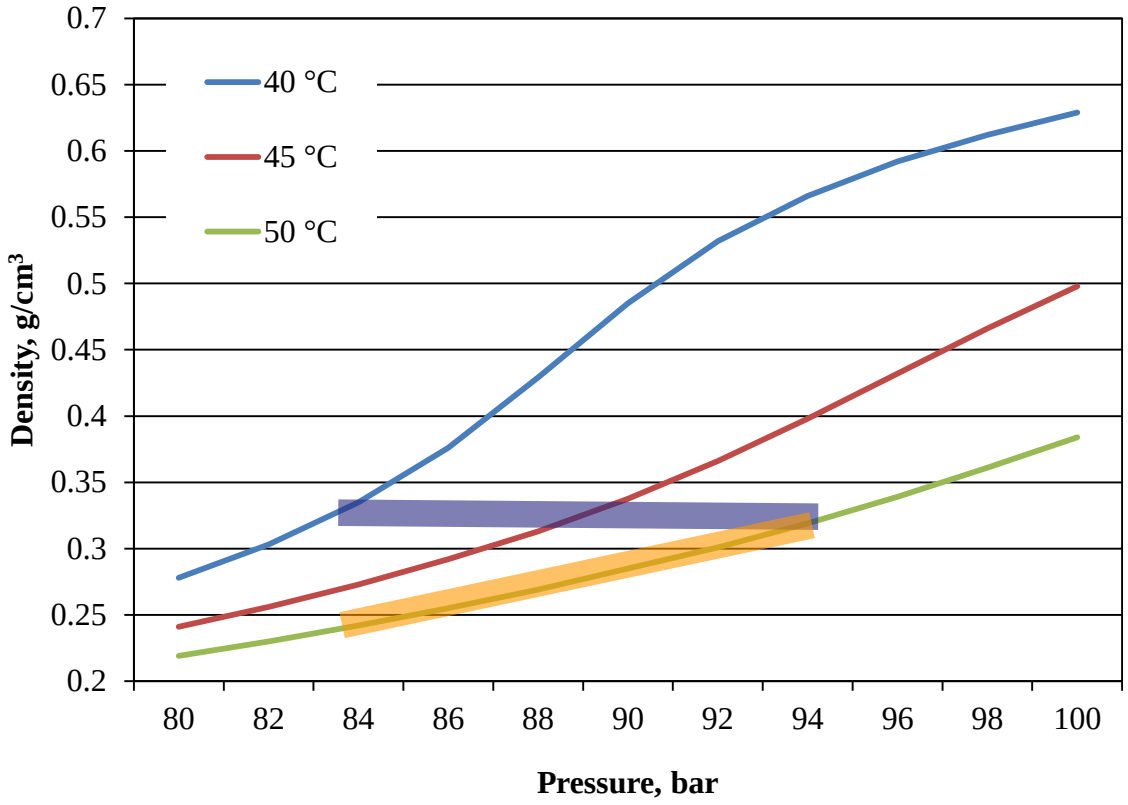

Figure 3.2 Experimental conditions displayed on carbon dioxide density vs pressure diagram. The symbols represent two sets of experimental conditions: fixed density and fixed temperature. The lines represent isotherms of pure CO_2 at the operating temperatures calculated from the NIST chemistry webbook

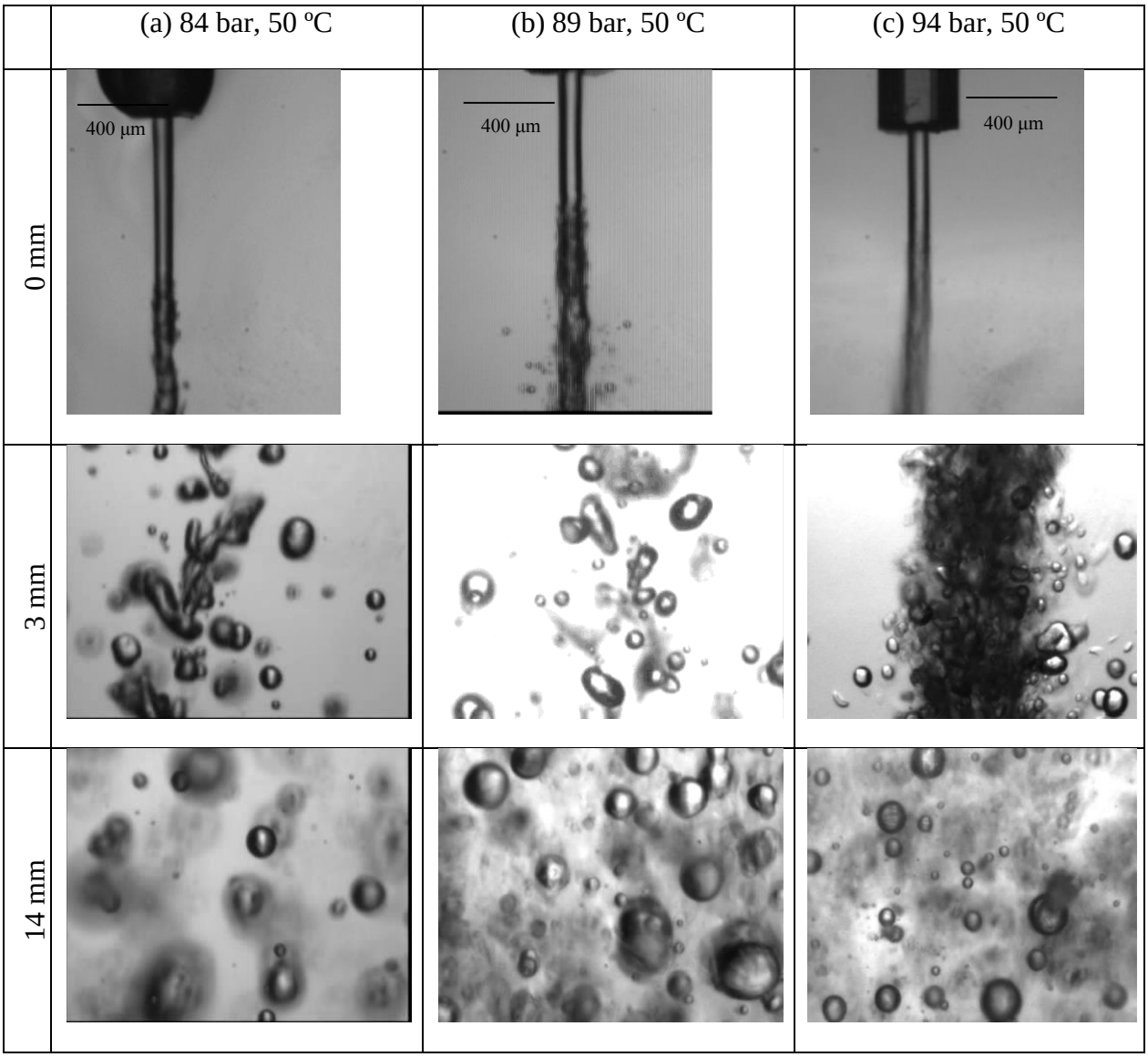

Figure 3.3 Selected frames taken from movies of 1 wt% budesonide in ethanol in the fixed temperature SAS experiments

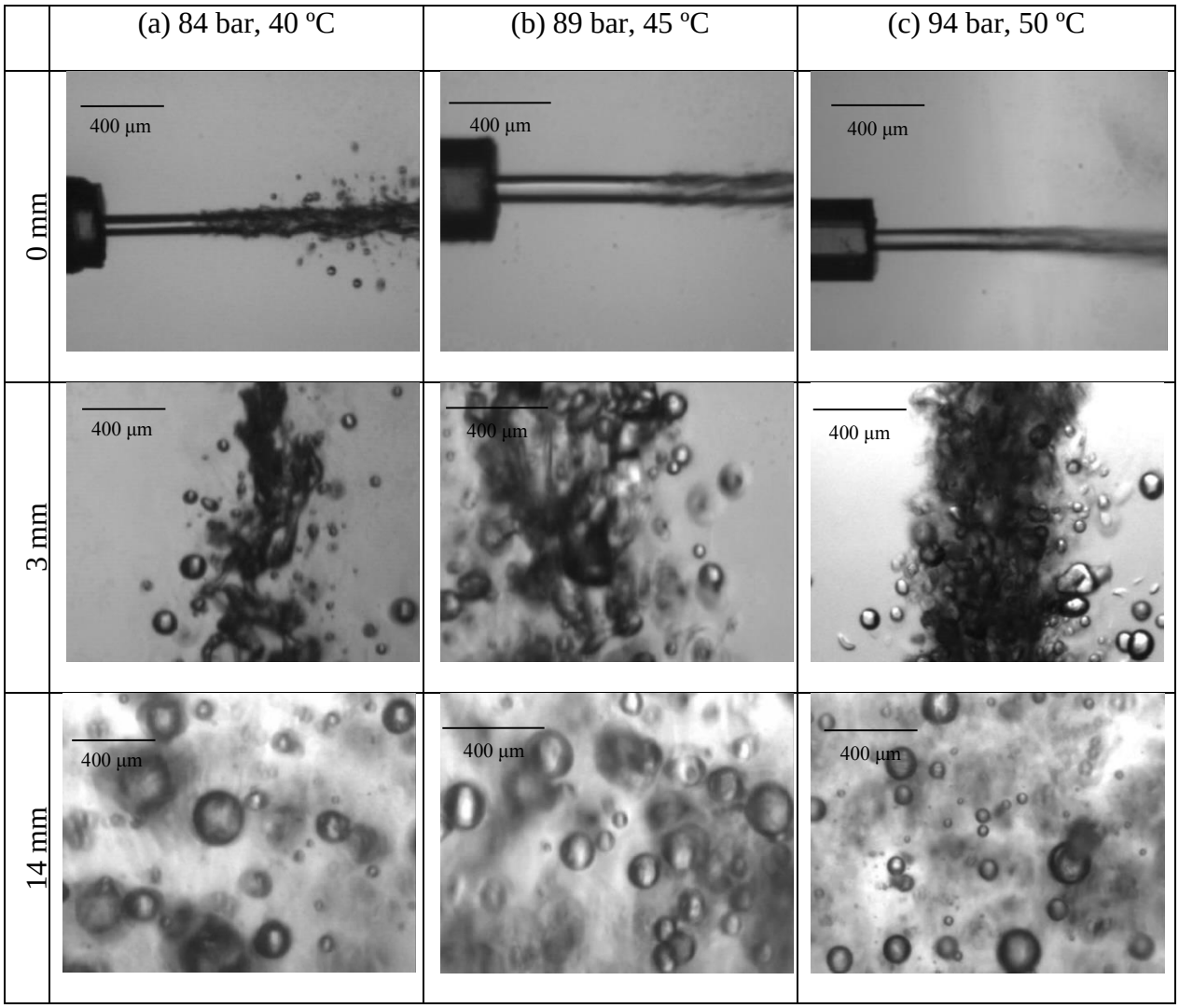

Figure 3.4 Selected frames taken from movies of 1 wt% budesonide in ethanol spray at given distances from the nozzle in the fixed density SAS experiments, bulk CO2 density of 0.32 g/cm^3

Bulk Supercritical CO_2				1 wt% Budesonide in Ethanol Solution		Visualizations
Density (g/cm^3)	Temperature (^oC)	Pressure (bar)	Viscosity (cP)	Flow Rate (cm^3/min)	Nozzle Velocity (m/s)	Distances from the Nozzle (mm)
Fixed Density						
0.32	40	84	0.025	1.6	0.8	0,3,14
0.32	45	89	0.025	1.6	0.8	0,3,14
0.32	50	94	0.025	1.6	0.8	0,3,14
Fixed Temperature						
0.24	50	84	0.021	1.6	0.8	0,3,14
0.28	50	89	0.023	1.6	0.8	0,3,14
0.32	50	94	0.025	1.6	0.8	0,3,14

Table 3.1 List of experimental conditions used to perform SAS as well as the distances from the nozzle imaged at each condition for 1 wt% budesonide in ethanol solution

Density (g/cm^3)	Temp (^oC)	Pressure (bar)	Distance from Nozzle (mm)	Average Droplet Diameter (μm)	Standard Deviation (μm)	Number of Droplets Measured	Jet Break Up Length (μm)	Measured Jet Images	Standard Deviation of Jet Length (μm)
Fixed Density									
0.32	40	84	0				456	200	62
			3	71	30	558			
			14	163	95	245			
0.32	45	89	0				589	183	31
			3	92	35	603			
			14	149	71	235			
0.32	50	94	0				508	84	53
			3	28	12	160			
			14	87	57	967			
Fixed Temperature									
0.24	50	84	0				871	195	67
			3	88	39	698			
			14	140	89	348			
0.28	50	89	0				549	200	42
			3	72	36	615			
			14	127	80	445			
0.32	50	94	0				508	84	53
			3	28	12	160			
			14	87	57	967			

Table 3.2 Analysis of 1 wt% budesonide in ethanol processed via the SAS precipitation process

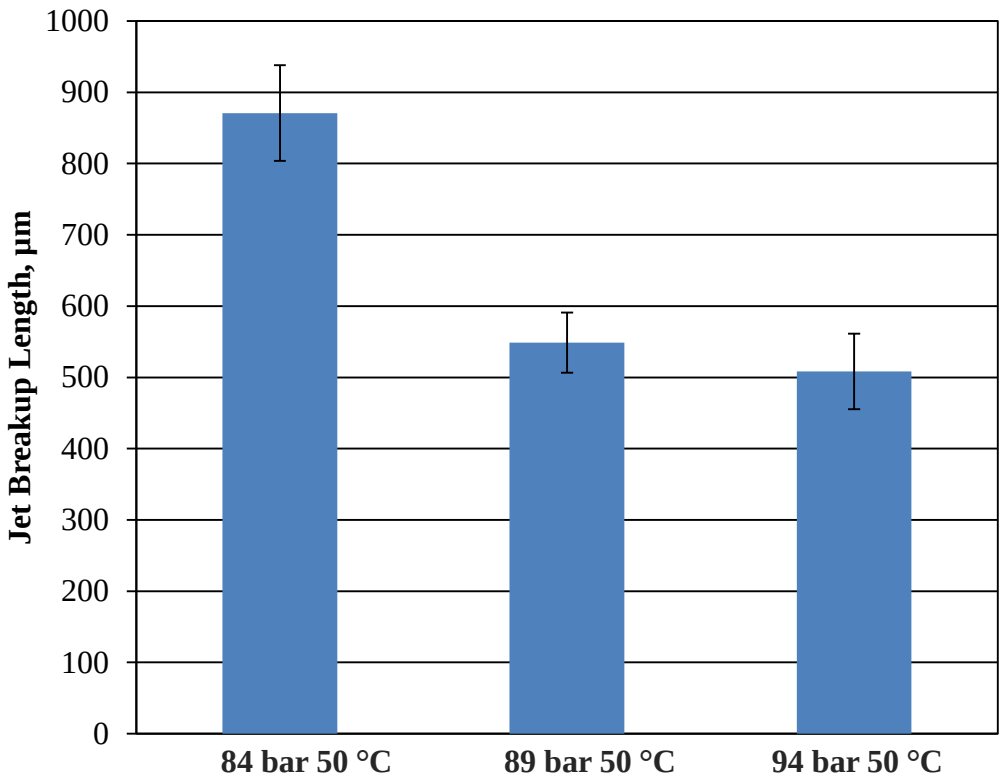

Figure 3.5 Jet breakup length for 1 wt% budesonide in ethanol solution sprayed through a capillary nozzle of 100 µm at a constant temperature of 50 ºC

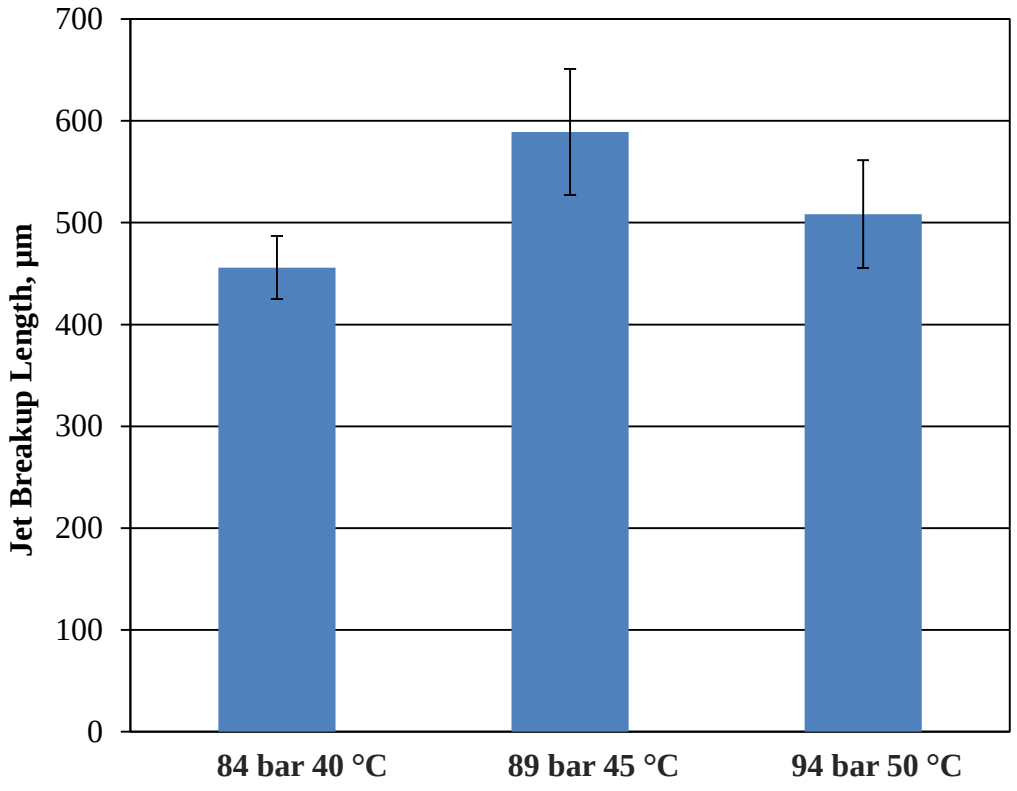

Figure 3.6 Jet breakup length for 1 wt% budesonide in ethanol solution sprayed through a capillary nozzle of 100 µm at a constant density of 0.32 g/cm^3

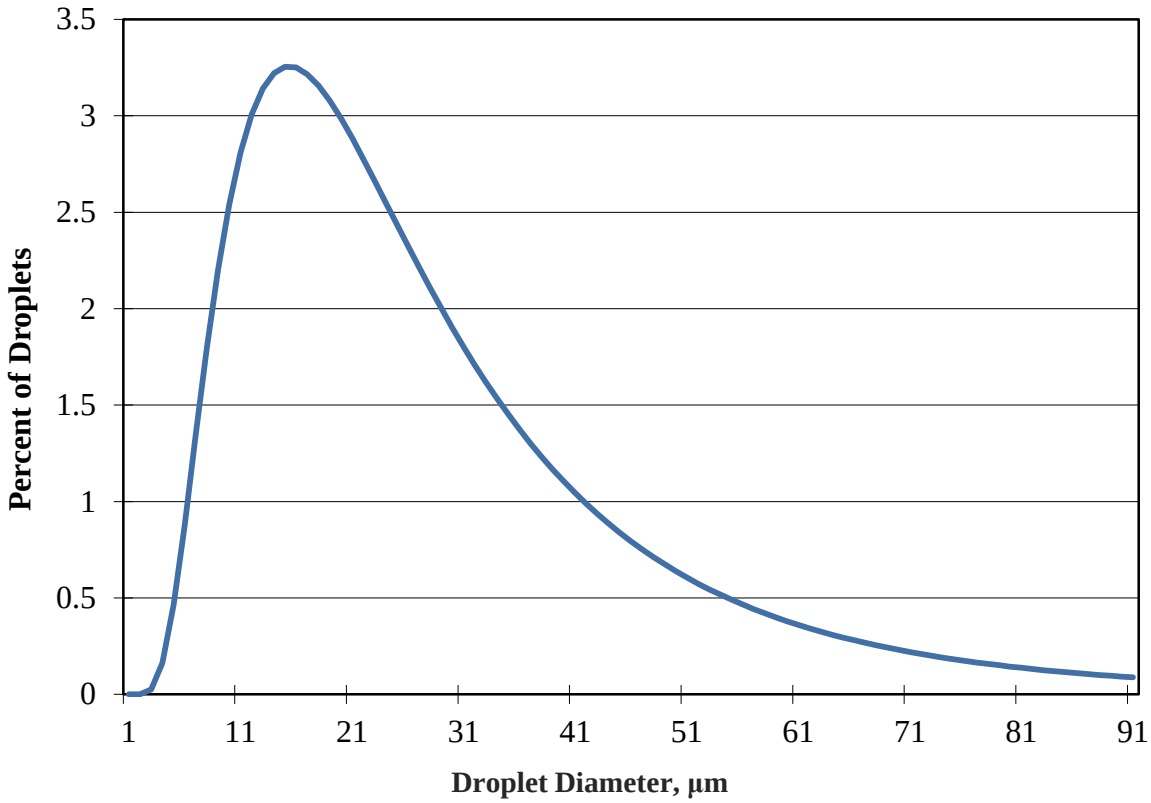

Figure 3.7 The droplet distrubtion for 1 wt% budesonide in ethanol solution at 14 mm from the nozzle in the SAS precipitation process at 84 bar and 50 ºC

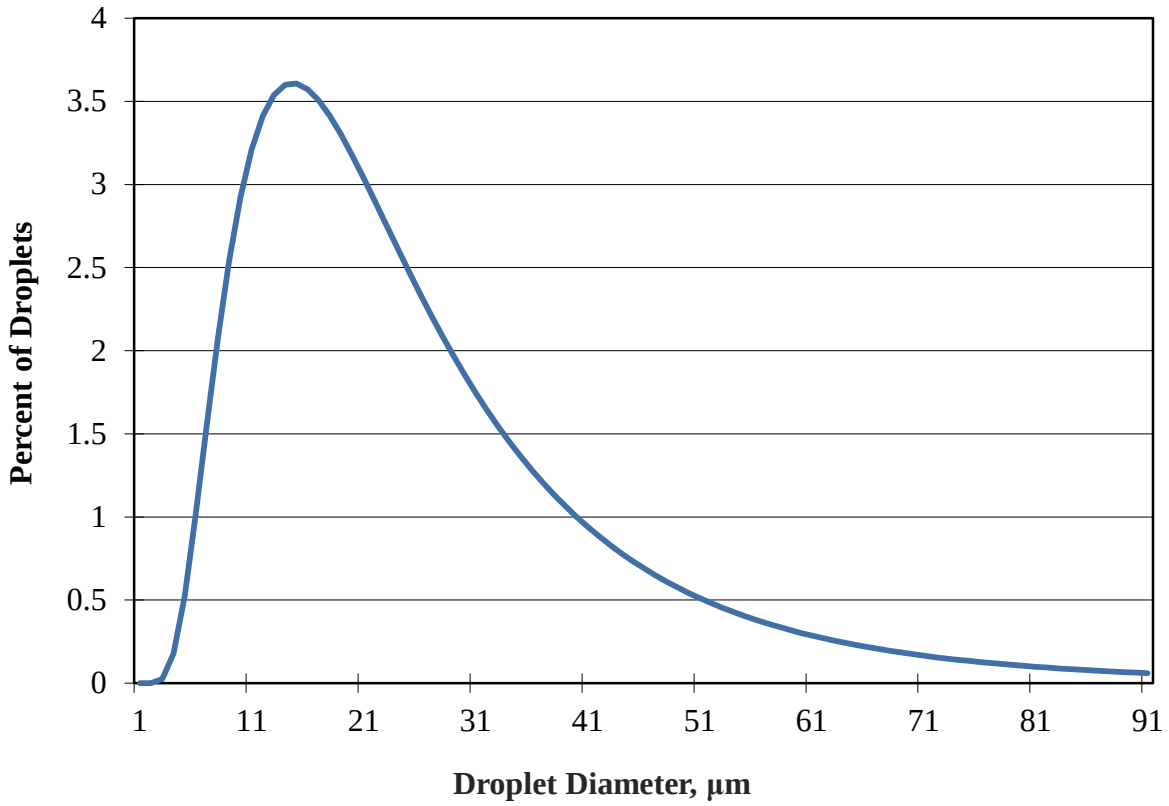

Figure 3.8 The droplet distrubtion for 1 wt% budesonide in ethanol solution at 14 mm from the nozzle in the SAS precipitation process at 89 bar and 50 ºC

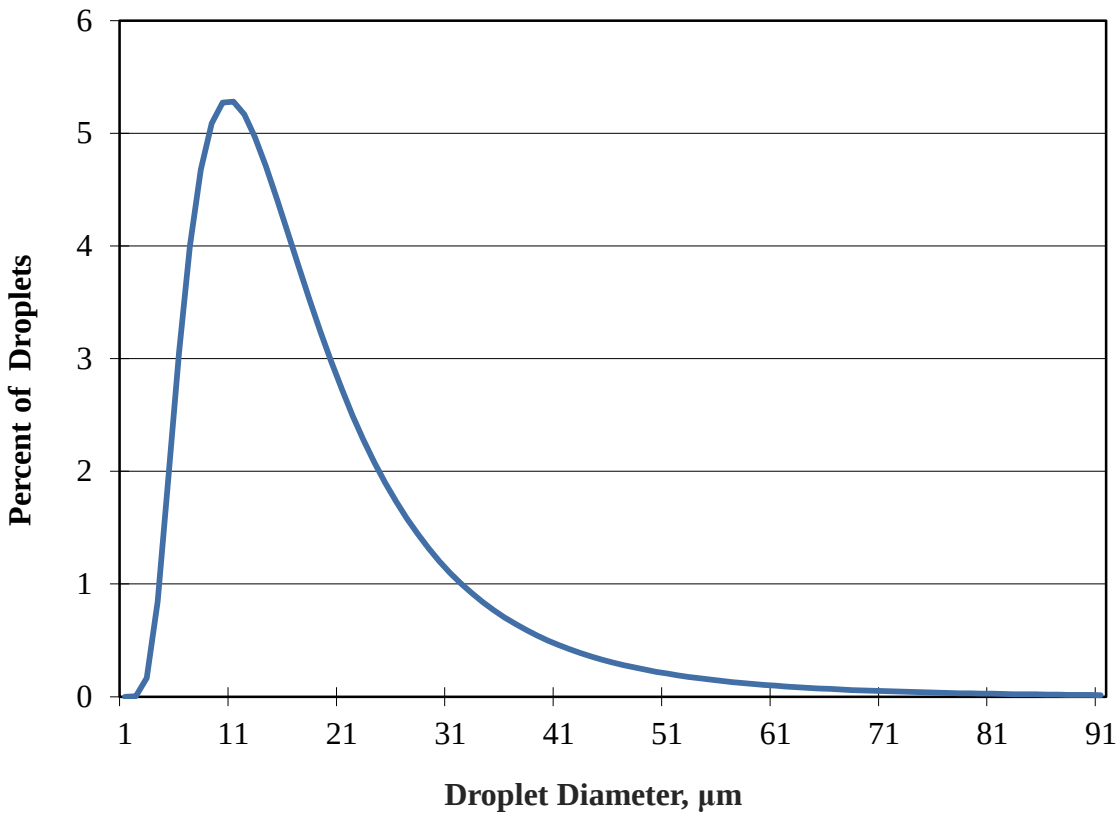

Figure 3.9 The droplet distrubtion for 1 wt% budesonide in ethanol solutin at 14 mm from the nozzle in the SAS precipitation process at 94 bar and 50 ºC

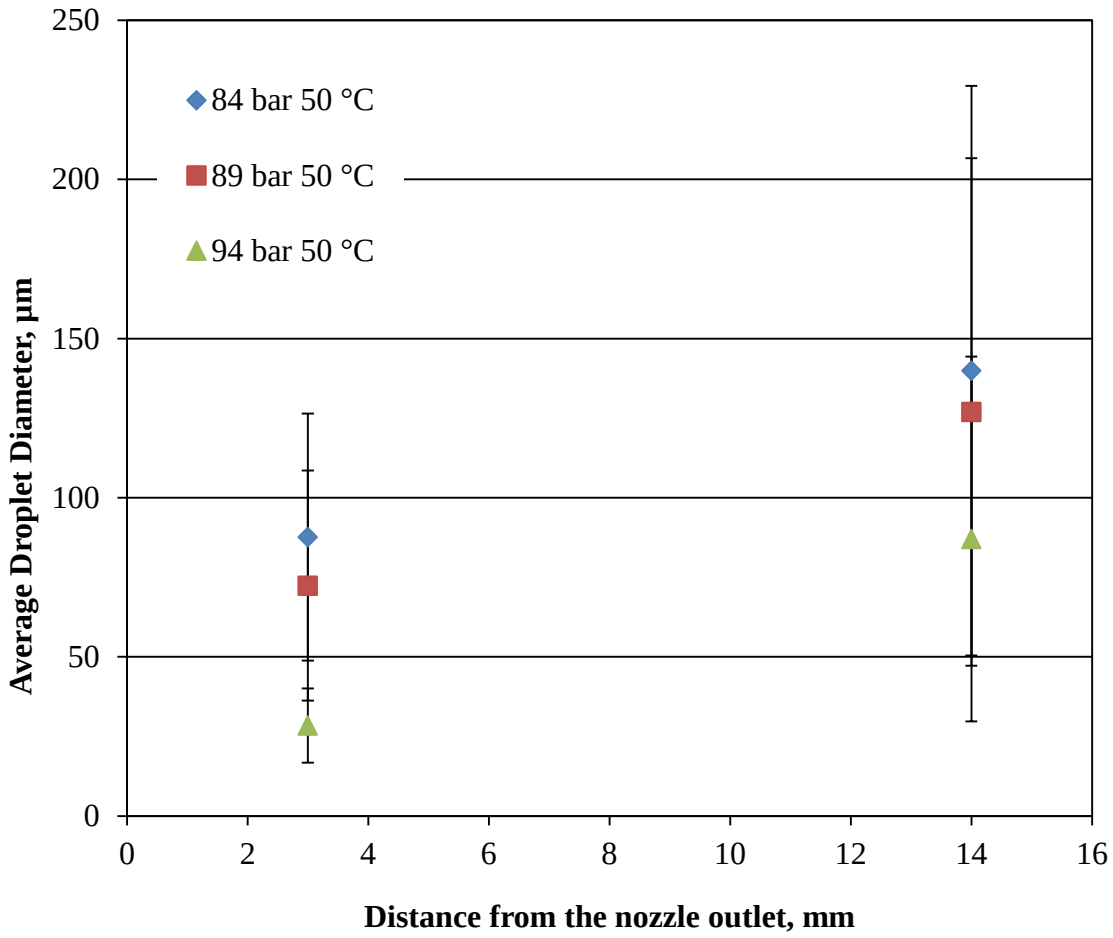

Figure 3.10 The average droplet diameter of 1 wt% budesonide in ethanol solution sprayed into supercritical CO_2 at a constant temperature of 50 ºC

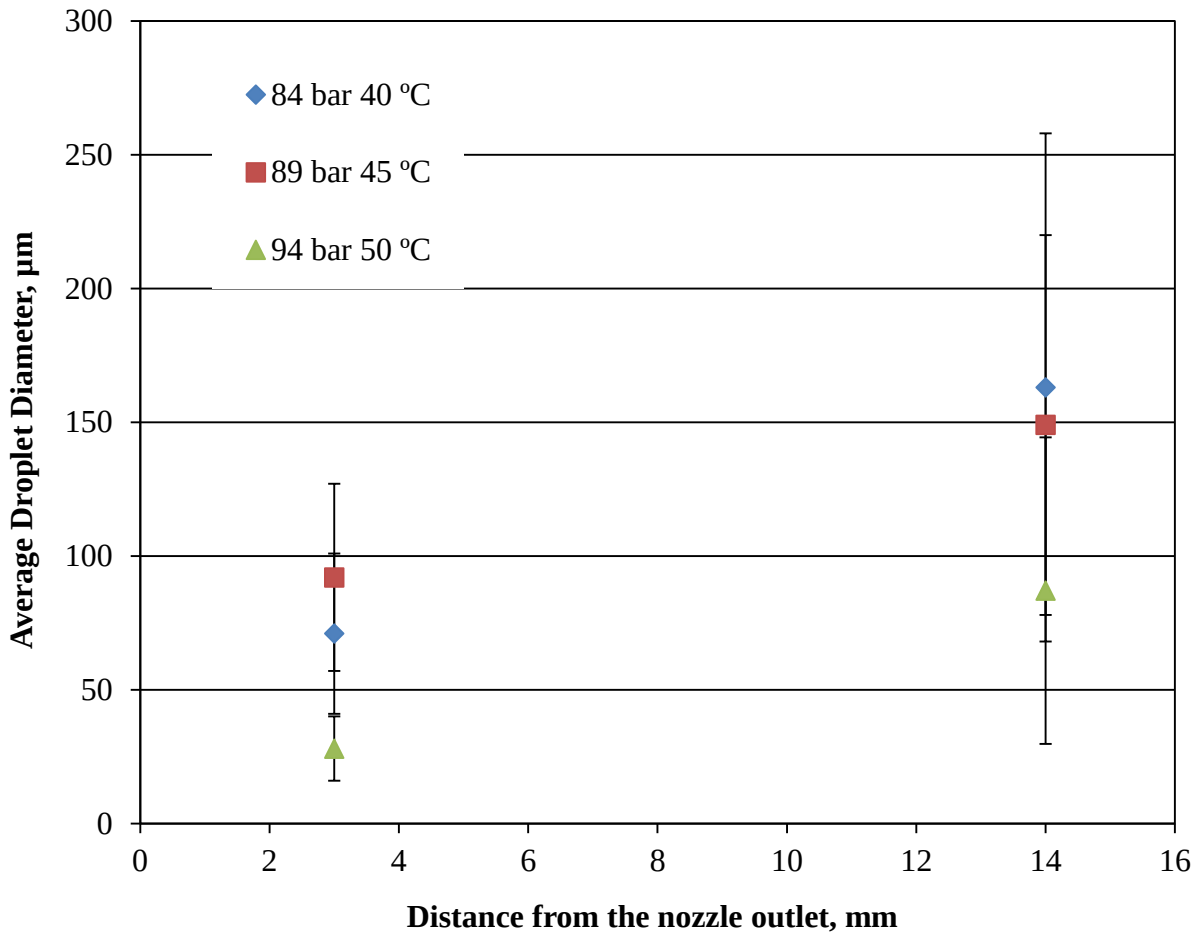

Figure 3.11 The average droplet diameter of 1 wt% budesonide in ethanol solution sprayed into supercritical CO_2 at a constant density of 0.32 g/cm^3

84 bar 50 ºC	89 bar 50 ºC	94 bar 50 ºC
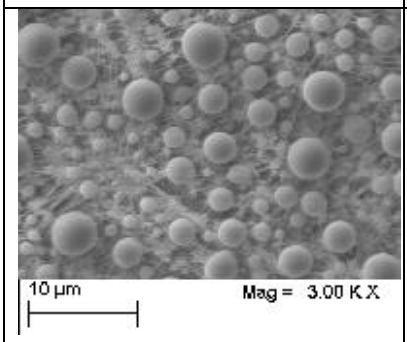	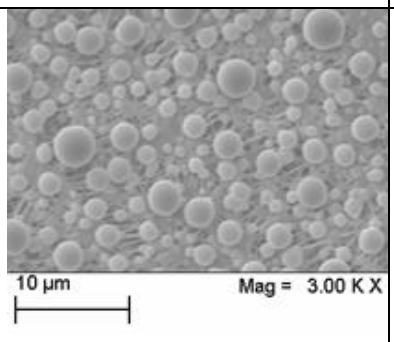	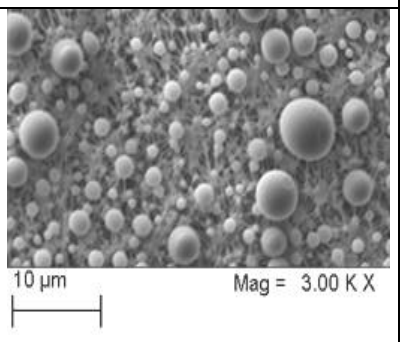

Figure 3.12 Scanning electron microscope images of 1 wt% budesonide in ethanol particles produced via SAS experiments at a constant temperature of 50 ºC

84 bar 40 ºC	89 bar 45 ºC	94 bar 50 ºC
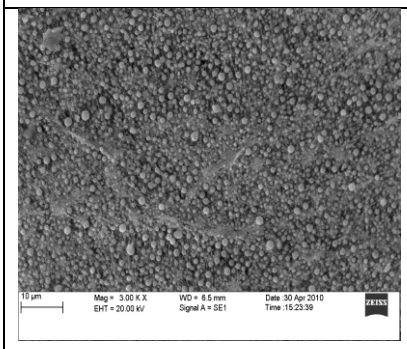	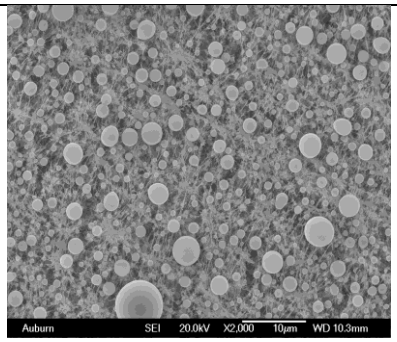	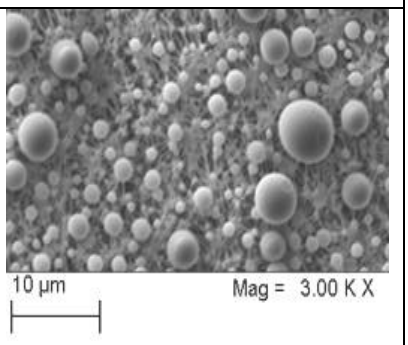

Figure 3.13 Scanning electron microscope images of 1 wt% budesonide in ethanol particles produced via SAS experiments at a constant density of 0.32 g/cm^3

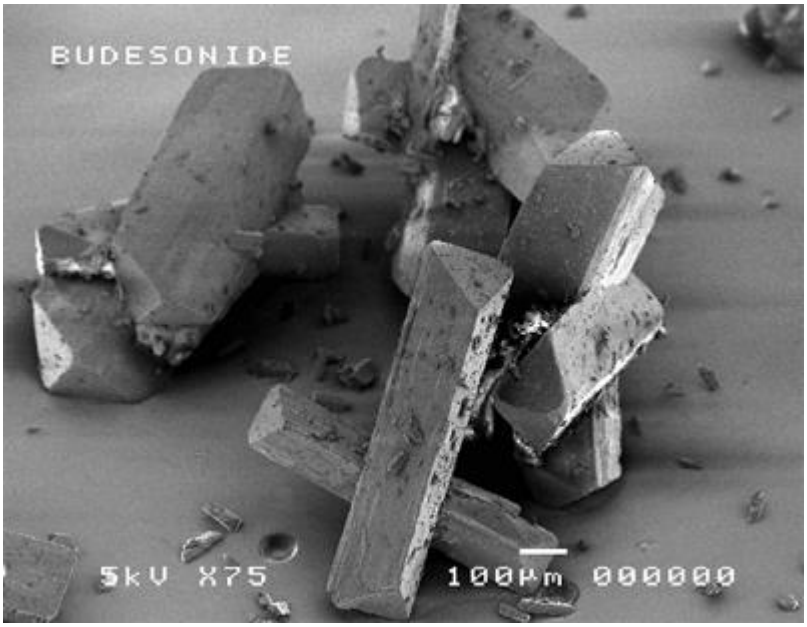

Figure 3.14 SEM image of unrefined budesonide (Source: AstraZeneca, 2008)

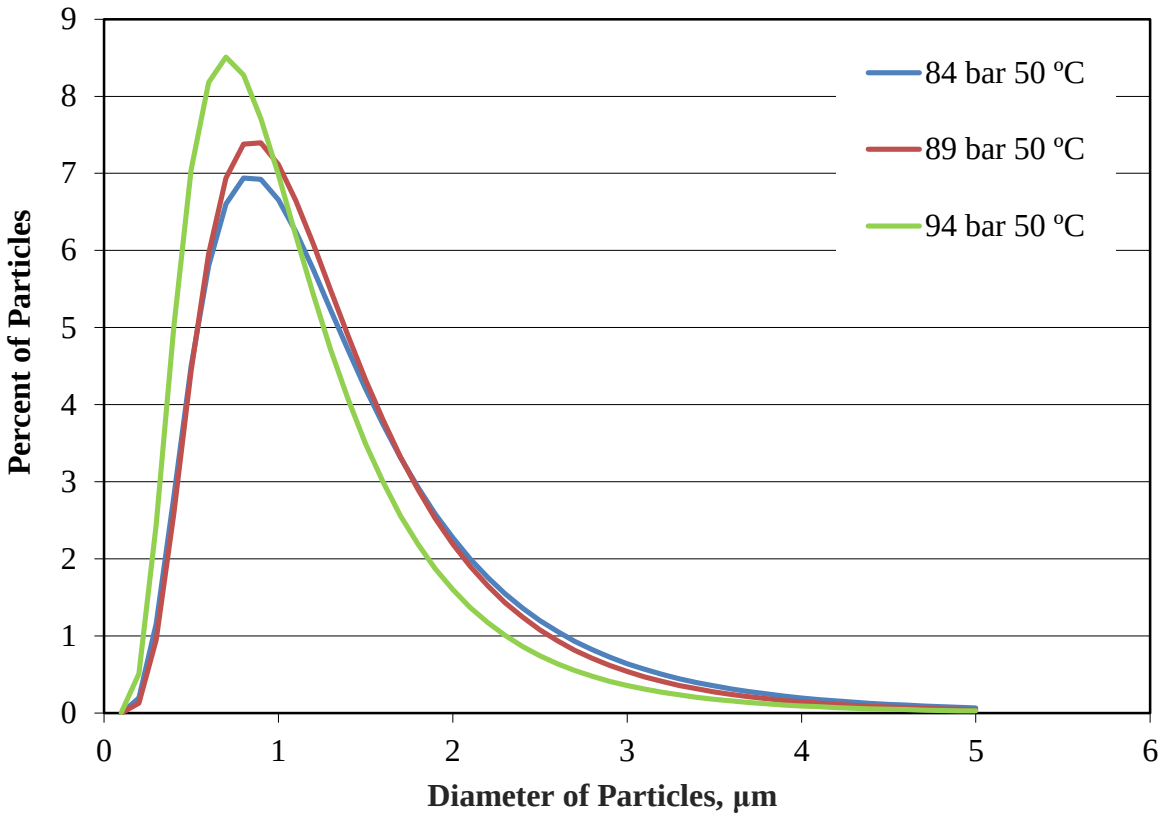

Figure 3.15 Size distribution of budesonide particles produced via the SAS precipitation process during the fixed temperature experiments performed at 50 ºC

Chapter 4

Effect of process conditions on the spray characteristics and particle size of PMMA+budesonide in acetone via the SAS precipitation process

4.1 Introduction

This study uses the supercritical antisolvent (SAS) precipitation process to create micro particles of PMMA+budesonide particles at various operating conditions. 1 wt% PMMA+budesonide (90+10) in acetone solution is processed via the SAS precipitation process using carbon dioxide as an antisolvent. This study is specifically tailored to simulate biodegradable polymers used in pulmonary drug delivery. An anti-inflammatory corticosteroid, budesonide, used in the treatment of lung conditions such as asthma, is co-precipitated with a polymer carrier, PMMA, using the SAS precipitation process. In order for an inhaler to deliver the drug particles to the lungs most effectively, the particles must have an average particle size in the 1-5 micron range. If the particles are too big or too small, they will not be deposited in the lungs (Finlay et al. 2008). The shape of the particles also plays a factor in ideal drug delivery to the alveolar region of the deep lung (O'Donnell et al. 2011).

The goal of this research is to be able to design drug-polymer particles of specific size, morphology, and drug loading by controlling underlying mechanisms of the SAS precipitation process. A specific objective of this study was to form PMMA+budesonide particles with the SAS precipitation process at various conditions and to design and develop a method for determining the composition of these polymer-drug particles.

Another objective of this study was to visualize the SAS precipitation process at varying conditions using a high magnification, high-resolution camera. Using the video captured as well as scanning electron micrographs of the particles collected, the aim was to determine the relations between the spray characteristics, process conditions, particles sizes, and the particle size distributions. Past research has studied the spray characteristics of precipitating particles using a solution with just one solute (Obzrut et al. 2007, Bell et al. 2005), but in this study the supercritical antisolvent process of co-precipitation is visualized.

I was assisted by undergraduate research fellow Matthew LaChance and NSF REU fellow Lara Tucci while carrying out the experiments and the data collection of these studies.

4.2 Materials

Experiments were conducted using a solution of the solute polymethyl methacrylate (PMMA) in acetone, the solvent. PMMA was obtained from Sigma Aldrich and has a molecular weight of ~15000 Daltons. Acetone was obtained from Fisher Scientific. Carbon dioxide of grade 5.5 was obtained from Airgas (Opelika, AL). Budesonide (99.9%), was obtained from Sigma-Aldrich. All the materials were used as received.

4.3 Experimental setup and imaging system

The apparatus shown in Figure 4.1 used to perform the supercritical antisolvent precipitation process was adapted from Obrzut et al. 2007. An ISCO 500D syringe pump was

used to pump the carbon dioxide and an Acuflow Series II HPLC pump was used to pump solution. The precipitation chamber used was a Jerguson gage, model 19TM40, with volume of 57 cm^3, height of 48 cm. The precipitation chamber has transparent windows in front and back which facilitates the visualization of the spray. The solution was delivered at constant flow rate of 1.6 cm^3/min with a metering pump, the Acuflow Series II HPLC pump with pulse dampener, Scientific Systems, through a spray nozzle of 100 μm ID fused silica capillary tubing. The nozzle was made by cutting capillary tubing with a wire cutter and inspecting the ends with an optical microscope to achieve a flat tip. To safely operate the high pressure precipitation chamber a pressure gage, McDaniel Controls, and a blowout plug, HIP 16-63AF1, were attached. A RTD in the precipitation chamber was used as the input device for the temperature controller, Omega CSC32. The temperature controller regulated a heating tape, Omegaflux SRT051-080, to maintain the temperature of precipitation chamber. One more thermocouple was installed at the center of precipitation chamber to measure the temperature along the depth of the precipitation vessel. The membrane filter, Millipore FLGP02500, separates the precipitated particles from the vessel effluent. The membrane filter has a pore diameter of 0.22 μm and was mounted in a 25 mm filter holder, Millipore XX4502500, at the bottom of the precipitation chamber. The imaging system (Figure 4.1) was used to video the spray in a Jerguson gage during the SAS precipitation process. It was adapted from the imaging systems used by Obzrut et al. 2008 and Bell et al. 2005. A Questar QM 100 MK III lens and CCD camera combination on an adjustable tripod was used to visualize the spray. The camera records at 60 frames per second, and the lens has a maximum magnification of 0.9 μm/pixels. A Pinnacle converter was used to convert the video from analog to digital and displayed it on a computer. The video was captured and saved using Pinnacle

Studio Ultimate software. The Pinnacle converter was also connected to a VCR and TV so that the spray could be clearly viewed while we adjusted the focus of the camera lens during the spray. The output of the COHU camera was digitized by an analog to digital video converter, Pinnacle Studio Moviebox Ultimate. The video was collected on a computer in .mpg format using Pinnacle Studio 12 software. The frames of the video were separated into individual .bmp images using QuickTime media player. The images were then analyzed using image processing software, ImageJ. Jet break up length was the distance measured using the Straight Line tool, in ImageJ, from the edge of the capillary tubing to the point where the jet edge exhibits rippling. The same tool was used to measure the droplet diameters. Only droplets that were completely in focus were measured. To find pixel/μm, in-situ images of the 400 μm outer diameter nozzle with the same magnification as the droplet images were obtained and the known distances measured for pixel length.

The precipitated particles were analyzed using a scanning electron microscope (SEM), Zeiss EVO 500. Samples for the scanning electron microscope were prepared by transferring particles from the filter holder to a stub with double-sided carbon tape on the surface. The stub was sputter-coated for 2 minutes with gold. Images of the particles were obtained in .tif format. The particles were analyzed using ImageJ by measuring the diameter using the straight line tool.

4.4 Experimental procedure

To perform these experiments, the apparatus shown in Figure 4.1 was operated in batch mode. The precipitation chamber was initially filled with CO_2 using syringe pump, which was

set to maintain the operating pressure in the precipitation chamber. The precipitation chamber was heated by using temperature controlled heating tape. The system was run until the temperature and pressure reached equilibrium. 1 wt% PMMA+budesonide in acetone solution was pumped by the HPLC pump with all valves closed. The solution was sprayed at a fixed flow rate of 1.6 cm^3/ min for 30 to 45 sec. The valve on the syringe pump was opened to resume the pressure control by the Isco syringe pump. Then, the two valves, downstream of precipitation chamber, were adjusted to control the chamber outflow. Usually outflow rate was adjusted to 5-7 cm^3/min, which can be monitored through the change in the volume of the Isco syringe pump. Four chamber volumes of CO_2 were purged through the precipitation chamber. Once the chamber reached atmospheric pressure, the filter holder was removed to collect the dried PMMA+budesonide particles on the membrane filter.

The visualization of the spray was done while spraying the solution in the precipitation chamber. The camera was positioned at the desired vertical distance from the tip of the nozzle. Images were typically obtained with the center of the spray in frame. In the case of visualization at 0 mm from the tip of nozzle (jet breakup visualization), the camera was rotated by 90º to take the greater advantage of the aspect ratio.

4.5 Experimental conditions

The SAS precipitation experiments were conducted with 1wt% PMMA+budesonide in acetone solution sprayed into supercritical CO_2 at 1.6 cm^3/min for 30 to 45 seconds. Experimental conditions are listed in Table 4.1, grouped as three fixed density conditions and

three fixed temperature conditions. The operating conditions were chosen to allow for characterization of the spray near the transition from two phases to one phase jet break up.

Experiments with a fixed initial carbon dioxide density of 0.32 g/cm^3 were performed at pressure and temperature combinations of 84 bar and 40 ºC, 89 bar and 45 ºC, and 94 bar and 50 ºC. Fixed temperature experiments at 50 ºC were performed at three pressure and density combinations: 84 bar and 0.24 g/cm^3, 89 bar and 0.28 g/cm^3, and 94 bar and 0.32 g/cm^3. The pressure values were selected to correspond to those of the fixed density experiments. The phase diagram for the binary mixture of CO_2-acetone indicates that after spraying the solution into carbon dioxide a supercritical mixture will be present at these conditions.

Videos were captured through a viewing window in the precipitation chamber. Visualization was done, for all the experimental conditions, at 0 and 3 mm from the tip of the nozzle. The flow rate of 1 wt% PMMA+budesonide in acetone solution for these experiments was 1.6 cm^3/min, the pressure drop across the nozzle was estimated to be ~8 bar.

4.6 Results

Figure 4.2 represents the visualizations done by performing the SAS precipitation process at a fixed bulk CO_2 density of 0.32 g/cm^3 and select pressure and temperature combinations with 1 wt% PMMA+budesonide in acetone solution flow rate of 1.6 cm^3/min. Figure 4.3 represents the visualization done by performing the SAS precipitation process at a fixed temperature of 50 ºC and select pressure and density combinations with 1 wt% PMMA+budesonide in acetone

solution flow rate of 1.6 cm^3/min. The data obtained from all the experiments is listed in Table 4.2. Figure 4.4 and Figure 4.5 show the jet break up length plots for experiments performed at fixed density and fixed temperature conditions, respectively. Figure 4.6 presents the plots of average droplet diameter at 3 mm from the tip of the nozzle for experiments performed at fixed density and fixed temperature conditions, respectively. Error bars on all the plots represent the standard deviation due to the droplet size distribution.

4.6.1 Fixed density experiments

Figure 4.2 shows images of 1 wt% PMMA+budesonide in acetone sprayed in CO_2 at fixed density of 0.32 g/cm^3. Column (a), column (b), and column (c) represent the images of 1 wt% PMMA+budesonide sprayed in CO_2 at 84 bar and 40 ºC, 89 bar and 45 ºC, and 94 bar and 50 ºC, respectively. In all these conditions, the spray is clearly in the atomization regime as evidenced by the coherent jet and the presence of distinct droplets. Visualizations taken at 3 mm from the nozzle outlet show a section of the spray with the jet unbroken and droplets present. The average jet break up lengths for these three conditions was 736 ± 55 μm, 768 ± 75 μm and 847 ± 84 μm, respectively. Jet break up length for these fixed density conditions remains similar. For column (a), the average droplet diameter was 64 μm at 3mm. For column (b), the average droplet diameter was 64 μm at 3mm. For column (c), the average droplet diameter was 58 μm at 3mm.

4.6.2 Fixed temperature experiments

Figure 4.3 shows images of 1 wt% PMMA+budesonide in acetone sprayed in CO_2 at fixed temperature at 50 ºC. Column (a), column (b), and column (c) represent the images of 1

wt% PMMA+budesonide sprayed in CO_2 at 84 bar and 0.24g/cm^3, 89 bar and 0.28g/cm^3, 94 bar and 0.32g/cm^3, respectively. In all these conditions, the spray is clearly in the atomization regime as evidenced by the coherent jet and the presence of distinct droplets. But, the numbers of droplets seen in column (c) are fewer. This shows the transition regime for a gas like plume. Visualizations taken at 3 mm from the nozzle outlet show a section of the spray with the jet unbroken and droplets present. For column (a), the average droplet diameter was 41 μm at 3 mm. For column (b), the average droplet diameter was 56 μm at 3mm. For column (c), the average droplet diameter was 58 μm at 3mm.

4.7 Discussion

Figure 4.4 shows that the jet breakup length was similar, for the fixed density experiments. Figure 4.5 shows that the jet breakup length decreased as pressure was increased, for the fixed temperature experiments. Jet breakup length decreases with an increase in temperature or/and pressure which is consistent with the finding of Obrzut et al. 2007 and Lengsfeld et al. 2000. In fixed density experiments, an increase in pressure was accompanied by a decrease in temperature, hence no significant change in jet breakup length. But in fixed temperature experiments, an increase in pressure increased affinity of the solvent towards the bulk CO_2 which contributes to a decrease in surface tension of the sprayed solution, and hence results in a decrease of the jet breakup length.

Figure 4.2 shows the jet breakup through atomization and droplets formation was seen throughout the images for the fixed density experiments. The droplets occur due to the lack of

coherence in the jet. Figure 4.3 shows the jet break up through atomization and droplet formation was seen throughout the images for the fixed temperature experiments. But, the number density of the droplets decreases from the experiment at 84 bar and 0.24 g/cm^3 to 89 bar and 0.28 g/cm^3 to 94 bar and 0.32 g/cm^3. This trend is attributed to the fact that an increase in the pressure created a more miscible system.

For all three operating conditions, spherical PMMA+budesonide micro particles were found. The morphology of the particles was typically characterized as solid spheres as shown in Figure 4.8 and Figure 4.9. In the fixed density experiments, the average particle size for 84 bar and 40 ºC was 1.07 ± 2.03 µm, for 89 bar and 45 ºC was 1.67 ± 1.28 µm, for 94 bar and 50 ºC was 1.36 ± 0.93 µm. In the fixed temperature experiments, the average particle size for 84 bar and 0.24 g/cm^3 was 1.34 ± 0.59 µm, for 89 bar and 0.28 g/cm^3 is 1.51 ± 0.79 µm, for 94 bar and 0.32 g/cm^3 is 1.54 ± 1.89 µm. The particle sizes are also shown in Table 4.2. Despite the different spray characteristics at different operating conditions, the particle characteristics were similar, as shown in Figure 4.9. The particles collected at these operating conditions were spherical in shape with similar average diameter and size distribution.

4.8 Conclusion

This study shows that spherical, micron-sized PMMA+budesonide particles can be created via the SAS precipitation process. The high magnification visualization system was used to study the spray characteristics of the SAS precipitation process. In fixed temperature experiments, an increase in pressure and density caused a decrease in jet break up length. In

fixed density experiments, jet break up length was similar. Atomization of 1 wt% PMMA+budesonide in acetone was observed in all the experimental conditions. Despite different spray characteristics at different conditions, the particle size and particle size distribution of PMMA+budesonide was similar. This suggests that the spray characteristics are not the only phenomena influencing the particle characteristics in the SAS precipitation process.

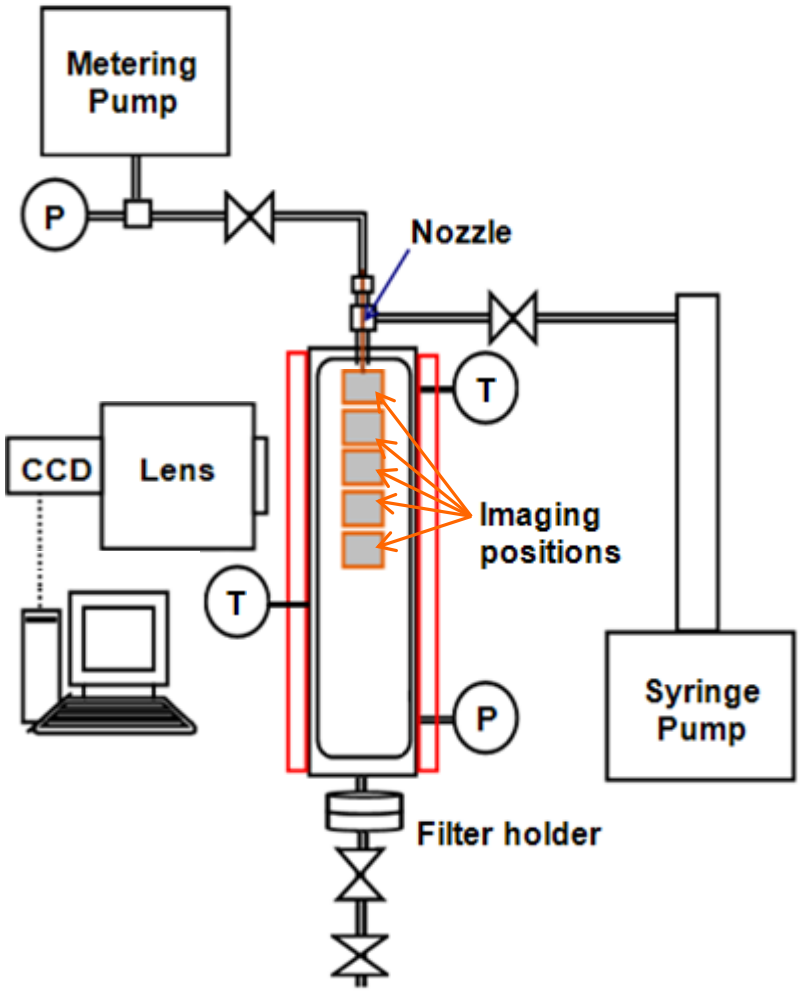

Figure 4.1 Diagram of the imaging system and the apparatus used to perform the supercritical antisolvent precipitation process. The imaging positions in the spray are represented by the shaded boxes inside the precipitation vessel

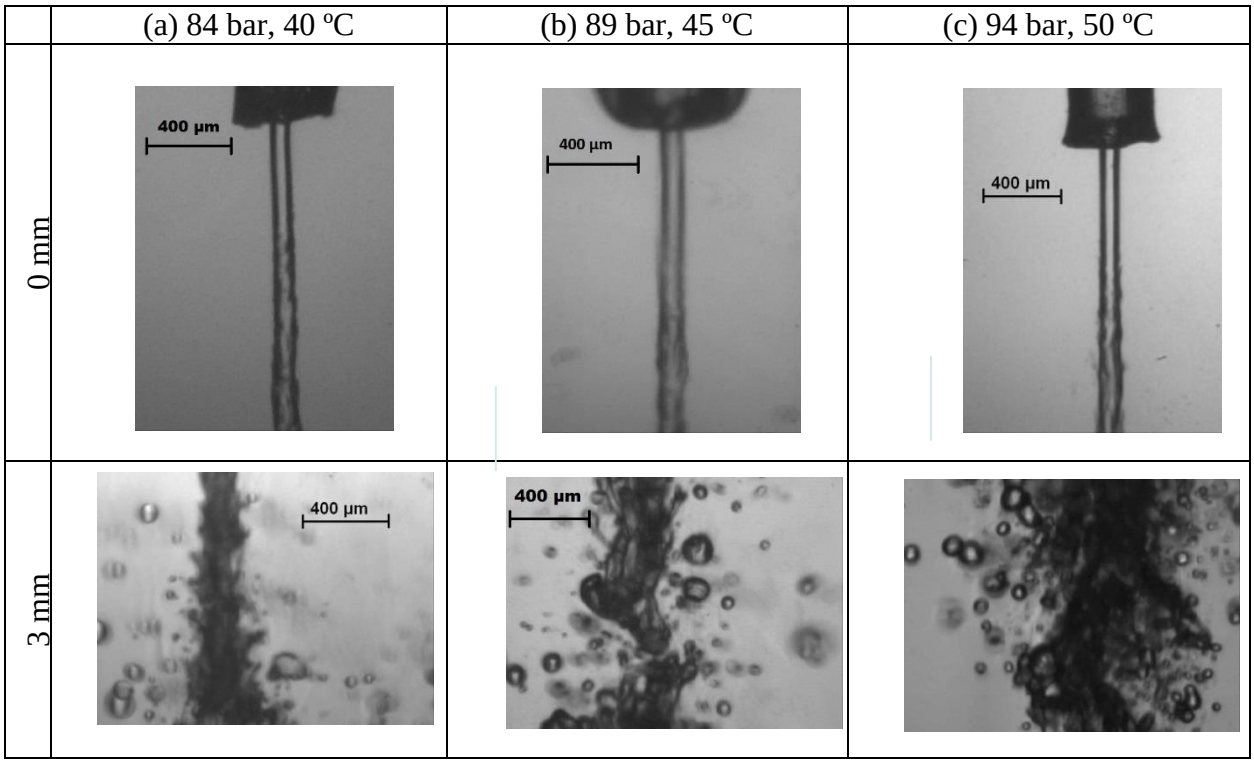

Figure 4.2. Selected frames taken from movies of 1 wt% PMMA+budesonide (90+10) in acetone spray at given distances from the nozzle in the fixed density SAS experiments, bulk CO_2 density of 0.32 g/cm^3

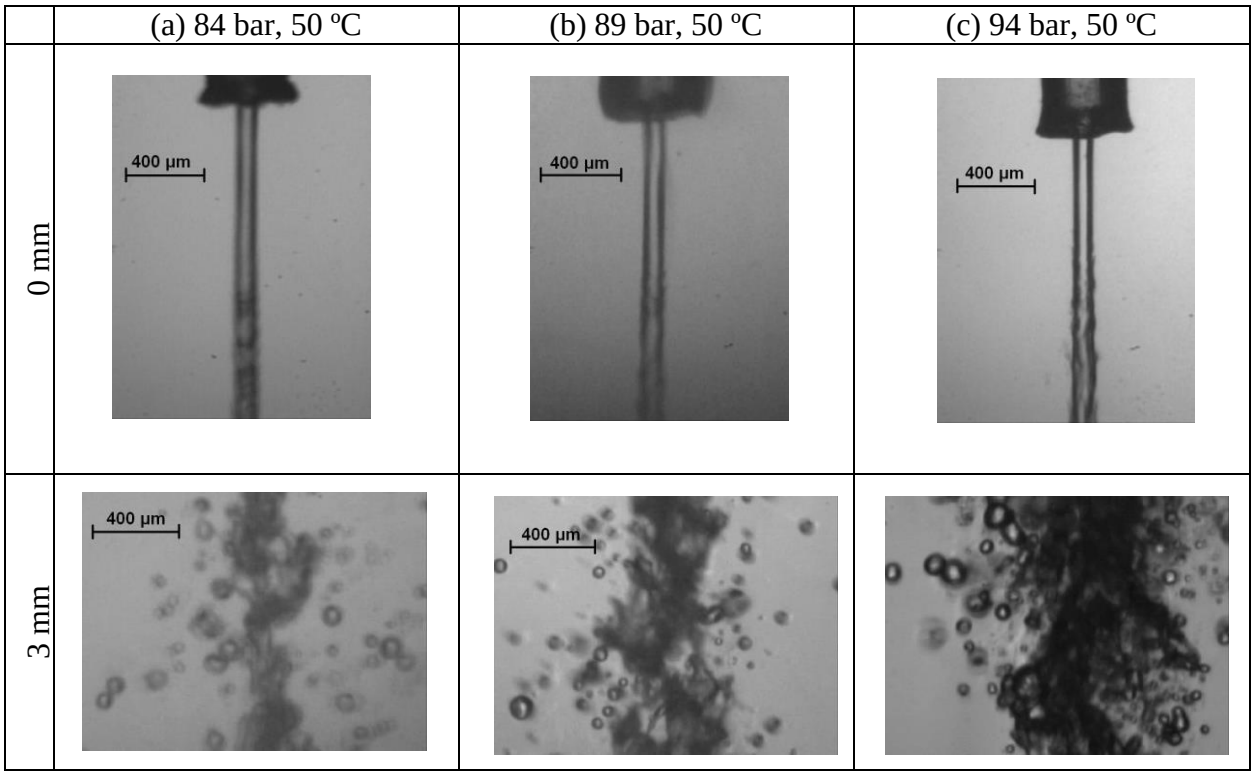

Figure 4.3. Selected frames taken from movies of 1 wt% PMMA+budesonide (90+10) in acetone spray at given distances from the nozzle in the fixed temperature SAS experiments

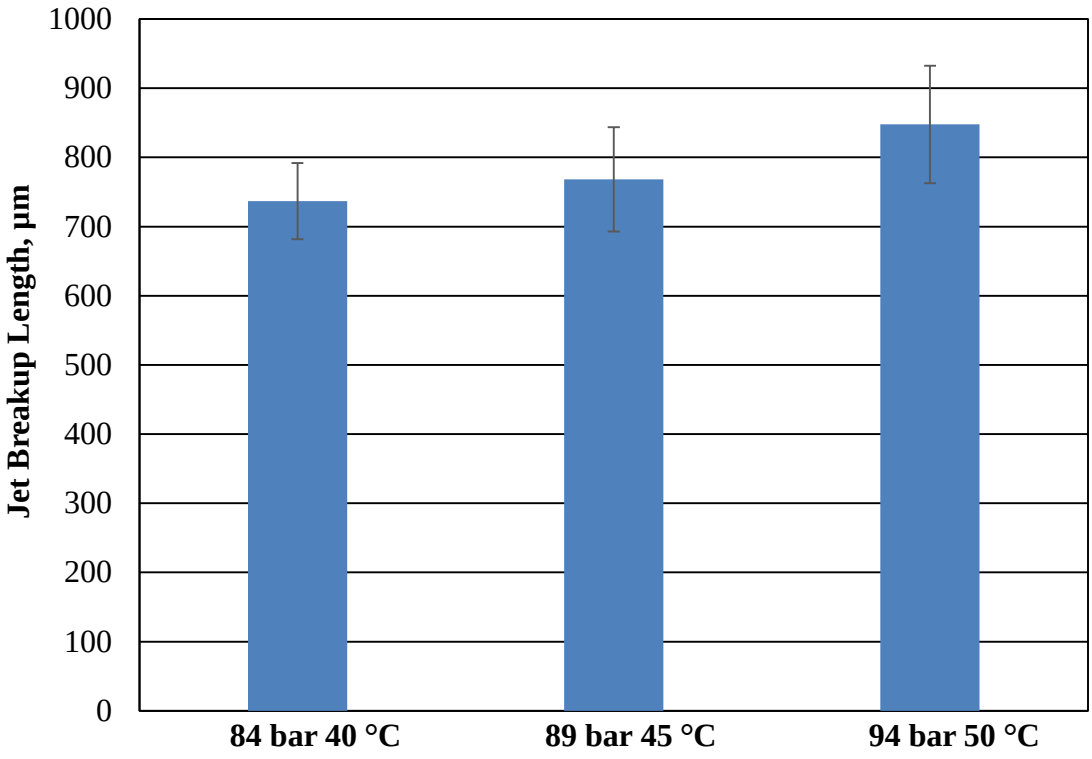

Figure 4.4 Jet breakup length for 1 wt% PMMA+budesonide in acetone solutions processed via the SAS precipitation process at a constant density of 0.32 g/cm^3

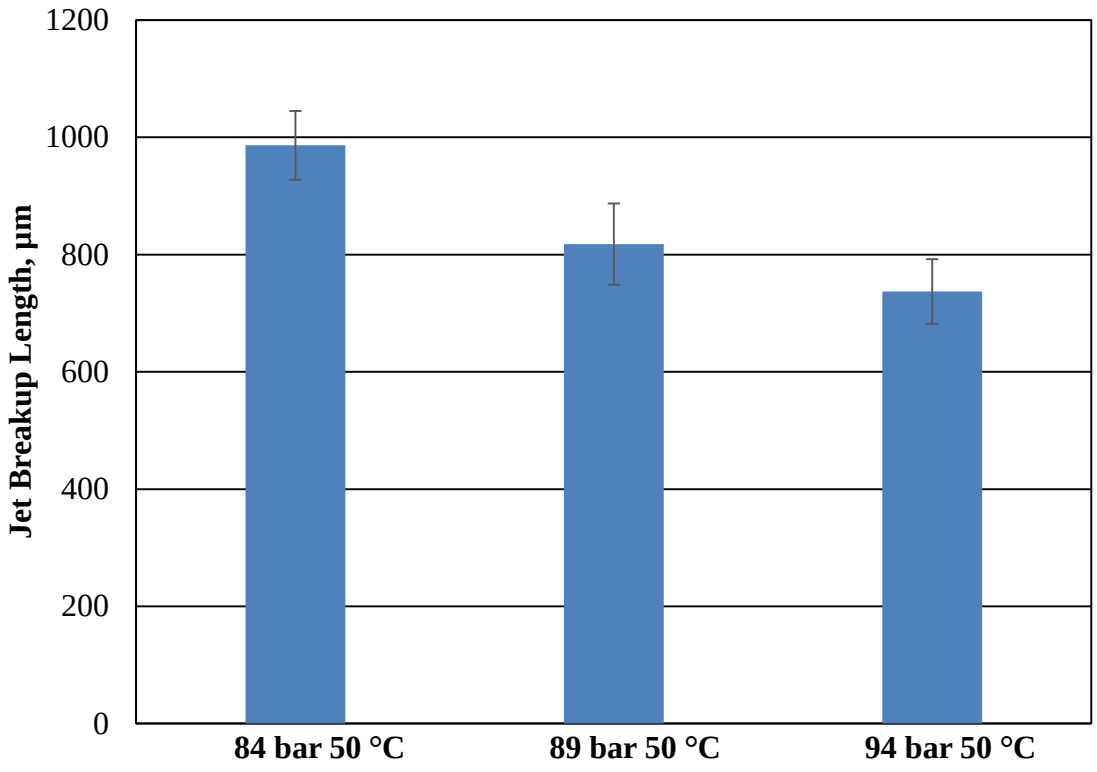

Figure 4.5 Jet breakup length for 1 wt% PMMA+budesonide in acetone solutions processed via the SAS precipitation process at a constant temperature of 50 ºC

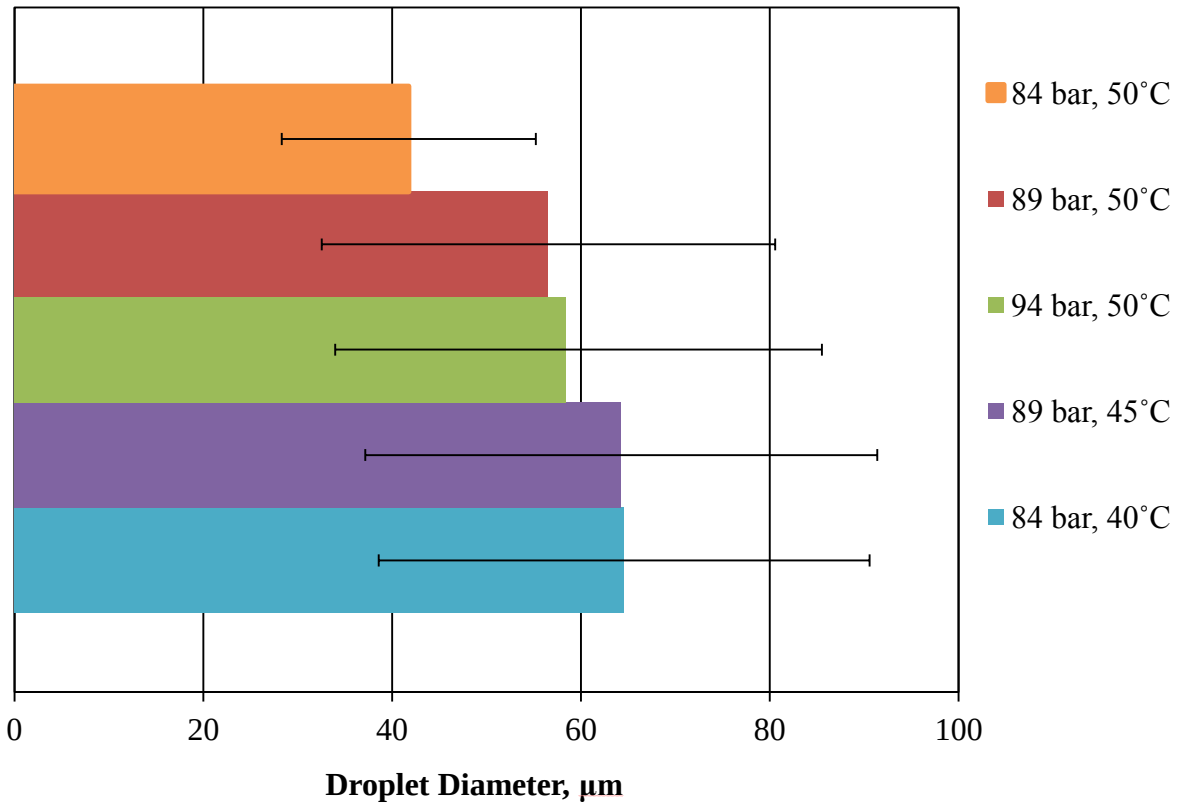

Figure 4.6 Average droplet diameter of 1 wt% PMMA+budesonide in acetone solution sprayed into supercritical CO_2 during the fixed density and the fixed temperature SAS experiments

Bulk Supercritical CO_2				1 wt% PMMA+budesonide in Acetone Solution		Visualizations
Density (g/cm^3)	Temperature (^oC)	Pressure (bar)	Viscosity (cP)	Flow Rate (cm^3/min)	Nozzle Velocity (m/s)	Distances from the Nozzle (mm)
Fixed Density						
0.32	40	84	0.025	1.6	0.8	0,3
0.32	45	89	0.025	1.6	0.8	0,3
0.32	50	94	0.025	1.6	0.8	0,3
Fixed Temperature						
0.24	50	84	0.021	1.6	0.8	0,3
0.28	50	89	0.023	1.6	0.8	0,3
0.32	50	94	0.025	1.6	0.8	0,3

Table 4.1 List of experimental conditions used to perform SAS as well as the distances from the nozzle imaged at each condition for 1 wt% PMMA+budesonide in acetone

Density (g/cm^3)	Temp (ºC)	Pressure (bar)	Distance from Nozzle (mm)	Average Droplet Diameter (μm)	Standard Deviation (μm)	Number of Droplets Measured	Jet Break Up Length (μm)	Measured Jet Images	Standard Deviation of Jet Length (μm)
Fixed Density									
0.32	40	84	0				847	122	84
			3	64.6	26	356			
0.32	45	89	0				768	135	75
			3	64.3	27.1	312			
0.32	50	94	0				736	84	55
			3	63.2	23.4	156			
Fixed Temperature									
0.24	50	84	0				986	95	58
			3	41.8	13.5	371			
0.28	50	89	0				817	61	69
			3	56.6	24	402			
0.32	50	94	0				736	73	55
			3	63.2	23.4	415			

Table 4.2 Analysis of 1 wt% PMMA+budesonide processed via the SAS precipitation processes

(a) 84 bar and 40 ºC	(b) 89 bar and 45 ºC	(c) 94 bar and 50 ºC
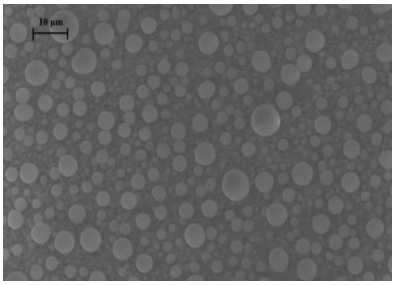	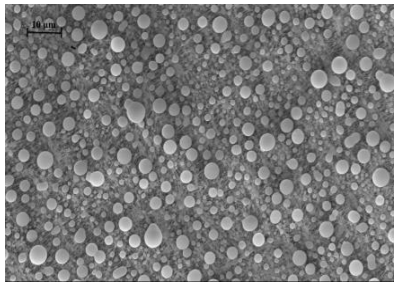	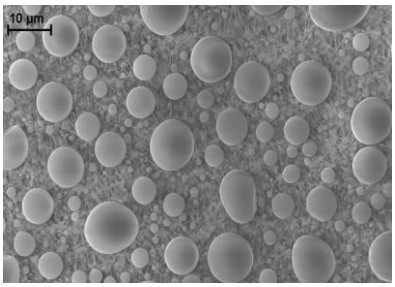

Figure 4.7 Scanning electron microscope images of PMMA+budesonide particles produced via the SAS precipitation process during the fixed density the SAS experiments with 1 wt% PMMA+budesonide (90+10) in acetone solution, bulk CO_2 density of 0.32 g/cm^3

(a) 84 bar and 0.24 g/cm^3	(b) 89 bar and 0.28 g/cm^3	(c) 94 bar and 0.32 g/cm^3
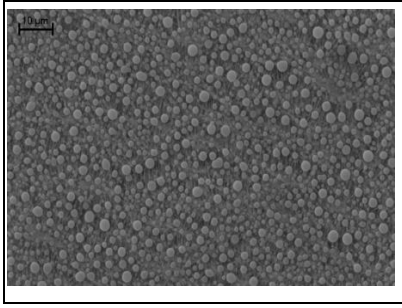	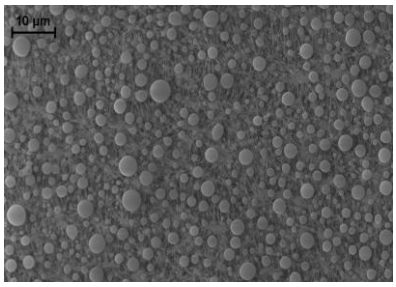	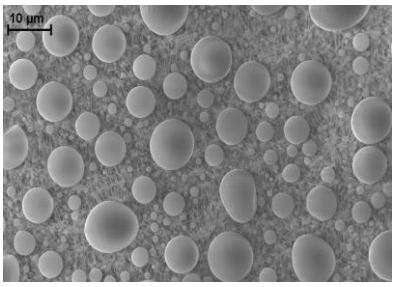

Figure 4.8 Scanning electron microscope images of PMMA+budesonide particles produced via the SAS precipitation process during the fixed temperature experiments performed at 50 ºC with 1 wt% PMMA+budesonide (90+10) in acetone solution

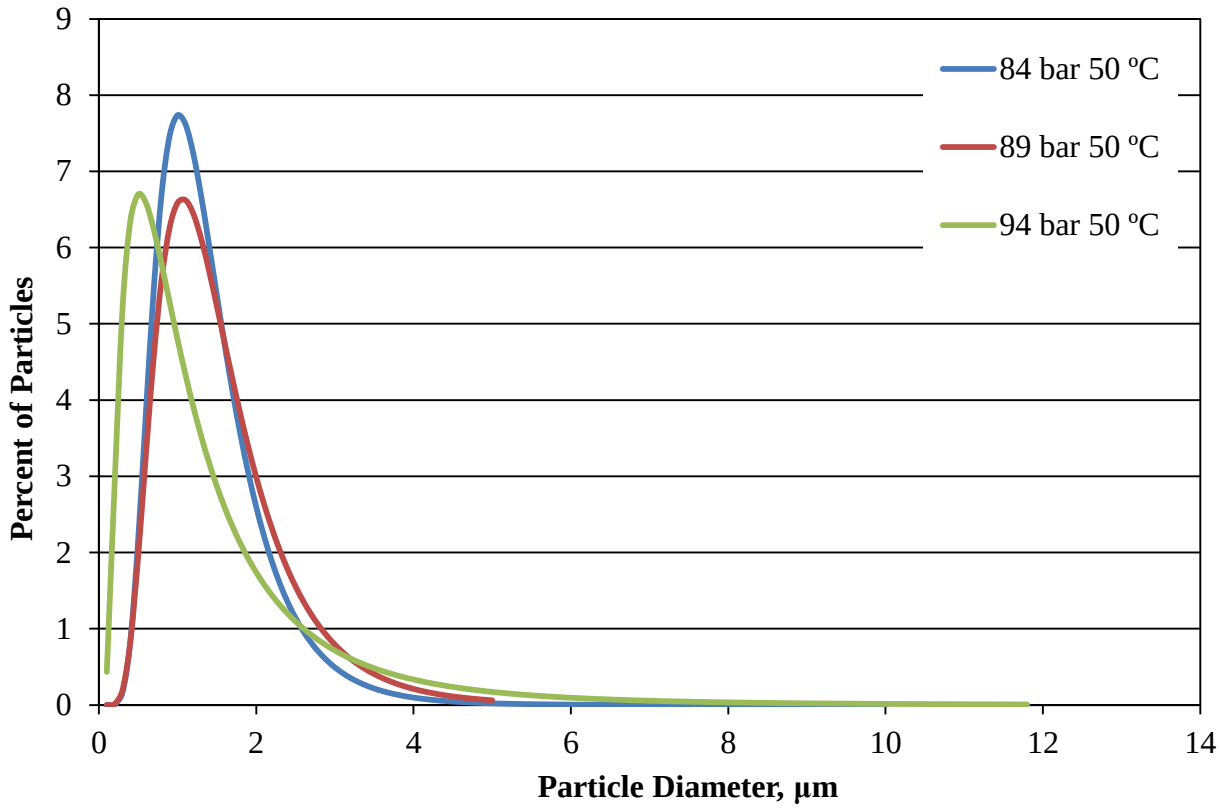

Figure 4.9 Size distribution of PMMA+budesonide particles produced via the SAS precipitation process during the fixed temperature experiments performed at 50 ºC with 1 wt% PMMA+budesonide (90+10) in acetone

Chapter 5

Effect of process conditions on the spray characteristics and particle size of different compositions of PMMA+budesonide in acetone via the SAS precipitation process

5.1 Introduction

This study uses the supercritical antisolvent (SAS) precipitation process to create micro particles of PMMA+budesonide particles at various operating conditions. 1 wt% PMMA+budesonide in acetone solution with three different compositions of PMMA+budesonide (99+1, 95+5, and 90+10) were processed via the SAS precipitation process using carbon dioxide as an antisolvent. A specific objective of this study was to form PMMA+budesonide particles with the SAS precipitation process at various conditions and to determine the composition of the resulting polymer-drug particles. This study is specifically tailored to simulate biodegradable polymers used in pulmonary drug delivery. An anti-inflammatory corticosteroid, budesonide, used in the treatment of lung conditions such as asthma, is co-precipitated with a polymer carrier, PMMA, using the SAS precipitation process. Another objective of this study was to visualize the SAS precipitation process at varying conditions using a high magnification, high-resolution camera. Using the video captured as well as scanning electron micrographs of the particles collected, the aim was to determine the relations between the spray characteristics, process conditions, particles sizes, and the particle size distributions.

I was assisted by undergraduate research student fellow Matthew LaChance and NSF REU fellow Lara Tucci while carrying out the experiments and the data collection of these studies.

5.2 Materials

Experiments were conducted using a solution of the solute PMMA and budesonide in acetone. PMMA was obtained from Sigma Aldrich and had the molecular weight of ~15000 Daltons. Acetone was obtained from Fisher Scientific. Carbon dioxide of grade 5.5 was obtained from Airgas (Opelika, AL). Budesonide (99.9%), was obtained from Sigma-Aldrich. All the materials were used as received. HPLC grade acetone was obtained from Mallinckrodt Baker Inc. (Phillipsburg, NJ). All the materials were used as received.

5.3 Experimental setup and imaging system

The apparatus shown in Figure 5.1 was used to perform the supercritical antisolvent precipitation process and was adapted from Obrzut et al. (2007). An ISCO 500D syringe pump was used to pump the carbon dioxide and an Acuflow Series II HPLC pump was used to pump solution. The precipitation chamber used was a Jerguson gage, model 19TM40, with volume of 57 cm^3, height of 48 cm. The precipitation chamber has transparent windows in front and back, which facilitates the visualization of the spray. The solution was delivered at constant flow rate of 1.6 cm^3/min with a metering pump, the Acuflow Series II HPLC pump with pulse dampener, Scientific Systems, through a spray nozzle of 100 μm ID fused silica capillary tubing. The nozzle was made by cutting capillary tubing with a wire cutter and inspecting the ends with an optical

microscope to achieve a flat tip. To safely operate the high pressure precipitation chamber a pressure gage, McDaniel Controls, and a blowout plug, HIP 16-63AF1, were attached. A RTD in the precipitation chamber was used as the input device for the temperature controller, Omega CSC32. The temperature controller regulates a heating tape, Omegaflux SRT051-080, to maintain the temperature of precipitation chamber. One more thermocouple was installed at the center of precipitation chamber to measure the temperature along the depth of the precipitation vessel. The membrane filter, Millipore FLGP02500, separates the precipitated particles from the vessel effluent. The membrane filter has a pore diameter of 0.22 μm and was mounted in a 25 mm filter holder, Millipore XX4502500, at the bottom of the precipitation chamber. The imaging system (Figure 5.1) was used to video the spray in the Jerguson gage during the SAS precipitation process. It was adapted from the imaging systems used by Obzrut et al. 2008 and Bell et al. 2005. A Questar QM 100 MK III lens and CCD camera combination on an adjustable tripod was used to visualize the spray. The camera records at 60 frames per second, and the lens has a maximum magnification of 0.9 μm/pixels. A Pinnacle converter was used to convert the video from analog to digital and displayed on computer. The video was captured and saved using Pinnacle Studio Ultimate software. The Pinnacle converter was also connected to a VCR and TV so that the spray could be clearly viewed while we adjusted the focus of the camera lens during the spray. The output of the COHU camera was digitized by an analog to digital video converter, Pinnacle Studio Moviebox Ultimate. The video was collected on a computer in .mpg format using Pinnacle Studio 12 software. The frames of the video were separated into individual .bmp images using QuickTime media player. The images were then analyzed using image processing software, ImageJ. Jet break up length was the distance measured using the Straight Line tool, in

ImageJ, from the edge of the capillary tubing to the point where the jet edge exhibits rippling. The same tool was used to measure the droplet diameters. Only droplets that were completely in focus were measured. To find pixel/μm, in-situ images of the 400 μm outer diameter nozzle with the same magnification as the droplet images were obtained and the known distances measured for pixel length.

The precipitated particles were analyzed using a scanning electron microscope (SEM), Zeiss EVO 500. Samples for the scanning electron microscope were prepared by transferring particles from the filter holder to a stub with double-sided carbon tape on the surface. The stub was sputter-coated for 2 minutes with gold. Images of the particles were obtained in .tif format. The particles were analyzed using ImageJ by measuring the diameter using the straight line tool.

5.4 Experimental procedure

To perform these experiments, the apparatus shown in Figure 5.1 was operated in batch mode. The precipitation chamber was initially filled with CO_2 using syringe pump, which was set to maintain the operating pressure in the precipitation chamber. The precipitation chamber was heated by using temperature controlled heating tape. The system was run until the temperature and pressure reached equilibrium. 1 wt% PMMA+budesonide in acetone solution, with different PMMA/budesonide composition, was pumped by the HPLC pump with all valves closed. The solution was sprayed at a fixed flow rate of 1.6 cm^3/ min for 30 to 45 sec. The valve on the syringe pump was opened to resume the pressure control by the Isco syringe pump. Then, the two valves, downstream of precipitation chamber, were adjusted to control the chamber

outflow. Usually outflow rate was adjusted to 5-7 cm^3/min, which can be monitored through the change in the volume of the Isco syringe pump. Four chamber volumes of CO_2 were purged through the precipitation chamber. Once the chamber reached atmospheric pressure, the filter holder was removed to collect the dried PMMA+budesonide particles on the membrane filter.

The visualization of the spray was done while spraying the solution in the precipitation chamber. The camera was positioned at the desired vertical distance from the tip of the nozzle. Images were typically obtained with the center of the spray in frame. In the case of visualization at 0 mm from the tip of nozzle (jet breakup visualization), the camera was rotated by 90º to take the greater advantage of the aspect ratio.

In this study a protocol for determining the composition of the particles was established. The method for determining the composition was chosen to be high performance liquid chromatography (HPLC), as suggested by previous work (Martin et al. 2002). Dr. Mark Byrne provided consultation in determining the materials needed and allowed the use of the HPLC equipment in The Byrne Lab at Auburn University. The HPLC system (Shimadzu, Columbia, MD) had a UV absorbance detector and GMHHRM column, a GPC column from Viscotek. The column has a 1M PS exclusion limit, particle size of 5 μm, and 7.8mm x 30cm dimensions. Standard solutions of budesonide in ethanol were measured for calibrations (range 1-10 $\mu g/cm^3$). Acetone was used as the mobile phase for the system with flow rate of 0.3 cm^3/min. Budesonide content was assayed at wavelength of 246 nm.

5.5 Experimental conditions

The SAS precipitation experiments were conducted with 1wt% PMMA+budesonide in acetone solution, with different PMMA/budesonide compositions, sprayed into supercritical CO_2 at 1.6 cm^3/min for 30 to 45 seconds. The operating condition chosen for these studies was 89 bar and 50 ºC, shown in Figure 5.2. A fixed initial carbon dioxide density of 0.32 g/cm^3 was used in all experiments. The phase diagram for the binary mixture of CO_2-acetone indicates that after spraying the solution into carbon dioxide, a supercritical mixture will be present at these conditions.

Videos were captured through a viewing window on the precipitation chamber. Visualization was done at 0, 3 and 14 mm from the tip of the nozzle. For the flow rate of 1.6 cm^3/min, the pressure drop across the nozzle was estimated to be ~8 bar.

5.6 Results

Figure 5.3 represents the visualizations done by performing the SAS precipitation process at 89 bar and bulk CO_2 density of 0.32 g/cm^3 with 1 wt% PMMA+budesonide in acetone solution, with different PMMA/budesonide compositions. During all these experiments, the spray was clearly in the atomization regime as evidenced by the coherent jet and the presence of distinct droplets. Visualizations taken at 3 mm from the nozzle outlet show a section of the spray with the jet unbroken and droplets present. Figure 5.4 shows the jet break up length plots for experiments performed alongside the jet break up length of 1 wt% PMMA in acetone run performed at the same operating condition of 89 bar and 50 ºC. The jet break up length was

similar for all the PMMA+budesonide compositions and PMMA in acetone solution processed via the SAS precipitation process. The droplet size measurements were not performed during these studies. The jet breakup lengths for all the compositions were similar, and as such, it is safe to assume that the droplet sizes will be similar to those from studies presented previously in this dissertation. Table 5.1 shows budesonide drug loading, as measured by the HPLC, in the particles produced during these studies.

5.7 Discussion

Figure 5.4 shows that the jet breakup length is similar for different compositions of PMMA+budesonide solutions in acetone sprayed in supercritical carbon dioxide at 89 bar and 50 ºC. The different compositions of the solute did not have a significant effect on the jet break up length. Figure 5.3 shows the jet breakup through atomization and droplet formation is seen throughout the images. The droplets occur due to the lack of coherence in the jet.

For all three compositions, spherical PMMA+budesonide microparticles were produced. The morphology of the particles was typically characterized as solid spheres as shown in Figure 5.5. The particle size distribution for PMMA+budesonide particles collected for different compositions experiments is shown in Figure 5.6. The average particle size for the solute PMMA+budesonide composition of 99+1 was 1.39 ± 0.72 µm, for the solute PMMA+budesonide composition of 95+5 the average particles size was 1.32 ± 0.65 µm, and for the solute PMMA+budesonide composition of 90+10 the average particle size was 1.51 ± 0.79 µm. Table 5.1 shows budesonide drug loading in the particles produced during these studies as

measured with the HPLC. The budesonide loading (wt%) for the PMMA+budesonide composition of 99+1 was 1.12, while the loading for the PMMA+budesonide composition of 95+5 was 6.17, and the loading for the PMMA+budesonide composition of 90+10 was 8.24. Based on this set of results, it can be said that the rate of precipitation of PMMA and budesonide during the SAS precipitation process were similar.

5.8 Conclusion

This study shows that spherical, micron-sized PMMA+budesonide particles can be created via the SAS precipitation process. The high magnification visualization system was used to study the spray characteristics of the SAS precipitation process. It was determined that the spray characteristics were similar to that of previous studies (shown in chapter 4) performed using acetone as a solvent. HPLC was used to determine the composition of the particles produced via the SAS precipitation process with different starting solute compositions. The starting composition of drug and polymer affects the drug loading in a directly.

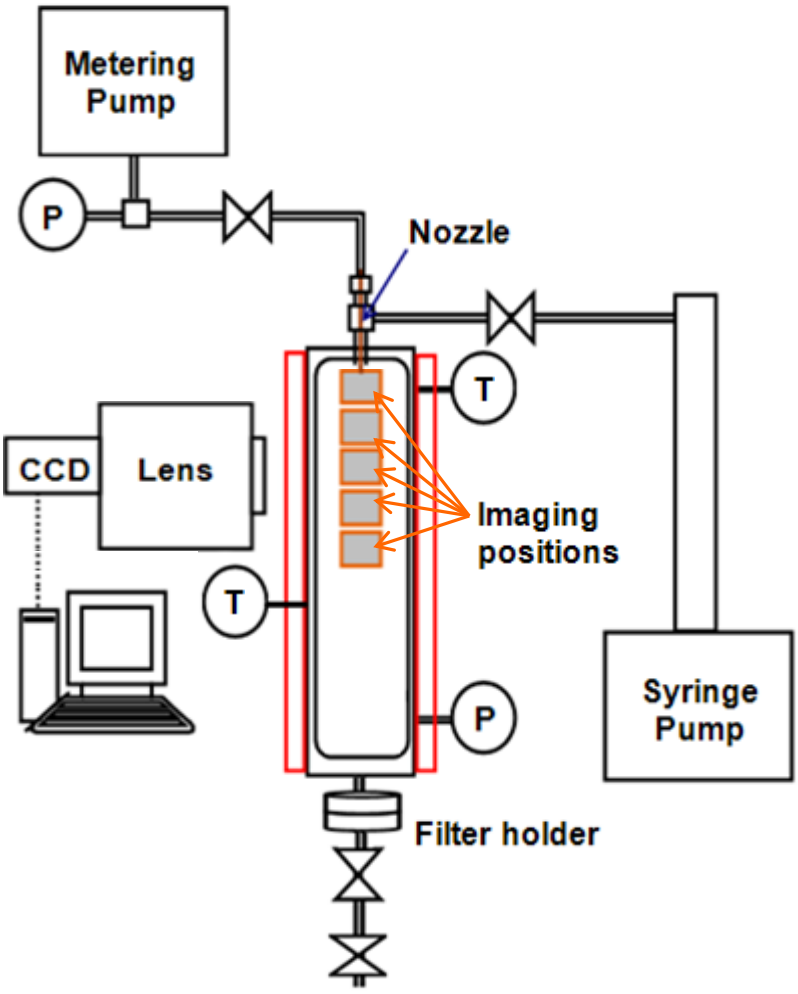

Figure 5.1 Diagram of the imaging system and the apparatus used to perform the supercritical antisolvent precipitation process. The imaging positions in the spray are represented by the shaded boxes inside the precipitation vessel

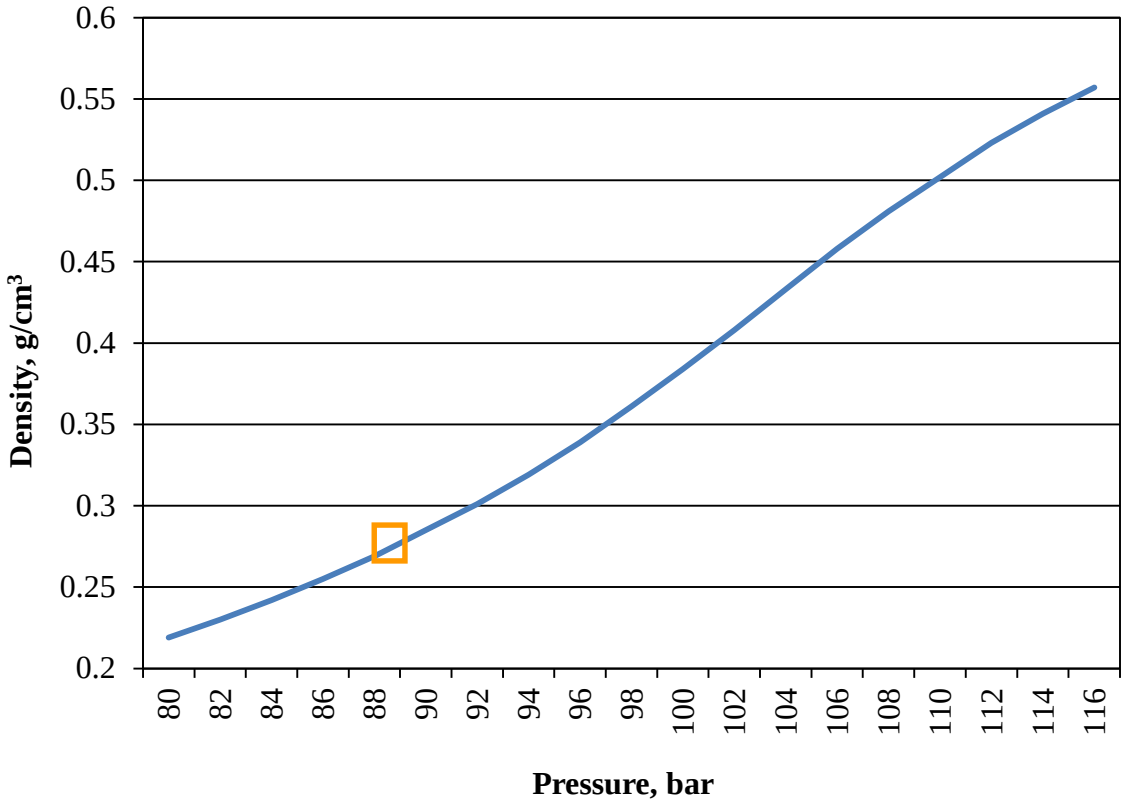

Figure 5.2 Experimental conditions displayed on carbon dioxide density vs pressure diagram. The symbols represent experimental conditions. The lines represent isotherms of pure CO_2 at the operating temperatures calculated from the NIST chemistry webbook

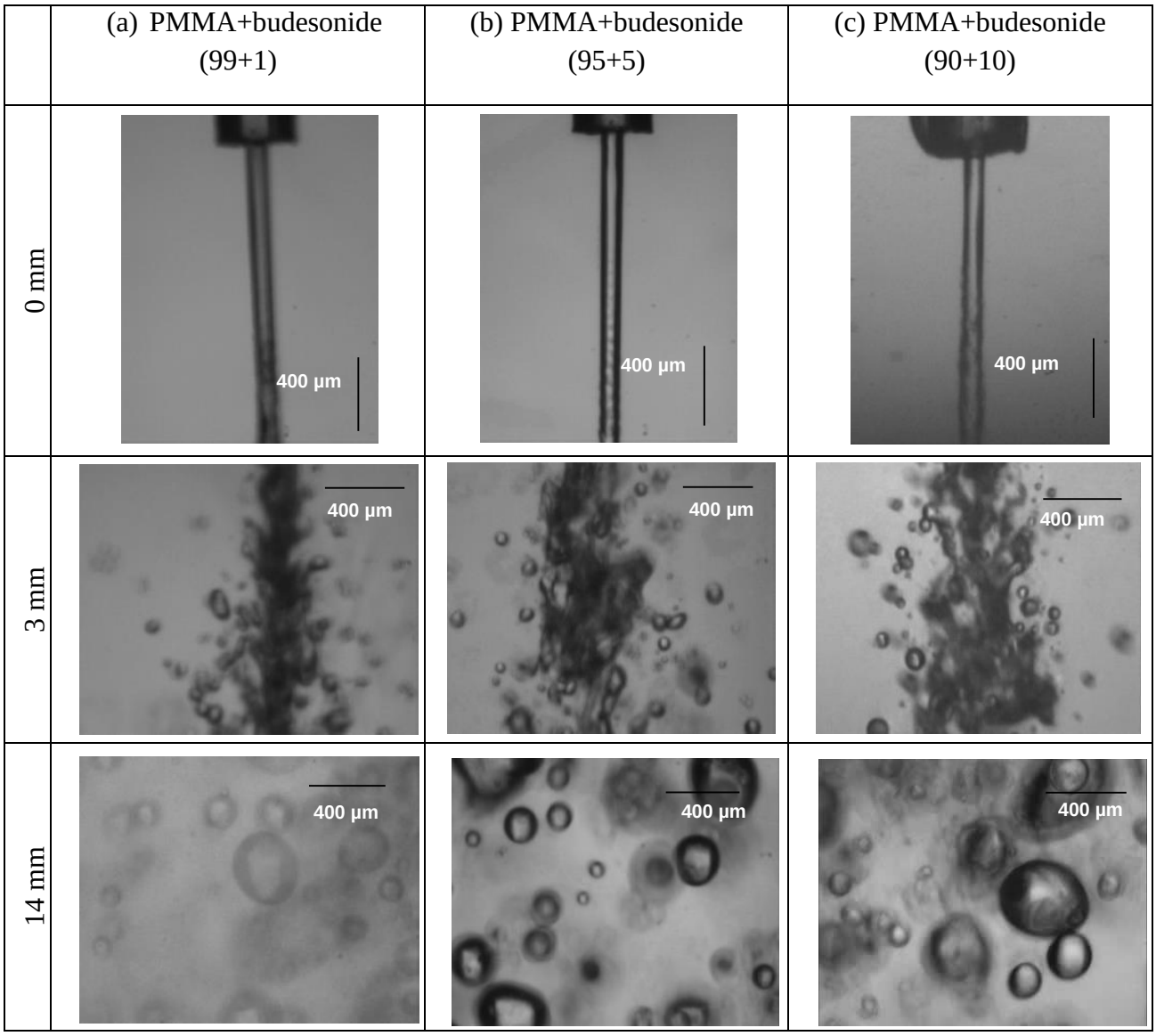

Figure 5.3 Selected frames taken from movies of the 1 wt% PMMA+budesonide in acetone spray at given distances from the nozzle at 89 bar and 50 ºC during the SAS precipitation process, bulk CO_2 density of 0.32 g/cm^3

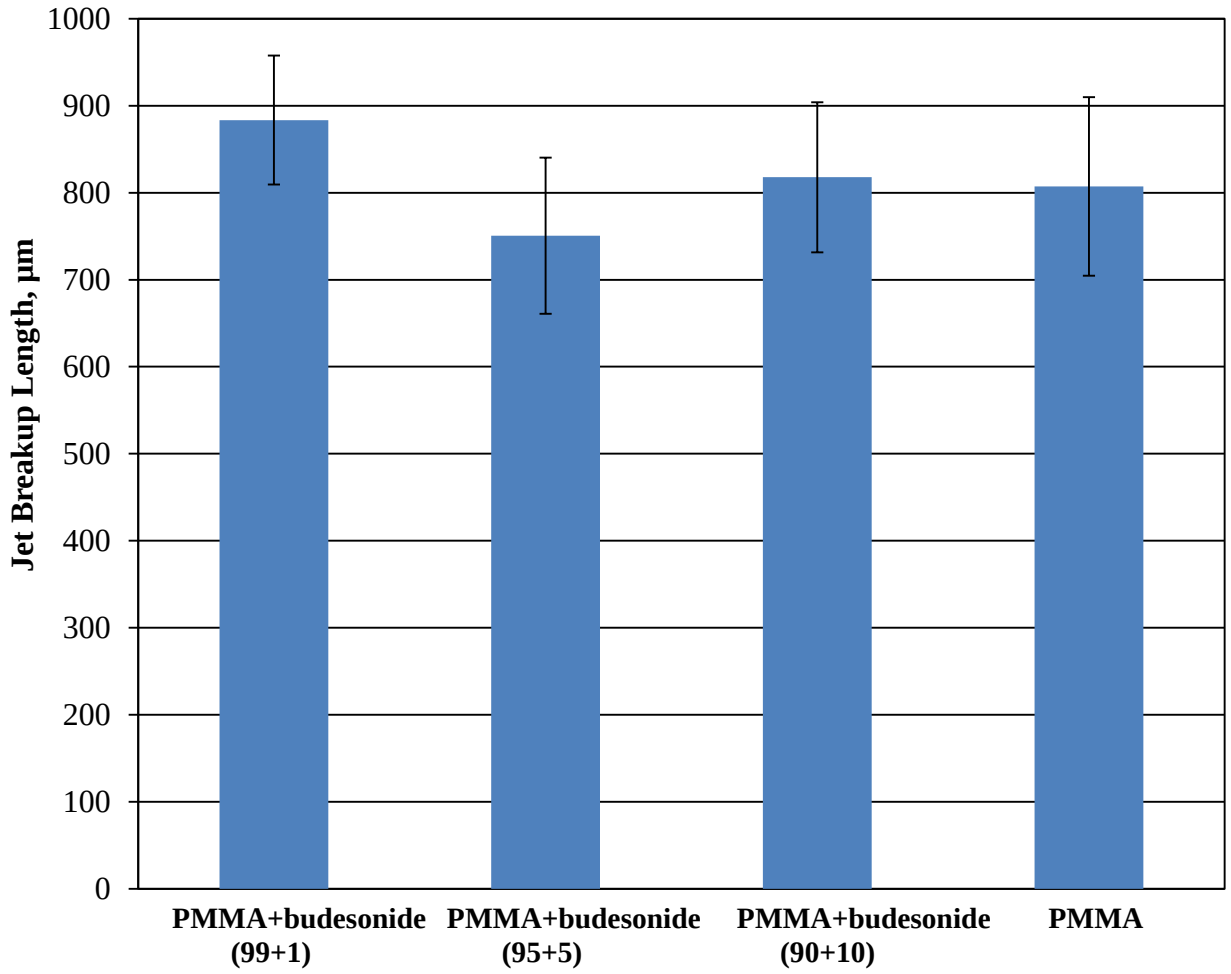

Figure 5.4 Jet breakup length for 1 wt% PMMA+budesonide and 1wt% PMMA in acetone solution processed via the SAS precipitation process at 89 bar and 50 ºC

PMMA+budesonide (99+1)	PMMA+budesonide (95+5)	PMMA+budesonide (90+10)
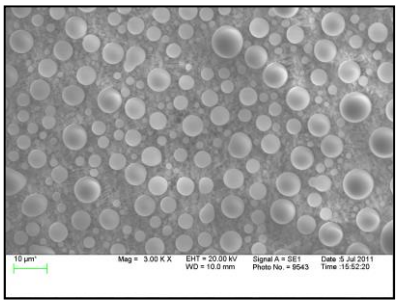	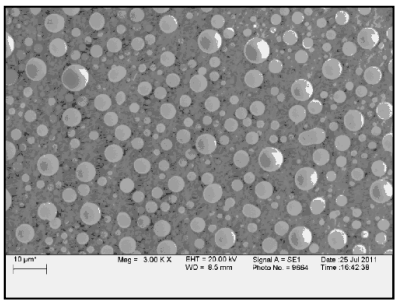	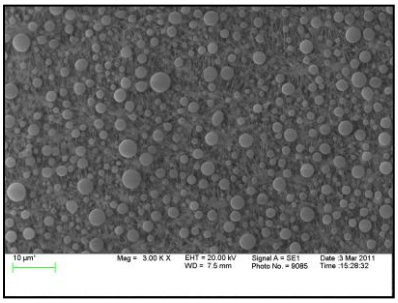

Figure 5.5 Scanning electron microscope images of 1wt% PMMA+budesonide, with different solute compositions, particles produced via the SAS precipitation process

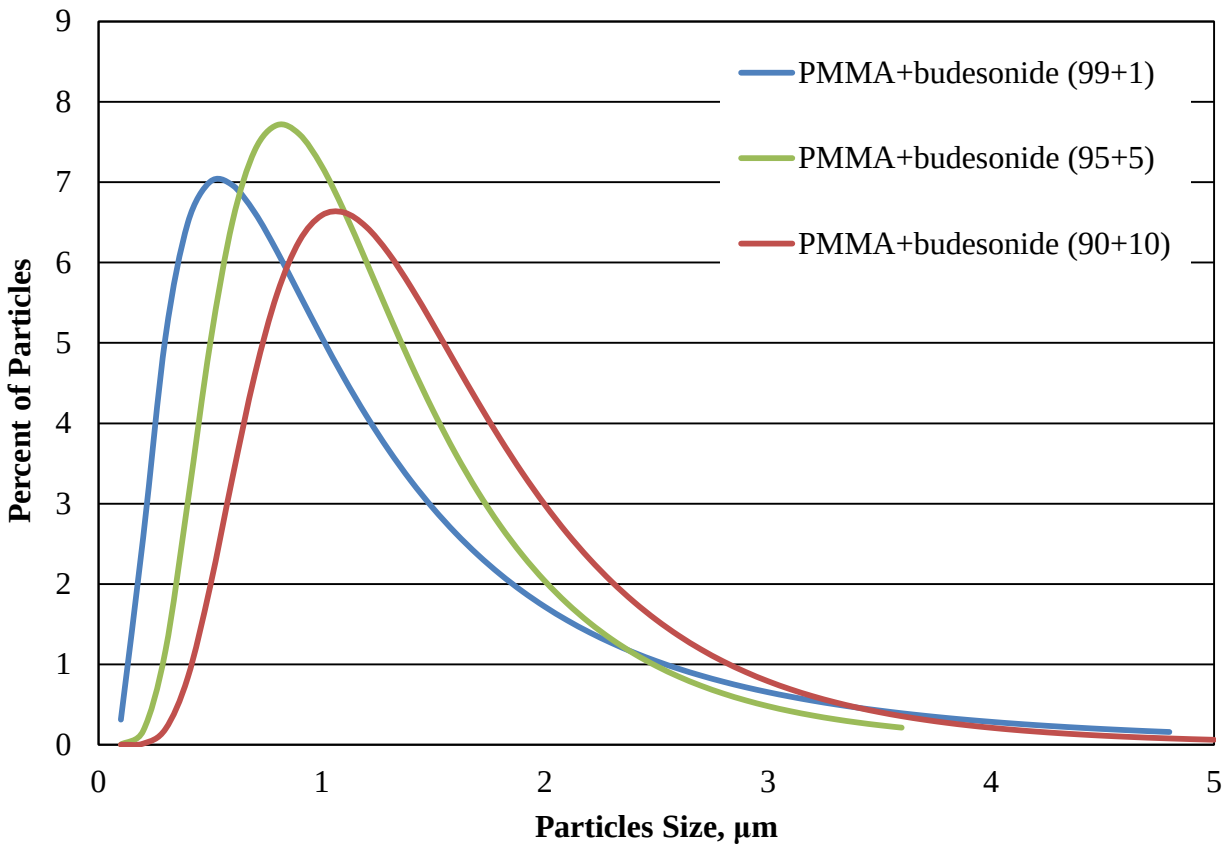

Figure 5.6 Size distribution of PMMA+budesonide particles produced via the SAS precipitation process at 89 bar and 50 ºC with 1 wt% PMMA+budesonide, with different solute compositions

Starting Composition in Acetone Solution	Budesonide Drug Loading, %wt
PMMA+budesonide (99+1)	1.12
PMMA+budesonide (95+5)	6.17
PMMA+budesonide (90+10)	8.24

Table 5.1 Budesonide drug loading in the particles produced during different compositions of PMMA+budesonide in acetone solution processed via the SAS precipitation process

Chapter 6

Effect of process conditions on the spray and particle size of gelatin in acetic acid via the SAS precipitation process

6.1 Introduction

Industrially made microparticles are used in the health care industry with other applications in electronics and the food and beverage industry. The United States tops the list in microparticles production, followed by East Asia and Europe (Ivansk 2013). In the food industry microparticles are used for packaging, additives, and other applications. Food additive applications include increasing the bioavailability of nutritional components, ensuring the quality of certain foods, and preventing bacterial growth. Functional foods are a potential use for microparticles. Functional foods are foods that deliver more than just nutritional benefits naturally found in a particular food (Bigliardi et al. 2013). They are similar in appearance to conventional foods, but they contain bioactive compounds, which have physiological benefits and reduce the risk of disease beyond that of conventional foods. Micro-scale particles can be used as vehicles for these bioactive compounds in functional foods. This growing branch of the food industry aims at improving general bodily conditions, decreasing the risk of some diseases, and even possibly curing select illnesses. The rise in popularity of functional foods can be partly attributed to the recent increase in health interest. Generally, these foods contain probiotics and/or prebiotics, with probiotics the more common. Probiotics are bacteria found in the body that aid in extracting nutrients from food, while prebiotics are nutrients that stimulate the growth

of such bacteria. As stated before, this is a growing industry with nearly limitless potential in applications as far reaching as helping to solve world hunger.

Gelatin was chosen as the polymer for this research. Synthetic polymers have been used to create microparticles for use in the immunotherapy application. Gelatin provides a natural polymer that can be formed into microparticles using the SAS precipitation process, and importantly the gelatin is not destroyed during the processing. As a biodegradable and biocompatible derivative of collagen, gelatin provides an optimum starting point for research in the area of microparticles drug delivery. Due to the already widespread use of gelatin as a food additive, little resistance would exist in its usage in functional foods and medicinal applications, such as inhaled steroids, which tends to be a problem for synthetic polymers. Gelatin has been used to make microparticles for the delivery of proteins, genetic materials, and small-molecule drugs. This is a major advantage of using gelatin over other polymers, which may have the potential for harmful degradation in the body. Also, because collagen is already a substance in the human body, the immune system is less likely to target a drug carrier made of gelatin. Possible disease transmission, such as mad cow disease, has been discussed related to the consumption of gelatin, but no evidence has been found to support this suspicion. Even though the potential spread of disease is a nonissue, pork gelatin can be used just as easily as bovine. Research is currently being conducted on fish derived gelatin as well, due to the religious ramifications associated with pork products.

This chapter shows the collaborative work with Dr. Yifen Wang, Biosystems Engineering at Auburn University. Dr. Wang has worked extensively with functional foods, and his PhD student Bangping Wang is continuing research in gelatin particle formation for functional food

and drug deliver applications. I was assisted by NSF REU fellow Andre Hansford and the Department of Biosystems Engineering PhD candidate Bangping Wang during data collection of these studies.

6.2 Materials

The gelatin is Type-A pork skin gelatin, product number 9764-500G, and was obtained from Amersco (Solon, OH). The glacial acetic acid was obtained from Sigma-Aldrich, product number 695092-500ML. The carbon dioxide was obtained from Airgas (Opelika, AL). All the materials were used as received.

6.3 Experimental setup and imaging system

The setup used to perform the SAS precipitation process (Figure 6.1) was modified from the system used by Obrzut et al. (2007). The precipitation chamber used was a Jerguson gage, model 19TM40, with volume of 57 cm^3 and height of 48 cm. The precipitation chamber has transparent windows in front and back, which facilitates the visualization of the spray. The solution was delivered at constant flow rate of 1.6 cm^3/min with a metering pump, the Acuflow Series II HPLC pump with pulse dampener, Scientific Systems, through a spray nozzle of 100 μm ID fused silica capillary tubing. An ISCO 500D syringe pump delivered the CO_2 to the precipitation chamber through the annular space between a capillary nozzle and a stainless steel sheath. The nozzle was made by cutting capillary tubing with a wire cutter and inspecting the ends with an optical microscope to achieve a flat tip. To safely operate the high pressure

precipitation chamber a pressure gage, McDaniel Controls, and a blowout plug, HIP 16-63AF1, were attached. A RTD in the precipitation chamber was used as the input device for the temperature controller, Omega CSC32. The temperature controller regulated a heating tape, Omegaflux SRT051-080, to maintain the temperature of precipitation chamber. One more thermocouple was installed at the center of precipitation chamber to measure the temperature along the depth of the precipitation vessel. The membrane filter, Millipore FLGP02500, separated the precipitated particles from the vessel effluent. The membrane filter has a pore diameter of 0.22 μm and was mounted in a 25 mm filter holder, Millipore XX4502500, at the bottom of the precipitation chamber.

SAS involves jet spraying of the solution into a compressed antisolvent. Imaging and visualization techniques are often used to study the jet flows, atomization and droplets (Lengsfeld et al. 2000, Obrzut et al. 2007). A high resolution monochrome CCD camera, COHU 2122, was used to image the SAS precipitation process. The camera has a chip size of 768 x 494 pixels with the pixel size of 8.4 x 9.8 μm. The shutter speed is 60 fps. Attached to the camera was a Questar QM100 MKIII long distance microscopic lens. The lens working distance ranges from 8 to 35 cm allowing visualization inside the precipitation chamber. The camera and lens were mounted on a tripod which facilitates X-Y-Z direction movement. A stroboscope, Monarch Nova Strobe DA Plus 115 with the pulse duration of 30 μs, provided backlight illumination (Bell et al. 2005).

The output of the COHU camera was digitized by an analog to digital video converter, Pinnacle Studio Moviebox Ultimate. The video was collected on a computer in .mpg format

using Pinnacle Studio 12 software. The frames of the video were separated into individual .bmp images using QuickTime media player. The images were then analyzed using image processing software, ImageJ. Jet break up length is the distance measured using the Straight Line tool, in ImageJ, from the edge of the capillary tubing to the point where the jet edge exhibits rippling. The same tool was used to measure the droplet diameters. Only droplets that were completely in focus were measured. To find pixel/μm, in-situ images of the 400 μm outer diameter nozzle with the same magnification as the droplet images were obtained and the known distances measured for pixel length.

The precipitated particles were analyzed using a scanning electron microscope (SEM), Zeiss EVO 500. Samples for the scanning electron microscope were prepared by transferring particles from the filter holder to a stub with double-sided carbon tape on the surface. The stub was sputter-coated for 2 minutes with gold. Images of the particles were obtained in .tif format. The particles were analyzed using ImageJ by measuring the diameter using the Straight Line tool.

6.4 Experimental procedure

To perform these experiments, the apparatus shown in Figure 6.1 was operated in batch mode. The precipitation chamber was initially filled with CO_2 using the syringe pump, which was set to maintain the operating pressure in the precipitation chamber. The precipitation chamber was heated by using temperature-controlled heating tape. The system was run until the temperature and pressure reached equilibrium. 1 wt% gelatin in acetic acid solution was pumped

by the HPLC pump into the chamber with all valves closed. The solution was sprayed at a fixed flow rate of 1.6 cm^3/min for 30 to 45 sec. After the spray, the valve on the syringe pump was opened to resume the pressure control by the Isco syringe pump. Then, the two valves, downstream of precipitation chamber, were adjusted to control the chamber outflow. Usual outflow rate was adjusted to 5-7 cm^3/min, which was monitored through the change in the volume of the Isco syringe pump. Four chamber volumes of CO_2 were purged through the precipitation chamber. Once the chamber reached atmospheric pressure, the filter holder was removed to collect the membrane filter with the dried gelatin particles.

The visualization of the spray was done while spraying the solution in the precipitation chamber. The camera was positioned at the desired vertical distance from the tip of the spray nozzle. Images were typically obtained with the centerline of the spray in frame. In the case of visualization at 0 mm from the tip of nozzle (jet breakup visualization), the camera was rotated by 90º to take advantage of the longer axis of the frame aspect ratio.

6.5 Experimental conditions

The SAS precipitation experiments were conducted with 1wt% gelatin in acetic acid solution sprayed into supercritical CO_2 for 30 to 45 seconds. The experimental conditions are listed in Table 6.1, grouped as two sets of fixed pressure conditions. The operating conditions were chosen to allow for characterization of the spray near the transition from two phases to one phase (gas-like plume) jet break up.

Videos were captured through a viewing window on the precipitation chamber. Visualizations were done at 0, 3 and 14 mm from the tip of the spray nozzle. For the flow rate of 1.6 cm^3/min of 1 wt% gelatin in acetic acid solution, the pressure drop across the nozzle was estimated to be ~8. The process was repeated for trials using a 5 wt% gelatin in acetone solution.

6.6 Results

The use of the SAS Precipitation Process proved to be a success in the creation of micronized gelatin particles. Experiments were performed for 1 and 5 wt% gelatin in acetic acid solutions at combinations of three temperatures, 40, 50 and 60 °C, and two pressures, 85 bar and 120 bar. Spray characteristics were obtained for 1 wt% solution of gelatin in acetic acid. Video was not recorded for the 5 wt% solution of gelatin in acetic acid. Figure 6.4 shows the jet break up lengths plots for experiments performed for 1 wt% gelatin in acetic acid at three different temperatures, 40, 50 and 60 °C, and two different pressures, 85 bar and 120 bar.

Particles produced from processing 1 wt% gelatin in acetic acid at 120 bar and 40 °C were of an average diameter of 1.19 ± 0.76 μm. 5wt% gelatin in acetic acid solution was sprayed into supercritical carbon dioxide at 120 bar and 40 °C and produced particles were of an average diameter of 1.11 ± 0.81 μm. In experiments conducted at 85 bar, no particles were collected on the Teflon filter at any of the three operating conditions. Figure 6.5 and Figure 6.6 shows the size distribution of particles collected from 1 wt% and 5 wt% gelatin in acetic acid, respectively. SEM images of particles collected are shown in Figure 6.7.

Average jet breakup length was measured for 1 wt% gelatin in acetic acid solution at six different operating conditions with the pressure and temperature parameters previously stated. At

120 bar and 40, 50 and 60 °C, average jet breakup length was measured to be 211 ± 24 μm, 189 ± 19 μm, and 213 ± 18 μm, respectively. At 85 bar and 40, 50 and 60 °C, average jet breakup length was measured to be 958 ± 75 μm, 1180 ± 180 μm, and 1340 ± 110 μm, respectively.

6.7 Discussion

6.7.1 Analysis of particle size

Gelatin particles produced by processing 1 and 5 wt% in acetic acid solutions via the SAS precipitation process were of similar characteristics, with similar average diameter and distributions. This coincides with Reverchon et al. (2008) in that changes in solute concentration have little effect on average particle size. Natural biopolymers, such as chitosan and gelatins, as well as industry standard polymers, such as poly L lactic acid and polyglycolic acid, offer the opportunity to examine Reverchon's prediction that the molecular weight of the polymer controls average particle size. Once an average particle size is established for each polymer at specific operating conditions and solution concentration, the concentration of solute in solution can vary while holding the operating conditions stable and vice versa.

More SAS trials should be conducted at pressures lower than 120 bar, including more at 85 bar to determine the feasibility of particle creation at a pressure slightly above the 83 bar critical point of acetic acid-carbon dioxide mixture. It is quite possible that particles of gelatin may have been formed at the lower pressures in our studies, however we were not able to collect them.

6.7.2 Analysis of jet breakup length

In experiments conducted at 85 bar, and three different temperatures, jet breakup length increased as the temperature of the system increased. However, in experiments conducted at 120 bar and the same temperature differences, the results do not definitively demonstrate that an increase in temperature at this pressure will lead to a longer jet breakup length. Between the set of the experiments conducted at 120 bar and at 85 bar, this data suggests that jet breakup length will increases as pressure decreases. At pressures far above the 83 bar, critical point of acetic acid-carbon dioxide mixture, jet breakup length was less influenced by temperature because of the elevated pressure/density inside the vessel.

6.8 Conclusion

Using the supercritical antisolvent precipitation process, gelatin particles of approximately 1 μm in diameter were produced. Gelatin particles were produced when 1 wt% gelatin in acetic acid solution was sprayed into supercritical carbon dioxide at 120 bar and 40 °C. Similar particles were created when 5 wt% gelatin in acetic acid solution was sprayed into supercritical carbon dioxide at the same operating conditions. This demonstrates that gelatin particles can be created using the SAS precipitation process. Future work should include determining the effect of operating conditions on particle size to see if particle size and size distribution can be controlled effectively. Once conditions are established, particles can then be produced and used for drug encapsulation and measure the loading capacity of particles, encapsulations efficiency, and drug release rate. Although the research and knowledge of gelatin

microparticles is still in its early stages relative to other studies in this dissertation, the use of gelatin particles, produced via the SAS precipitation process, in the areas of food industry and medicine is promising.

Bulk Supercritical CO_2			1 wt% Gelatin in Acetic Acid Solution		Visualizations
Density (g/cm^3)	Temperature (^oC)	Pressure (bar)	Flow Rate (cm^3/min)	Nozzle Velocity (m/s)	Distances from the Nozzle (mm)
At 85 bar					
0.38	40	85	1.6	0.8	0,3,14
0.25	50	85	1.6	0.8	0,3,14
0.21	60	85	1.6	0.8	0,3,14
At 120 bar					
0.69	40	120	1.6	0.8	0,3,14
0.51	50	120	1.6	0.8	0,3,14
0.42	60	120	1.6	0.8	0,3,14

Table 6.1 Experimental conditions used to perform the SAS precipitation processes as well as the distances from the nozzle imaged at each condition for 1 wt% gelatin in acetic acid

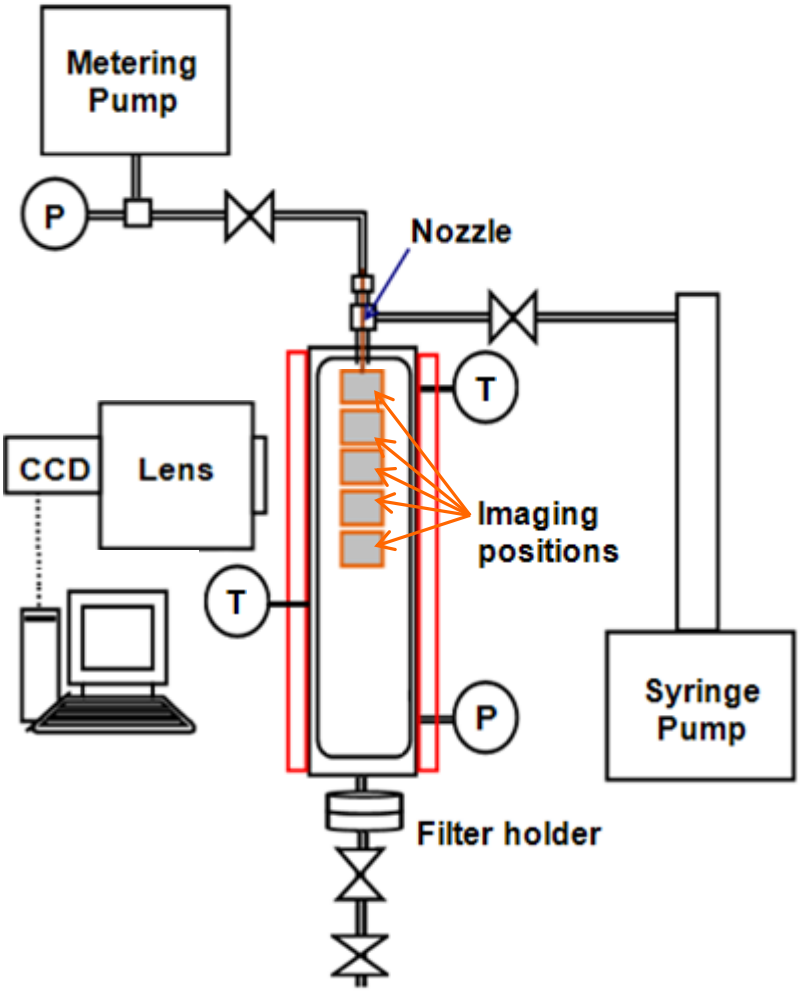

Figure 6.1 Diagram of the imaging system and the apparatus used to perform the supercritical antisolvent precipitation process. The imaging positions in the spray are represented by the shaded boxes inside the precipitation vessel

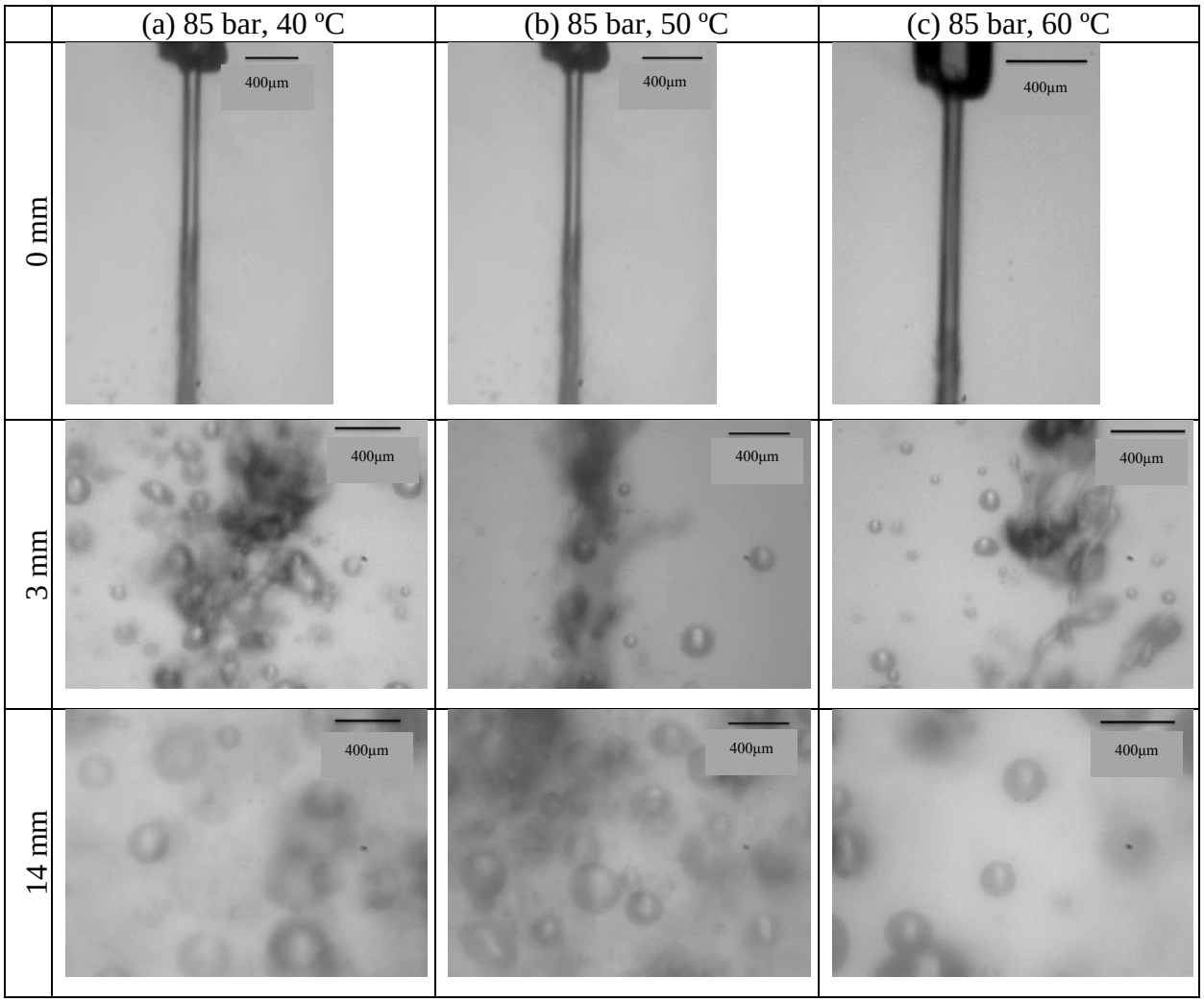

Figure 6.2 Selected frames taken from movies of 1 wt% gelatin in acetic acid spray at given distances from the nozzle in 85 bar SAS experiments

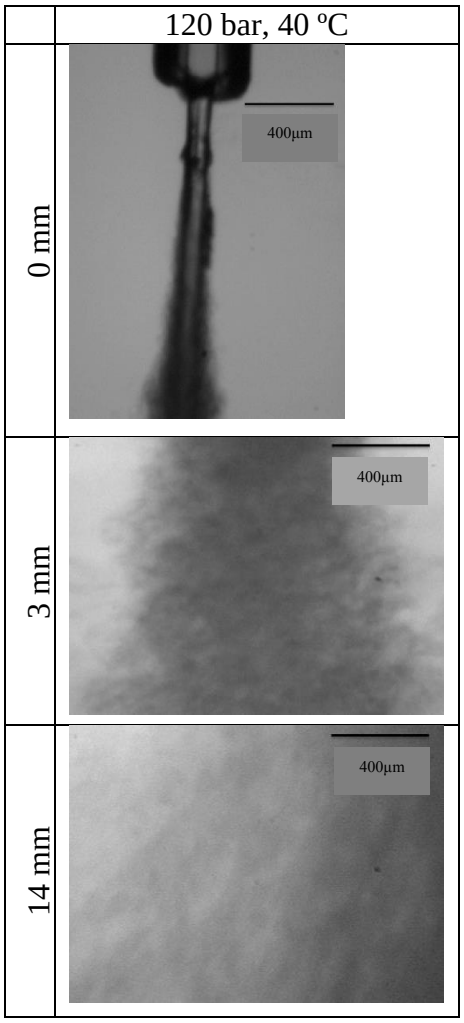

Figure 6.3 Selected frames taken from movies of the spray at given distances from the nozzle in 120 bar and 40 ºC SAS experiments

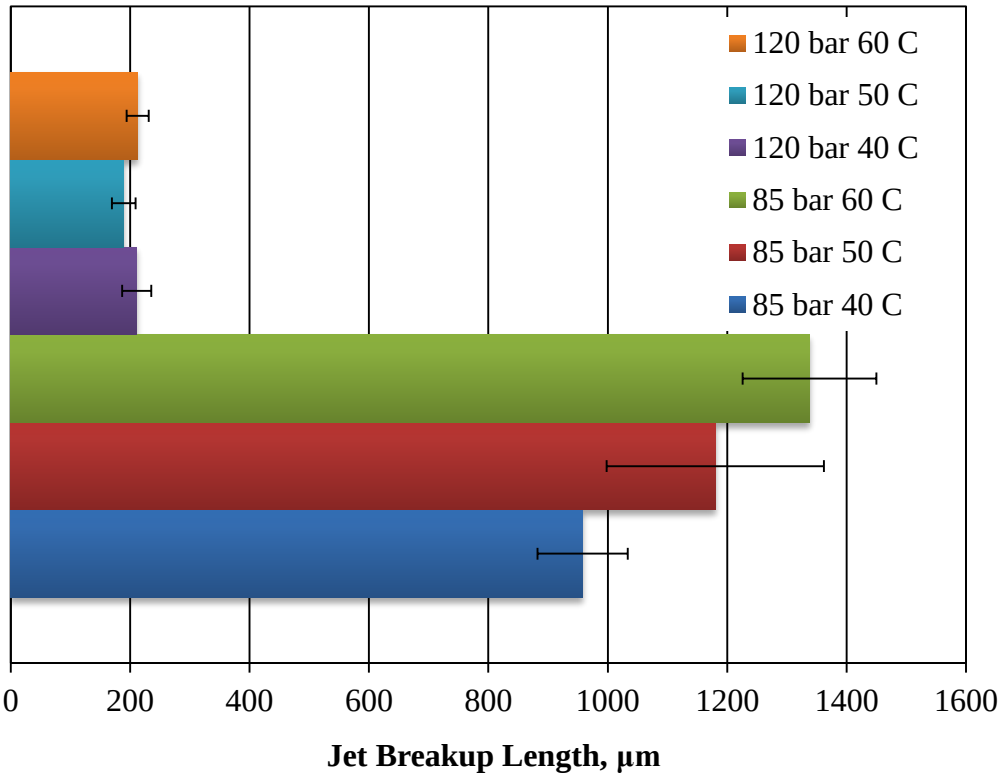

Figure 6.4 Jet breakup lengths of 1wt% gelatin acetic acid processed via the SAS precipitation process at different operating conditions

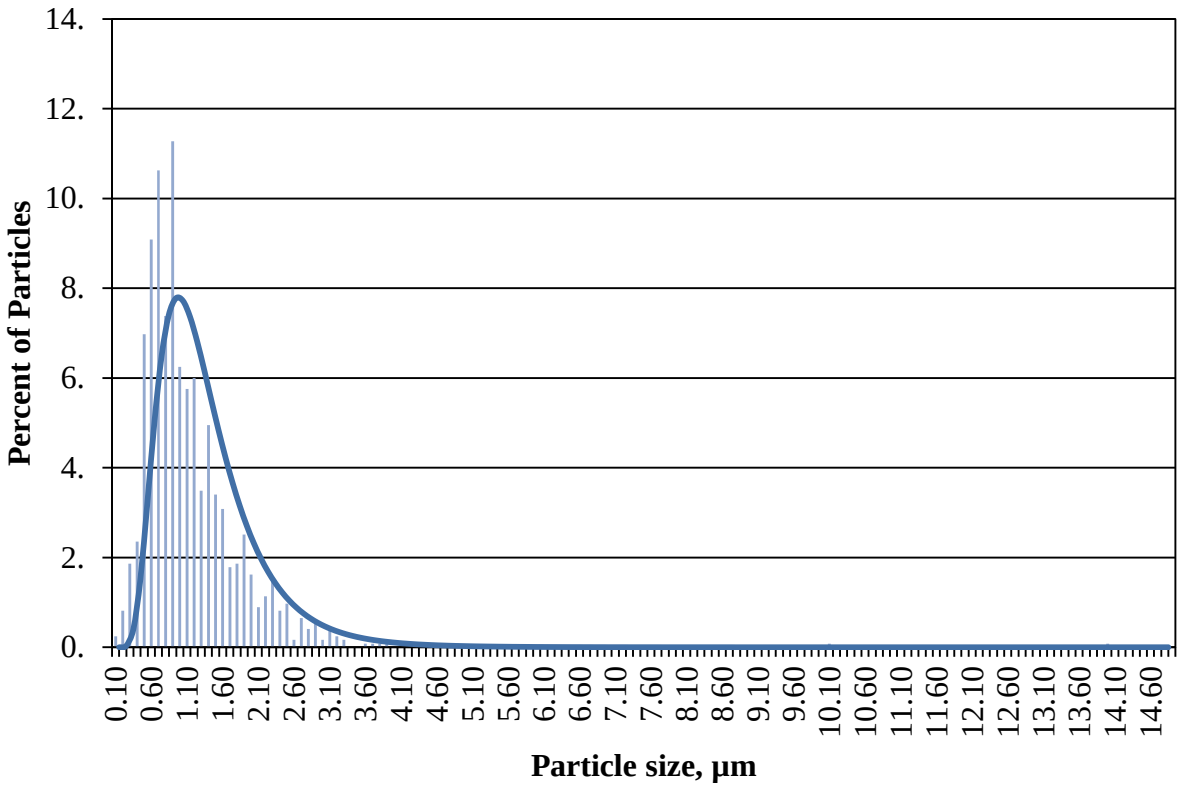

Figure 6.5 Particles size distribution of particles produced from 1 wt% gelatin in acetic acid solution processed via the SAS precipitation process at 120 bar and 40 ºC, that fall on a scale from ≤0.1 µm to 14.50 µm

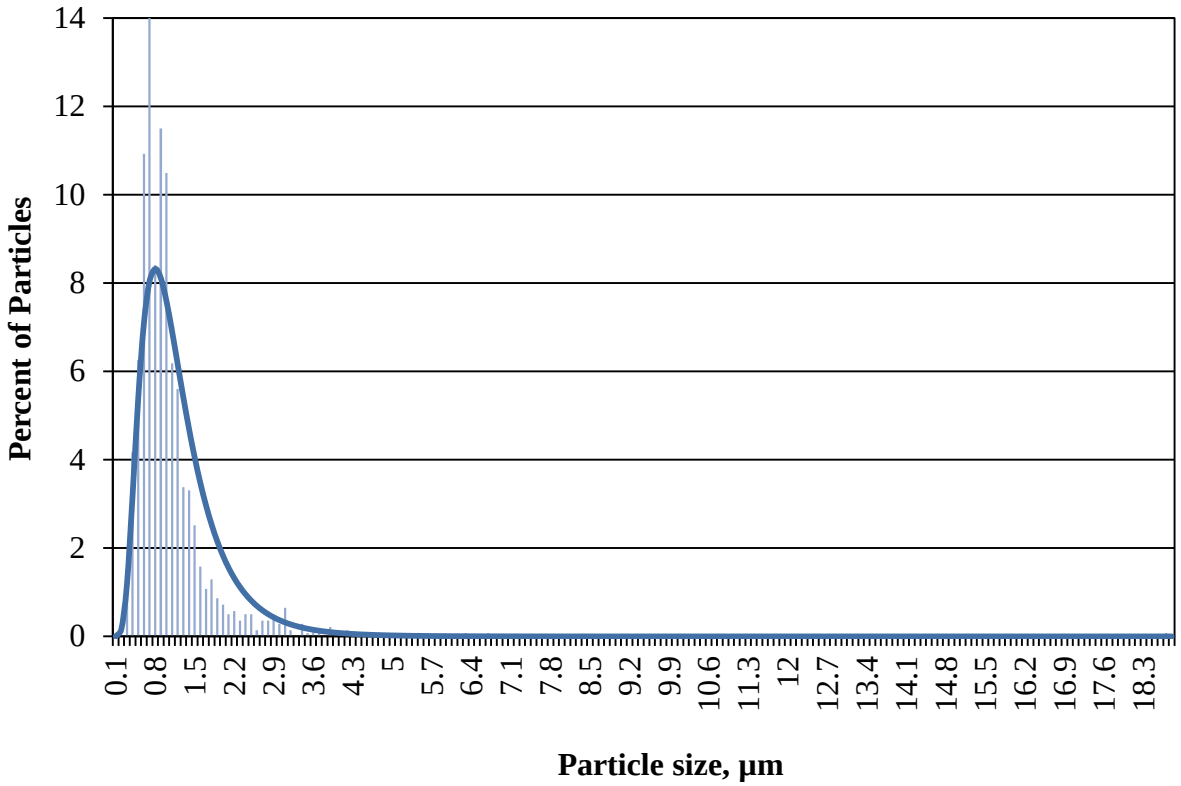

Figure 6.6 Particles size distribution of particles produced from 5 wt% gelatin in acetic acid solution processed via the SAS precipitation process at 120 bar and 40 ºC, that fall on a scale from ≤0.1 µm to 18.30 µm

1wt% gelatin in acetic acid	5 wt% gelatin in acetic acid
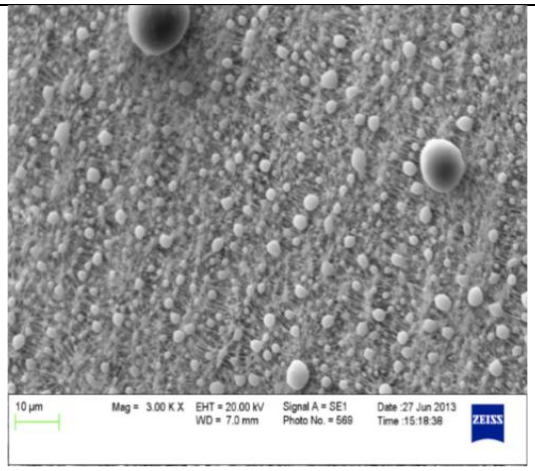	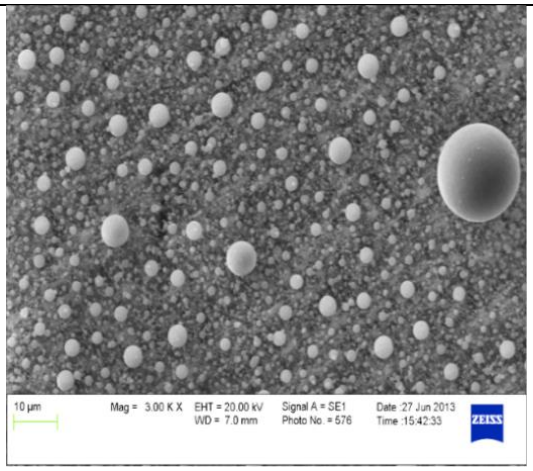

Figure 6.7 Scanning electron microscope images of gelatin particles produced from gelatin in acetic acid solution processed via the SAS precipitation process at 120 bar and 40 ºC

Chapter 7

Conclusion

Many studies have been conducted in the past to understand the mechanisms that control particle size in the SAS precipitation process. We carried out a number of SAS experiments to determine the relationship between SAS spray characteristics and particle characteristics. To study the link between spray characteristics and the resulting particles, a high magnification setup was used to visualize the spray of solution into supercritical carbon dioxide at several pressure and temperature combinations. The effect of the affinity of the solute for the solvent on the SAS precipitation process was tested by processing several solutions of polymers and (polymer+drug) in a solvent via the SAS precipitation process. Despite different spray characteristics at different operating conditions, the size and size distribution of resulting particles was very similar. From these studies we found that characteristics of the spray provided an insufficient correlation with particle characteristics; therefore other phenomena were heavily influencing the particle formation in the SAS precipitation process.

A high magnification visualization system was used to characterize the spray of 1 wt% PMMA in acetone solution into supercritical carbon dioxide at various pressure, temperature, and bulk carbon dioxide density combinations. The spray of a solution into supercritical carbon dioxide was characterized by visualizing the spray at various distances from the nozzle outlet to measure jet break up lengths and droplet diameters. In the fixed temperature experiments, an increase in pressure and density caused a decrease in jet break up length. In each of the fixed

density experiments, the jet break up length was similar. Atomization of solutions of 1wt% PMMA in acetone was observed under all of the experimental conditions studied. In the case of atomization, the average droplet diameter increased then decreased with the distance from the nozzle outlet. Despite different spray characteristics the particle characteristics were similar at different operating conditions. Similar studies were carried out using 1 wt% budesonide in ethanol solutions. This study demonstrated that spherical micro particles of budesonide can be created via the SAS precipitation process. The conclusions from previous studies were confirmed using a solution of drug in solvent.

We also carried out experiments on a solution of PMMA+budesonide in acetone via the SAS precipitation processes. The co-precipitation of poly methyl methacrylate and budesonide was studied by measuring the SAS spray characteristics and the particle characteristics. Acetone was chosen as the solvent since it readily dissolves PMMA while budesonide is slightly soluble in acetone. Precipitated particles were characterized using HPLC to find the relation between starting composition of PMMA+budesonide in solution and composition in produced particles. We found that the starting composition of PMMA+budesonide has a direct relation to composition of PMMA+budesonide in the particles produced via the SAS precipitation process.

We showed that it is feasible to produce gelatin particles using the SAS precipitation process. Gelatin particles of approximately 1 μm in diameter were obtained by processing 1 wt% gelatin in acetic acid solution via the supercritical antisolvent precipitation process. These particles were produced using the SAS precipitation process with supercritical carbon dioxide pressurized to 120 bar and heated to 40 °C. Future work should focus on determining the effect

of operating conditions on particle size for this substance. Although research related to gelatin microparticles is in early stages, the future of these particles is promising in many different areas of industry and medicine.

To better control the SAS precipitation process, a clearer understanding of the mass transfer and concentration fields in this process is required. This will give better understanding of parameters affecting the particle characteristics in the SAS precipitation process. We believe it can be achieved by mapping the two dimension concentrations of solute in the SAS precipitation process. I performed experiments to validate the feasibility of planar laser induced studies of SAS spray. In the future, more experiments can be performed to better understand the precipitation mechanism leading to particle formation in the SAS precipitation process. We developed a system to perform planar laser induced fluorescence (PLIF) of the SAS precipitation process for better understanding of the precipitation mechanism leading to particle formation in the SAS precipitation process. Please see the appendix B for more details. Modifications were made to the experimental setup and the precipitation vessel to allow a planar laser sheet to enter the precipitation vessel. I have laid the foundation for the studies to find the relationship between the particle characteristics and precipitation mechanism in the SAS precipitation process.

References

E.J. Beckman, Supercritical and near-critical CO_2 in green chemical synthesis and processing, The Journal of Supercritical Fluids, 28, 121-191, 2004

P.W. Bell, A.P. Stephens, C.B. Roberts, S.R. Duke, High-resolution imaging of the supercritical antisolvent process, Experiments in Fluids, 38, 708-719, 2005.

A. Bertucco, P. Pallado, L. Benedetti, Formation of biocompatible polymer microspheres for controlled drug delivery by supercritical antisolvent technique, High Pressure Chemical Engineering, 217, 1996.

B. Bigliardi and F. Galati, Innovation Trends in the Food Industry: The Case of Functional Foods, Trends in Food and Science Technology, 2013.

J.F. Brennecke, D.L. Tomasko, J. Peshkin and C.A. Eckert, Fluorescence spectroscopy studies of dilute supercritical solutions, Industrial & Engineering Chemistry Research, 29(8), 1682-1690, 1990.

P. Chattopadhyay, R.B. Gupta, Production of griseofulvin nanoparticles using supercritical CO_2 antisolvent with enhanced mass transfer, International Journal of Pharmaceutics, 228, 19-31, 2001.

D.J. Dixon, K.P. Johnston, R.A. Bodmeier, Polymeric materials formed by precipitation with a compressed fluid antisolvent, AIChE Journal, 39, 127-139, 1993.

S.S. Dukhin, C. Zhu, R. Dave, R. Pfeffer, J.J. Luo, F. Chavez, Y. Shen, Dynamic interfacial tension near critical point of a solvent-antisolvent mixture and laminar jet stabilization, Colloids and Surfaces: A Physicochemical and Engineering Aspects, 229, 181-199, 2003.

W.H. Finlay, C.F. Lange, M. King and D.P. Speert, Lung delivery of aerosolized dextran, American Journal of Respiratory and Critical Care Medicine, 161(1), 91-97, 2000.

A. Gokhale, B. Khusid, R.N. Dave, R. Pfeffer, Effect of solvent strength and operating pressure on the formation of submicrometer polymer particles in supercritical microjets, The Journal of Supercritical Fluids, 43, 341-356, 2007.

Y. Hakuta, H. Hayashi, K. Arai, Fine particle formation using supercritical fluids, Current Opinion Solid State Material Science, 7, 341-351, 2003.

M. Hanna, P. York, Patent WO 95/01221, 1994.

J. Heyder, M.U. Svartengren, Basic principles of particle behavior in the human respiratory tract, Edited H. Bisgaard, C. O'Callaghan, G.C. Smaldone, Drug Delivery to the Lung, Marcel Dekker, 21-45, 2002.

J.A. Hubbell, Synthetic biodegradable polymers for tissue engineering and drug delivery, Current Opinion Solid State Material Science, 3(3), 246-251, 1998.

A. Ivask, Potential and actual applications of nanoparticles as food ingredients and in food packaging, National Institute of Chemical Physics and Biophysics, Laboratory of Environmental Toxicology, Tallinn Estonia, 2013.

T.R. Kommuru, B. Gurley, M.A. Khan, I.K. Reddy, Self-emulsifying drug delivery systems (SEDDS) of coenzyme Q10: Formulation development and bioavailability assessment, International Journal of Pharmaceutics, 212(2), 233-246, 2001.

R. Langer, Drug delivery and targeting, Nature, 392(6679), 5-10, 1998.

C.S. Lengsfeld, J.P. Delplanque, V.H. Barocas, T.W. Randolph, Mechanism governing microparticle morphology during precipitation by a compressed antisolvent: atomization vs nucleation and growth, The Journal of Physical Chemistry B, 104, 2725-273, 2000.

G.G. Liversidge, K.C. Cundy, Particle size reduction for improvement of oral bioavailability of hydrophobic drugs: I. Absolute oral bioavailability of nanocrystalline danazol in beagle dogs, International Journal of Pharmaceutics, 125, 91-97, 1995.

T.M. Martin, N. Bandi, Ryan Shulz, C.B. Roberts, U.B Kompella, Preparation of budesonide-PLA microparticles using supercritical fluid precipitation technology, AAPS PharmSciTech, 3(3), 16-26, 2002.

A. Martin, M.J. Cocero, Numerical modeling of jet hydrodynamics, mass transfer, and crystallization kinetics in the supercritical antisolvent (SAS) process, The Journal of Supercritical Fluids, 32, 203-219, 2004.

S. Mawson, S. Kanakia, K.P. Johnston, Coaxial nozzle for control of particle morphology in precipitation with a compressed fluid antisolvent, Journal of Applied Polymer Science, 64, 2105-2118, 1997.

M. Mukhopadhyay, S.V. Dalvi, Mass and heat transfer analysis of SAS: effects of thermodynamic states and flow rates on droplet size, The Journal of Supercritical Fluids, 30, 333-348, 2004.

D.L. Obrzut, P.W. Bell, C.B. Roberts, S.R. Duke, Effect of process conditions on the spray characteristics of a PLA+Methylene chloride solution in the supercritical antisolvent precipitation process, Journal of Supercritical Fluids, 42(2), 299-309, 2007.

D.L. Obrzut, Investigation of the underlying phenomenon of precipitation in supercritical antisolvent process, PhD Thesis, Auburn University, 2008.

K.P. O'Donnell, H.D.C. Smyth, Macro- and Microstructure of the Airways for Drug Delivery, 2011.

T.W. Randolph, A.D. Randolph, M. Mebes, S. Yeung, Sub-micrometer-sized biodegradable particles of poly(L-lactic acid) via the gas antisolvent spray precipitation process, Biotechnology Progress, 9, 429-435, 1993.

N. Rasenack, B.W. Müller, Micron-size drug particles: common and novel micronization techniques, Pharmaceutical Development and Technology, 9, 1-13, 2004.

E. Reverchon, Supercritical antisolvent precipitation of micro- and nanoparticles, Journal of Supercritical Fluids, 15, 1-21, 1999.

E. Reverchon, G. Caputo, I. De Marco, Role of phase behavior and atomization in the supercritical antisolvent precipitation, Industrial & Engineering Chemistry Research, 42, 6406-6414, 2003.

E. Reverchon, I. De Marco, E. Torino, Nanoparticles production by supercritical antisolvent precipitation: A general interpretation, Journal of Supercritical Fluids, 43, 126-138, 2007.

E. Reverchon, R. Adami, G. Caputo, I. De Marco, Spherical microparticles production by supercritical antisolvent precipitation: interpretation of results, Journal of Supercritical Fluids, 47, 70-84, 2008.

S. Roy, S.R. Duke, Visualization of oxygen concentration fields and measurement of concentration gradients at bubble surfaces in surface-contaminated water, Experiments in Fluids, 36 (4), 654-662, 2004.

F. Shakeel, S. Baboota, A. Ahuja, J. Ali, S. Shafiq, Skin permeation mechanism and bioavailability enhancement of celecoxib from transdermally applied nanoemulsion, Journal of Nanobiotechnology, 6(8), 2008.

A. Shariati, C.J. Peters, Recent developments in particle design using supercritical fluids, Current Opinion Solid State Material Science, 7, 371-383, 2003.

B.Y. Shekunov, J. Baldyga, P. York, Particle formation by mixing with supercritical antisolvent at high Reynolds numbers, Chemical Engineering Science 56, 2421-2433, 2001.

R. Sih, N.R. Foster, Visualization and conception of the atomized rapid injection for solvent extraction (ARISE) process for the production of highly respirable powders, AICHE Annual Meeting, 2007.

P.J. Sinko, Martins Physical Pharmacy and Pharmaceutical Sciences, 2006, Lippincott, Williams & Wilkins, Baltimore.

S. J. Smith, J. A. Bernstein, Therapeutic uses of lung aerosols, edited by A.J. Hickey, Inhalation Aerosols: Physical and Biological Basis for Therapy. Marcel Dekker, 233-269, 1996.

A.P. Stephens, Visualization of particle formation processes in supercritical fluids, MS Thesis, Auburn University, 2003.

B. P. Sullivan, D.L. Obrzut, C.B. Roberts, S.R. Duke, Effect of Pressure on a PMMA-Ethanol Solution during the Supercritical Antisolvent Precipitation Process, 2009.

M.C. Thurber, R.K. Hanson, Simultaneous imaging of temperature and mole fraction using acetone planar-laser induced fluorescence, Experiments in Fluids, 30, 93-101, 2001.

J.W. Tom, P.G. Debenedetti, R. Jerome, Precipitation of poly(L-lactic acid) and composite of poly(L-lactic acid)-pyrene particles by rapid expansion of supercritical solutions, The Journal of Supercritical Fluids, 7, 9, 1994.

B. Valeur, Molecular Fluorescence: Principles and Applications, Wiley-VCH, Weinheim, 2002.

G. H. Ward, G.H. and R. K. Schultz, Process-induced crystallinity changes in albuterol sulfate and its effect on powder physical stability, Pharmaceutical Research, 12(5), 773–779. 1995.

J.O. Werling, P.G. Debenedetti, Thermal analysis of a natural circulation solar air heater with phase change material energy storage, The Journal of Supercritical Fluids, 16, 167-181, 1999.

J.O. Werling, P.G. Debenedetti, Numerical modeling of mass transfer in the supercritical antisolvent process: miscible conditions, The Journal of Supercritical Fluids, 20, 11-24, 2000.

P.T. Woodrow, S.R. Duke, LIF measurements of oxygen concentration gradients along flat and wavy air-water interfaces, Industrial & Engineering Chemistry Research, 40, 1985-1995, 2001.

P.T. Woodrow, S.R. Duke, LIF measurements of oxygen concentration gradients along flat and wavy air-water interfaces, Gas Transfer at Water Surfaces, Geophysical Monograph, 127, 83-88, 2002.

H.T. Wu, M.J. Lee, H. Lin, Nano-particles formation for pigment red 177 via a continuous supercritical anti-solvent process, The Journal of Supercritical Fluids, 33, 173-182, 2005.

S. Yeo, G. Lim, P.G. Debenedetti, H. Bernstein, Formation of microparticulate protein powders using a supercritical fluid antisolvent, Biotechnology and Bioengineering, 41, 341-346, 1993.

Appendix A

Mass Balance on the SAS precipitation process using FTIR technique

A.1 Experimental procedure

After performing the SAS experiments, the produced particles where collected on the membrane filter, Millipore FLGP02500, which separates the precipitated particles from the vessel effluent. The membrane filter has a pore diameter of 0.22 μm and was mounted in a 25 mm filter holder, Millipore XX4502500, at the bottom of the precipitation chamber. From the SEM we have learned that some of the particles produced are smaller than 0.22 μm, which might get washed away while drying the particles. Also, some of the particles get deposited on the inside wall of the precipitation vessel. To find the efficiency of particle collection on the filter paper during the SAS precipitation process we performed a mass balance on the SAS precipitation vessel.

The batch experiment was performed using 1wt% PMMA in acetone solution at operating conditions of 84 bar and 40 °C using the experimental set up shown in chapter 2. 1 wt% PMMA in acetone solution was pumped by the HPLC pump with all valves closed. The solution was sprayed at a flow rate of 1.6 cm^3/min for 45 sec. After the spraying, four chamber volumes of CO_2 were used to purge the precipitation chamber. Once the chamber reached atmospheric pressure, the filter holder was removed to collect the dried PMMA particles on the membrane filter. The membrane filter was removed from the filter holder and the particles on the filter were redissolved in acetone. To collect the particles deposited on the wall of the vessel, the

vessel was filled with acetone. After 30 min, the vessel was drained and the acetone was collected.

A.2 Characterization by FTIR

Liquid sample FTIR was chosen as the characterization technique. Data for these samples were recorded using a Shimadzu IRtracer-100 and scan from 400-4000 cm^{-1} with a resolution of 2 cm^{-1}. FTIR spectra peak at 2900 cm^{-1} was used which corresponds to CH_2 stretch. Figure A.1 shows the IR spectra of PMMA in acetone samples collected from filter and vessel, respectively. Sample solutions of PMMA in acetone were prepared and scanned scan from 400-4000 cm^{-1} with a resolution of 2 cm^{-1}.

A.3 Result

Total PMMA used during the process was calculated to be 9.48 mg (using 1 wt% PMMA sprayed at 1.6 cm^3/ min flowrate for 45 seconds). From FTIR, PMMA collected on the filter was 4.49 mg and PMMA deposited on the wall of vessel was 1.35 mg. The loss of PMMA during the drying the particles was determined to be the difference between total PMMA used and PMMA collected on filter and deposited on vessel wall, 3.64 mg. From this calculation, it was determined that the particle collection efficiency on the filter paper was 47%.

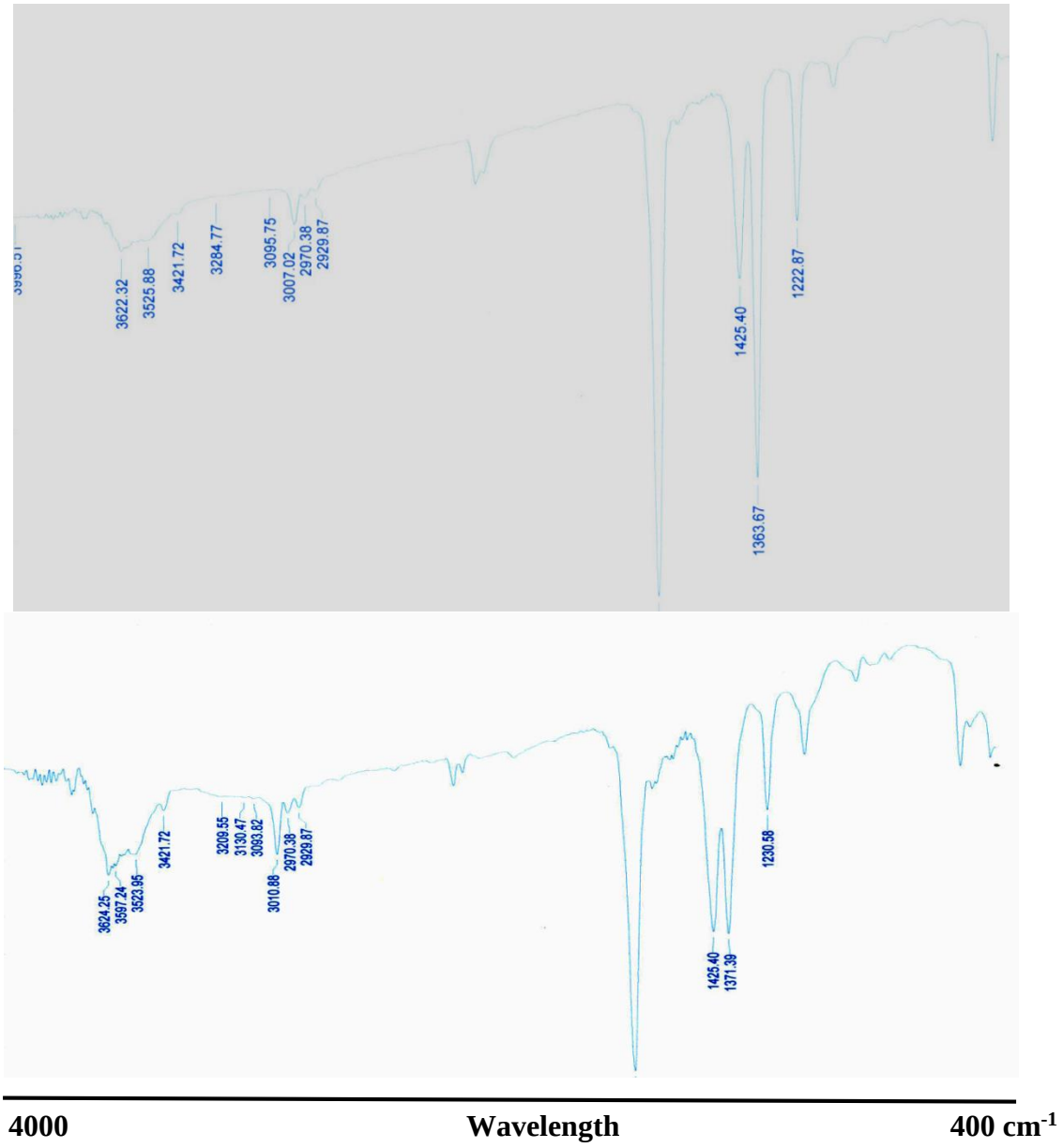

Figure A.1 FT-IR spectra of PMMA collected from filter and vessel, respectively, during the SAS precipitation process at 84 bar and 40 °C

Appendix B

Planar laser induced fluorescence of the SAS precipitation process spray and recommendations

B.1 Introduction

From the studies in Chapter 2, 3 and 4 we learned that spray characteristics are not the only phenomena influencing the particle characteristics in the SAS precipitation processes. To better control this precipitation process, a clearer understanding of the mass transfer and concentration fields in this process is required. By knowing SAS spray concentration profile at different process conditions, nucleation and mass transfer rates can be determined. Knowing concentration profile and mass transfer rates, growth rate of nucleated particle can be calculated. Growth rate of nucleated particle can be used to calculate the final particle size.

One method to obtain the concentration field in the precipitation chamber involves planar laser-induced fluorescence (PLIF) of SAS. A fluorescent molecule, as a solute, serves as a molecular probe. A high magnification imaging technique in combination with PLIF can be used to record the fluorescence from a small portion of the spray. These PLIF studies provide the two dimensional concentration field digital images, which can be used to calculate mass transfer rate coefficients. Previously studies have been done in our lab using laser induced fluorescence (LIF), to measure concentration fields and local mass transfer rate coefficients across air-water interface for oxygen absorption into water (Woodrow et al. 2002, Roy et al. 2004). Roy et al. (2004), Woodrow et al. (2001) and Woodrow et al. (2002) demonstrated high-magnification imaging

techniques in combination with PLIF to measure oxygen concentration fields near air-water interfaces; these techniques and systems can be modified to allow for the fluorescence from small portions of the spray to be recorded. Low magnification imaging could be used to obtain the overall fluorescent emission. Thurber at el. (2001) validated the technique of PLIF of acetone spray to determine the mole fraction of acetone for mixing investigation.

The objective of this work was to employ PLIF in the SAS precipitation process for better understanding of the precipitation mechanism leading to particle formation in the SAS precipitation process. In this study, the potential for use of PLIF to study SAS was validated by choosing a fluorescent molecule as a solute, which can be processed using the SAS precipitation process to make micro particles. The detailed description of use of high magnification imaging techniques in combination with PLIF to capture two dimensional images of the fluorescence occurring in the SAS sprays is provided. Using the techniques mentioned, PLIF experiments over a wide range of operating conditions can be performed in the SAS precipitation process.

B.2 Selection of fluorescent solute for PLIF of SAS experiments

While selecting a fluorescent solute we wanted to select a fluorescent molecule which we can use to compare the results mentioned in the Chapter 2, 3 or 4. Also it is important to consider the absorption and emission spectra of fluorescence. The light absorption and emission is dependent on temperature, pressure and solvent strength. But studies in supercritical fluids have shown that spectra and decay times of many fluorescent molecules remain intact at high pressure (Brennecke et al. 1990). The low quantum yield for single and double ringed aromatic

compounds makes them poor candidates for LIF though they are good solvent for the SAS precipitation process. Larger molecules like pyrene have higher quantum yields and strong emission spectra in certain wavelength. So we have decided to use a molecule, Poly[methylmethacrylate-co-(7-(4-trifluoromethyl)coumarin methacrylamide)] (PMMA-f), which is a copolymer of PMMA with a fluorescent entity. PMMA-f has a maximum absorbance of 339 nm; we had nitrogen laser with wavelength of 337.1 nm available in the lab, which is an appropriate excitation source. PMMA-f has a negligible solubility in $scCO_2$ and good solubility with many solvents used in SAS such as acetone. Figure B.1 and Figure B.2 shows the molecular structure and absorption spectrum of PMMA-f, respectively. The emission spectrum of PMMA-f was measured using a Shimadzu Spectrofluorophotometer RF-5301 in the Department of Polymer and Fiber Engineering, Auburn University. Figure B.3 shows the emission spectrum of PMMA-f in acetone. It generates an emission spectrum with maximum intensity at 449 nm. A CCD camera available in the lab can be used to capture the resulting fluorescence images of 449 nm. To confirm the selection of PMMA-f, we need to validate two conditions.

Validation I:

PMMA-f needed to precipitate the same way as PMMA while processing via the SAS precipitation process. To confirmed that, PMMA-f microparticles were produced, by processing 1wt% PMMA-f in acetone solution via the SAS precipitation process. The same experimental setup and imaging system described in chapter 2 was used. PMMA-f was obtained from Sigma-Aldrich (Product #56624-1), molecular weight of ~40000. Acetone was obtained from Fisher Scientific. Carbon dioxide of grade 5.5 was obtained from Airgas (Opelika, AL). The procedure

in this experiment follows closely with earlier studies. The solution was sprayed at the flowrate of 1.6 cm^3 /min. An experiment was performed at 84 bar and 50 ºC. Particles were collected for this experiment and analyzed using scanning electron microscopy. Figure B.4 shows the particles collected from this experiment were similar to PMMA particles collected previously at 84 bar and 50 ºC. Figure B.5 shows the particle size distribution for PMMA-f and PMMA at 84 bar and 50 ºC. The size and size distribution of PMMA-f and PMMA particles were similar. The morphology of the particles was typically characterized as solid spheres, as shown in Figure B.4. The average particle size for PMMA-f particles was 1.36 ± 0.89 μm and for PMMA particles was 1.15 ± 0.77 μm.

Validation II:

PMMA-f can fluoresce in acetone using PTI model GL-3300 N_2 laser available in the lab. In planar laser induced fluorescence, fluorescence indicates that an excited atom or molecule spontaneously emits light and then rests. In PLIF a laser sheet is exciting these atoms or molecules. In PLIF of the SAS precipitation process, a thin laser sheet will pass through the SAS spray. Fluorescence occurs when the excited electrons return to the ground state and release energy at a higher wavelength (Valeur 2002). We validated that the PMMA-f solution in acetone fluoresces by capturing the fluorescent images of PMMA-f solution in acetone.

A Nikkor 60 mm lens was used with a Photometric CH350/A CCD camera. A UV filter was placed on the Nikkor lens to discard light with wavelength below 350 nm, thus the light from the N_2 laser was filtered from the image. Initially the N_2 laser was turned ON. The N_2 laser is triggered by the CCD camera that fired a single pulse after a trigger indicating that, the camera

shutter was fully open. The laser sheet was passed through known concentration solution of PMMA-f in acetone placed in quartz cuvette. The laser sheet was oriented parallel to the viewing side of the cuvette. Camera operations were controlled by a computer with Photometric "V for Windows" software. The shutter exposure time was set to 100 ms. The effective exposure time was based on the fluorescence lifetime of PMMA-f and was assumed to be less than 10 ns. A focused image was acquired by the CCD camera. PMMA-f in acetone solutions of concentrations 0.08, 0.25, 0.5, 0.75 and 1 wt% were used to capture fluorescent images in the cuvette. Figure B.6 shows the 0.08 wt% PMMA-f in acetone fluorescence in a quartz cuvette. The image has highest intensity at the point where laser sheet enters the solution in the cuvette. The intensity of fluorescence decreases as light passes through the solution. Figure B.7 shows the intensity of fluorescence light along the cuvette, where the highest intensity is at the wall from which the laser sheet enters and then it decreases according to Lambert-Beer exponential decay. Figure B.8 shows the maximum intensity of fluorescent light in the cuvette plotted against concentration of PMMA-f in acetone. The maximum intensity increases with increase in concentration of PMMA-f in acetone.

B.3 Recommended experimental setup and imaging system

LIF techniques are being applied in numerous areas, such as, studies of gas transfer across bubble surfaces (Roy et al. 2004), the degree of combustion can be identified by planar LIF imaging (Thurber et al. 2001). Here, we are proposing use of PLIF technique to understand the precipitation of the solute in the SAS precipitation process. We spray the solution of

fluorescent PMMA-f in acetone while performing the SAS precipitation process in combination with PLIF. We can use high magnification imaging techniques to capture two dimensional images of the fluorescence occurring in the SAS spray. The SAS precipitation process in combination with PLIF is explained below.

PLIF of SAS can be performed in an apparatus mentioned in chapter 2, 3, 4 and, 5 with some modification. The main modification is installation of a sapphire window on the side of the precipitation chamber which allows laser sheet to pass through the SAS spray. Figure B.9 shows the installed sapphire window on the side of the precipitation chamber. A 1 inch diameter sapphire window of thickness 21mm was installed in such a way that a vertical laser sheet coming in the precipitation chamber is parallel to main visualization window. The side window was made of sapphire to maximize the transmittance of the light from nitrogen laser.

Figure B.10 shows the proposed experimental set up for the PLIF of SAS. N_2 laser, PTI model GL-3300, is available in the lab. The N_2 laser has emission wavelength of 339.1 nm with pulse energy of approximately 2.8 mJ and the pulse duration of 800 ps. The output beam has an elliptical cross section of 4 mm by 20 mm. The beam can be passed through a UV grade convex lens and then a plano-cylindrical lens to obtain a very thin planar laser sheet. The convex lens focuses the laser output from N2 laser and plano-cylindrical lens flattens the focused beam. The sheet of light is then reflected up and parallel to the main windows of the precipitation chamber using two 45^o UV-coated mirrors (reflection > 96%). A photometrics CH 350/A CCD camera (512 x 512 pixels) with a high magnification Questar QM100 MKIII long distance microscopic lens can be used to capture the fluorescence from the SAS spray. Photometrics CH 350/A CCD

camera is back-illuminated with quantum efficiency more than 60% at 449 nm. A 350 nm cutoff UV filter in front of the lens can be used to remove the N_2 laser light while capturing the fluorescence.

B.4 Discussion on recommended experiments

It is proposed that PLIF of SAS experiments could be conducted over a wide range of operating conditions in order to map the two dimensional solute concentration within the SAS precipitation process spray. Using this methodology, one could capture the two dimensional fluorescence images of the SAS precipitation process spray, which could then be converted to respective concentration profiles by knowing the relationship between fluorescence intensity and concentration of fluorescent solute. This would potentially allow identification of regions of high solute concentrations within the SAS precipitation process spray. Assuming that these high solute concentration regions lead to nucleation to form micro particles, Figure B.11 shows possible areas of nucleation. These cartoons are the still images of the SAS precipitation process spray at a particular distance from the nozzle.

In case I and case II, nucleation is occurring inside the solvent droplet hence the particle characteristics can be affected by the spray characteristics (like droplet size and droplet size distribution). In case III, nucleation of particles has occurred outside the droplet hence it will be controlled by inter diffusion of solvent and antisolvent rather than spray characteristics. Also there is possibility of seeing the combination of any number of cases. The location of the nozzle outlet relative to the top of the main windows could be altered to change the distance from the

nozzle at which the spray is visible through the sapphire window. Moving the nozzle outlet could be achieved by maintaining the same length of capillary tubing. The two dimensional fluorescent visualization done at different distances from the nozzle can give us the relative changes in the solute concentration profile with time. The obtained concentration profile should provide visual evidence as to where the particles are precipitating during the SAS precipitation process.

B.5 Conclusion

We validated the use of PMMA-f as a solute in the SAS precipitation process to perform PLIF of SAS. PMMA-f has similar behavior to PMMA in the SAS precipitation process. Modifications were made to the precipitation vessel to allow planar laser sheet to enter the precipitation vessel. A 1 inch diameter sapphire window of thickness 21 mm was installed in such a way that the laser sheet in the precipitation chamber is parallel to main visualization window. Using PLIF of SAS we can find the relationship between the particle size and the solute concentration profile in the SAS precipitation process spray. PLIF of SAS could be performed in an apparatus similar to that of previous studies with some modification. It is proposed that PLIF of SAS experiments could be conducted over a wide range of operating conditions in order to map the two dimensional solute concentration within the SAS precipitation process spray.

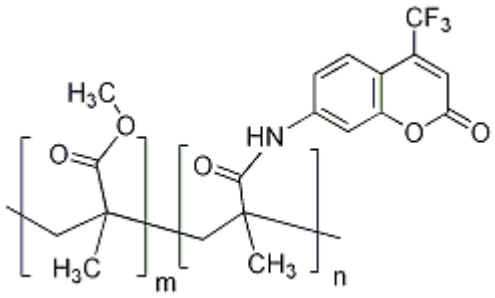

Figure B.1 Molecular structure of poly[methylmethacrylate-co-(7-(4-trifluoromethyl)coumarin methacrylamide)] (Source: Sigma-Aldrich)

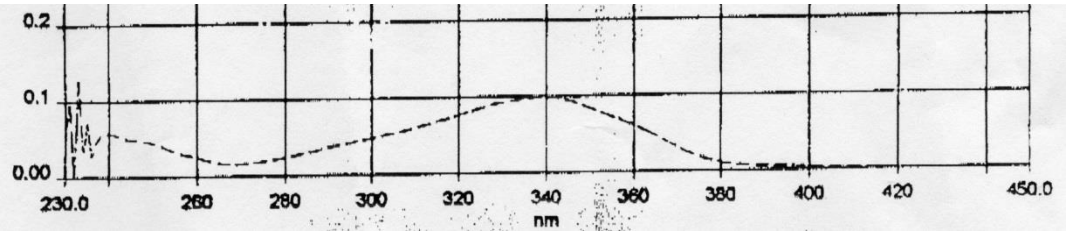

Figure B.2 Absorbance spectrum of poly[methylmethacrylate-co-(7-(4-trifluoromethyl)coumarin methacrylamide)] (Source: Sigma-Aldrich)

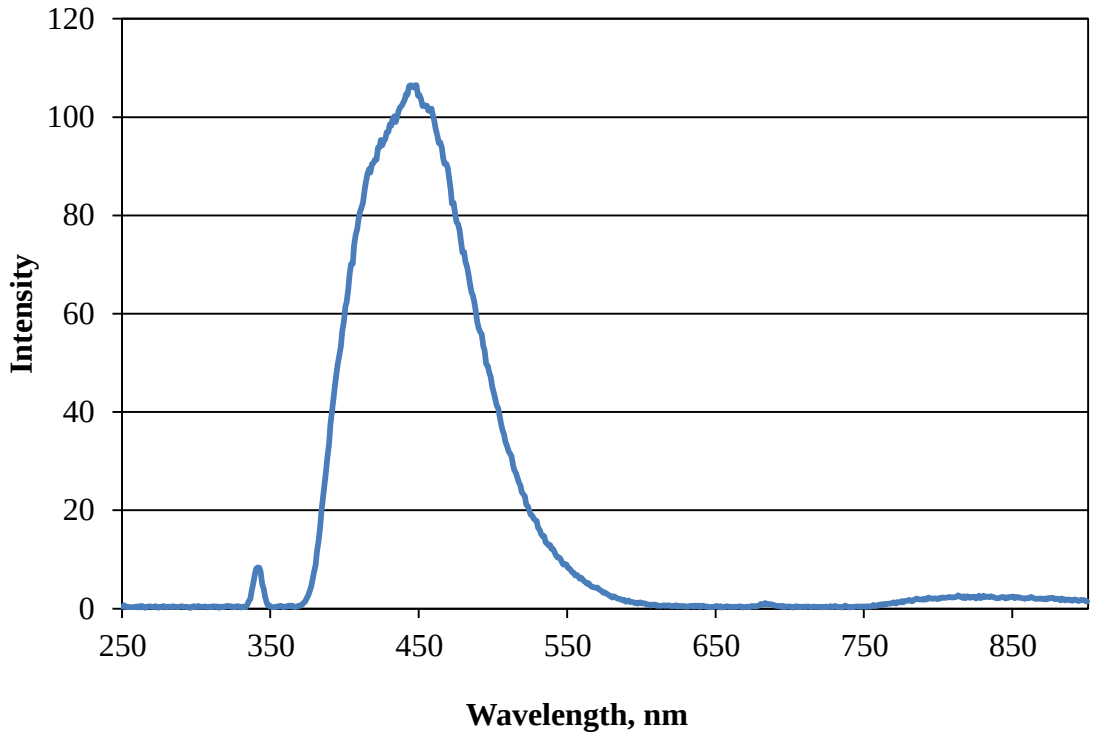

Figure B.3 Emission spectrum of PMMA-f was measured using a Shimadzu Spectrofluorophotometer RF-5301 in the Department of Polymer and Fiber Engineering, Auburn University

a) b)

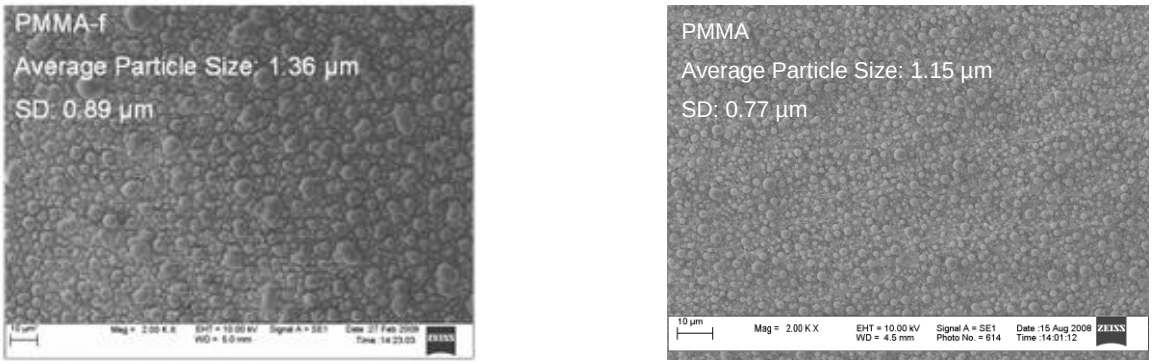

Figure B.4 Scanning electron microscope images of particles produced via the SAS precipitation process at 84 bar and 50 ºC, (a) PMMA-f particles and (b) PMMA particles

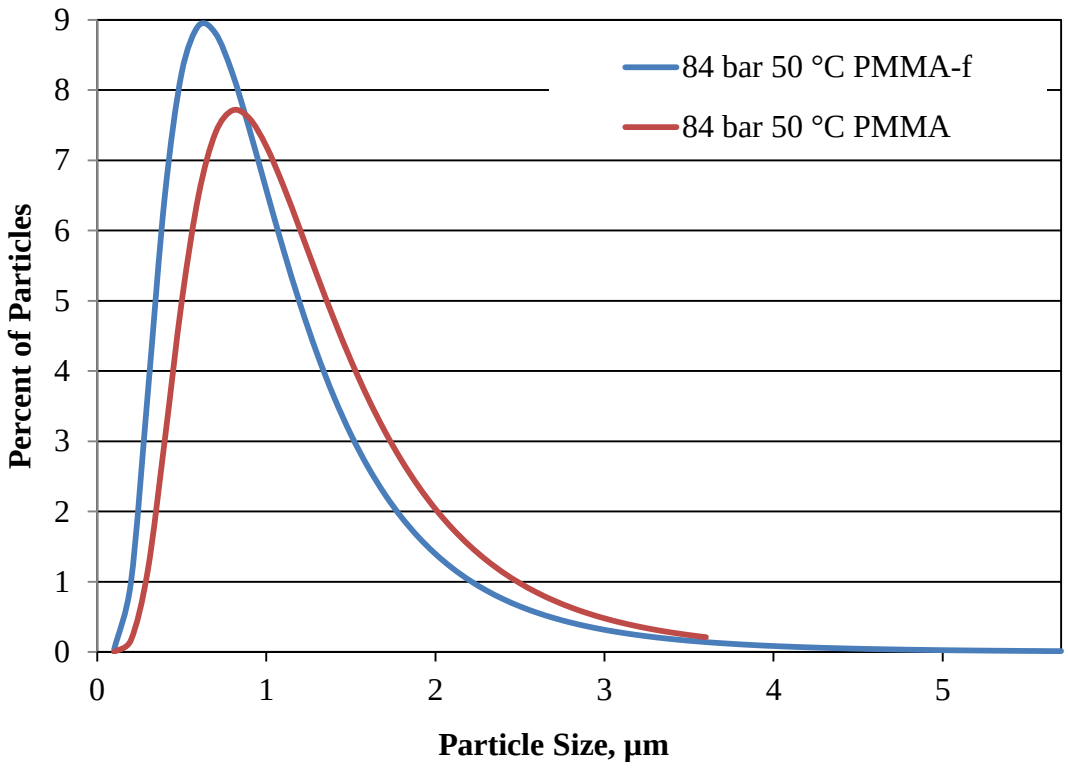

Figure B.5 Particle size distribution for PMMA-f and PMMA particles produced via the SAS precipitation process at 84 bar and 50 ºC

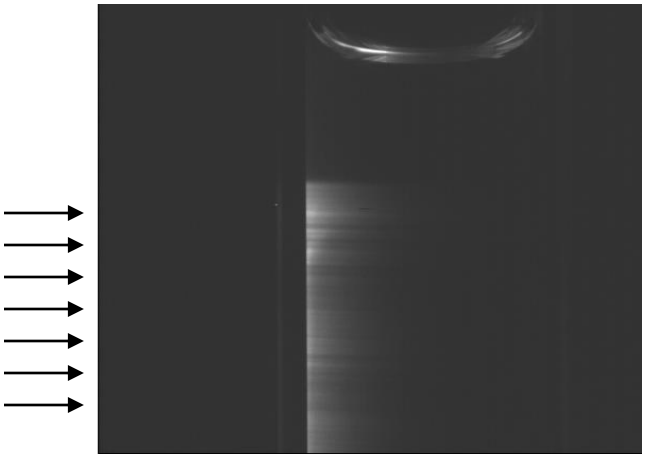

Figure B.6 Raw fluorescent image of 0.08 wt% PMMA-f in acetone solution in a quartz cuvette

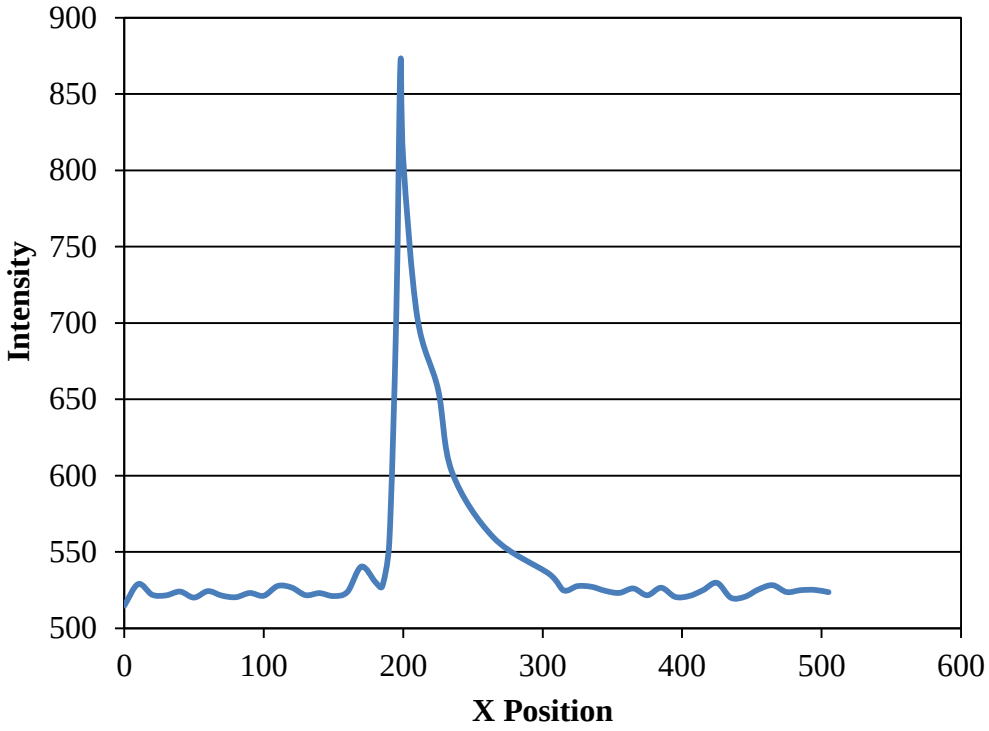

Figure B.7 Intensity of fluorescence of 0.08 wt% PMMA-f in acetone inside a quartz cuvette, the highest intensity is observed at the point where laser sheet enters the cuvette

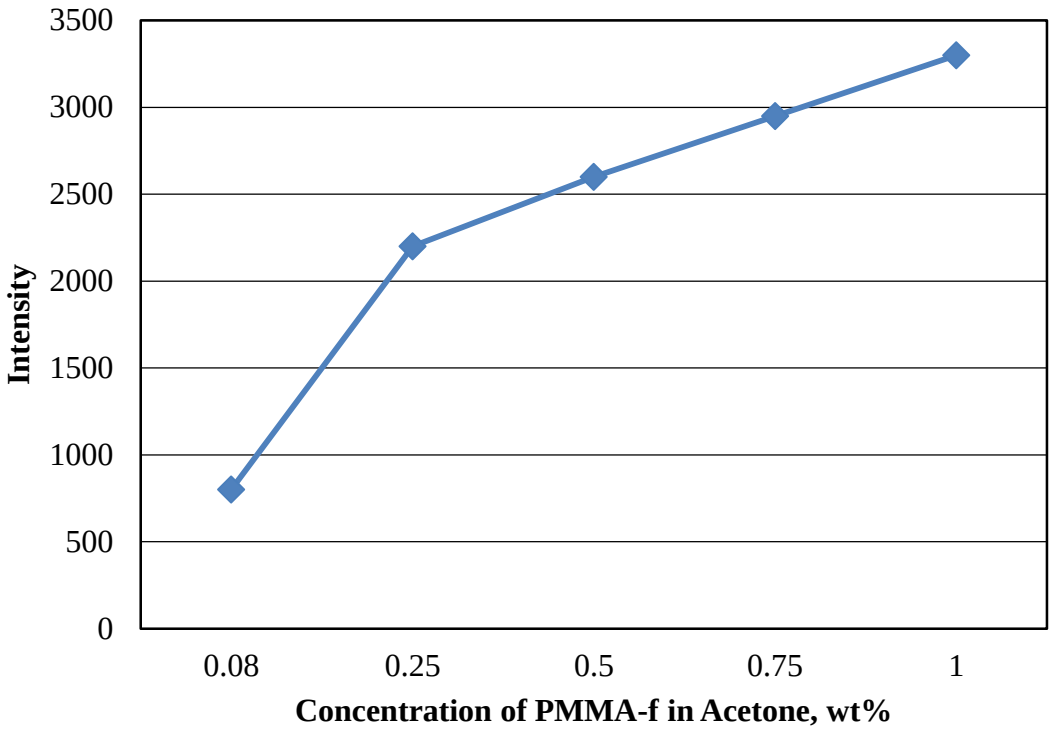

Figure B.8 Maximum intensity of fluorescence of PMMA-f in acetone solution light in a quartz cuvette plotted against concentration of PMMA-f in acetone (all the data is acquired from raw fluorescent images, no correction is applied on the images)

Figure B.9 Sapphire window on the side of the precipitation vessel

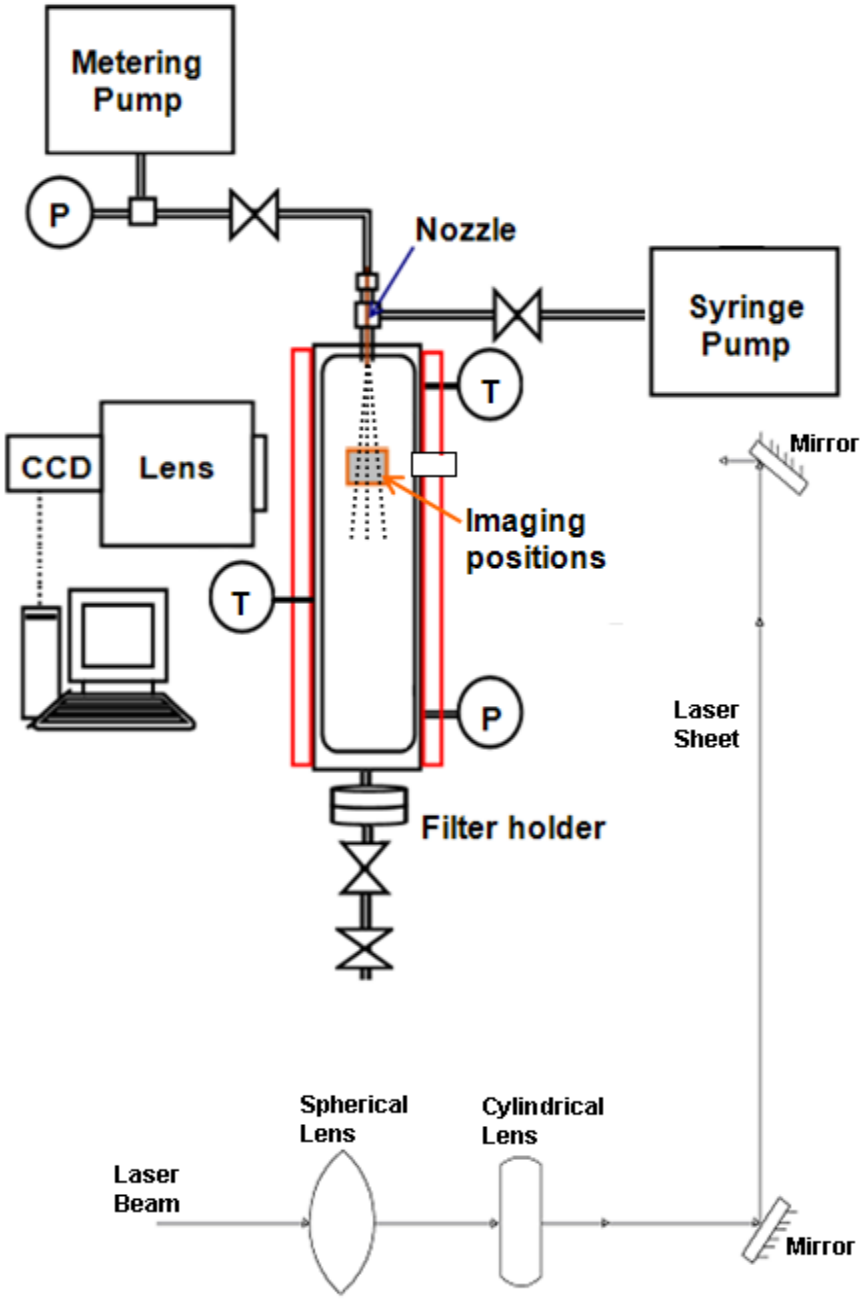

Figure B.10 Experimental set up of PLIF of SAS

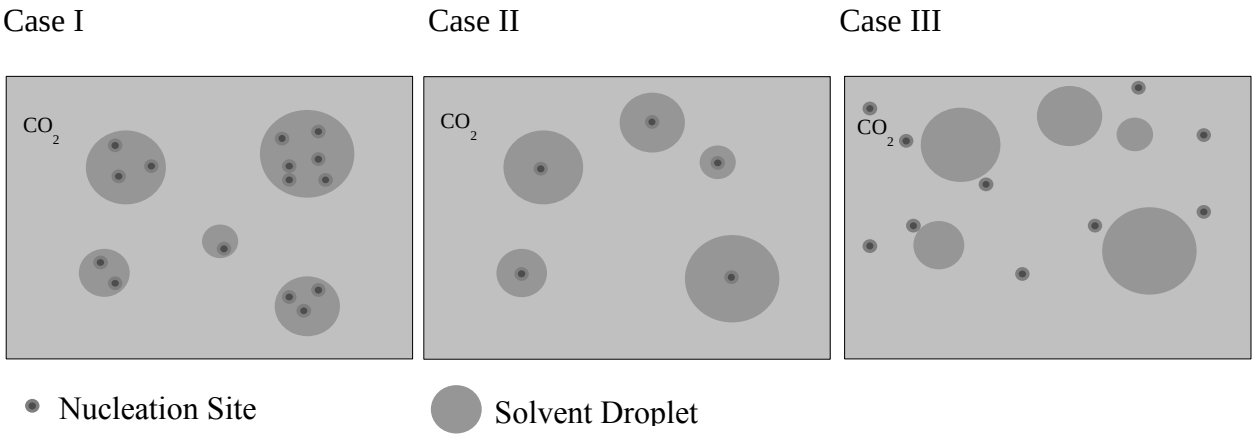

Figure B.11 Case I- One droplet of solution with many nucleation sites of particle formation, Case II- One droplet with one nucleation site of particle formation, Case III- Nucleation of particle formation outside the droplet